Lucia Hanh Tran Vu

Analysis Of Floater Supported Offshore Wind Turbines

Master's thesis in Marine Technology
Supervisor: Prof. Jørgen Amdahl
Co-supervisor: Tore Holmås
June 2022

Master's thesis

NTNU
Norwegian University of Science and Technology
Faculty of Engineering
Department of Marine Technology

NTNU
Norwegian University of
Science and Technology

Lucia Hanh Tran Vu

Analysis Of Floater Supported Offshore Wind Turbines

Master's thesis in Marine Technology
Supervisor: Prof. Jørgen Amdahl
Co-supervisor: Tore Holmås
June 2022

Norwegian University of Science and Technology
Faculty of Engineering
Department of Marine Technology

NTNU
Norwegian University of Science and Technology

NTNU
Norges teknisk-naturvitenskapelige universitet
Institutt for marin teknikk

Master thesis 2022

for

Stud. Lucia Hanh Tran Vu

Analysis of offshore floater supported wind turbines
Analyse av offshore flytende vindturbiner

Offshore wind energy is one of the most promising renewable energy resources in the coming decades. Compared to onshore turbines, offshore turbines provide higher wind speeds for electricity generation and more space is available and installation causes less damage to the surrounding environment. In recent years, the number of offshore wind farms is growing rapidly. By the end of 2019, Europe has a total of 22.1 GW of offshore winds installed, of which 3.62 GW is installed in 2019. The majority of installed offshore wind farms are bottom fixed turbines with monopile or jacket foundations in shallow water, i.e.<50 m. For areas with a water depth larger than 50 m, bottom fixed offshore turbines are not economically attractive and floating offshore wind turbines (FOWTs) are preferred. Floating offshore wind turbines consist of a floater, which is connected to the seabed by mooring lines. The most common floating foundations are the semi-submersible type, spar type, tension leg type and barge type floaters.

Analysis and design of wind turbines is well established for land based and fixed offshore wind turbines. For floating turbines, the experience is more limited.

The idea of the work in project and master thesis is to gain further insight into the governing parameters that drive the design of floating turbines. A key parameter for fatigue (FLS) design of the tower will the cyclic axial stresses due thrust force variation induced by the operating wind turbine and in the ultimate limit state (ULS) the maximum thrust force. Further, how much are these variations influenced by the dynamic behavior of the tower alone and under combined action with wave induced motions of the floater. The plan is to conduct analysis of the wind turbine in several steps with focus on thrust force variation for:

1. Fixed turbine operating alone
2. Turbine mounted on tower
3. Full model with floater

The software VpOne may be used for the simulations. Existing models for a 10 MW turbine with rotor blades will be made available. This design may be "stretched" to approx.12 MW turbine.

It is suggested that the tower may be designed like that used in the following reference_

Gaertner E, Rinker J, Sethuraman L, et al. Definition of the IEA 15-Megawatt Offshore Reference Wind Turbine. tech. rep., International Energy Agency; Denver, CO, US: 2020.

The tower is characterized by a large diameter/thickness ratio (270) compared to typical towers. This may make the design more susceptible to ULS failure.

The project work is proposed carried out in the following steps:

1. Describe briefly the most relevant FLS, ULS, and ALS failure modes of rotor blades, tower, and support structure. Give a brief overview of design cases that shall be investigated and determine which design conditions that will be focused on in the present work. Discuss characteristic wind spectra and corresponding turbulence intensities relevant for various regions in the North Sea and the Norwegian Sea.

2. Simulate control of the 10 MW turbine for various mean wind speeds above rated level and associated turbulence intensities. Estimate the mean and varying horizontal force component as well as the tilt and yaw induced moments at turbine level. On the basis of these responses calculate the mean and varying bending moments at various tower heights. Of particular concern is the stress ranges inducing fatigue. The evaluation should among others be based on the frequency content of the stress ranges, from which the no. of cycles during the expected lifetime of operation should be assessed. Choose a representative weld class and calculate a representative stress concentration factor for this weld class. On the basis of these simple considerations conduct the initial design of the tower (diameter and thickness of a tubular structure).

3. Mount the turbine on top of the designed tower. Calculate the eigenperiods of the assembled structure and assess the expected impact of tower dynamics on the tower responses at various heights using the force and bending moment histories at the tower top from pt 2. Perform time domain simulations of the operating turbine with the tower for the same wind conditions and compare with the results obtained above. Investigate if it is possible to obtain similar response statistics with the simplified calculations using an equivalent damping factor.

4. Choose a floater design supporting the tower. Determine the eigenperiods for the entire system and compare them with simplified hand calculations. Evaluate by simplified calculations the impact of the floater on the responses at the tower bottom. Assume in the first-place flat sea. Compare with full-scale simulations. Repeat analysis with realistic wave loads on the floater and compare the responses.

5. Conclusions and recommendations for further work.

Literature studies of specific topics relevant to the thesis work may be included.

The work scope may prove to be larger than initially anticipated. Subject to approval from the supervisors, topics may be deleted from the list above or reduced in extent.

In the thesis the candidate shall present his personal contribution to the resolution of problems within the scope of the thesis work.

Theories and conclusions should be based on mathematical derivations and/or logic reasoning identifying the various steps in the deduction.

The candidate should utilise the existing possibilities for obtaining relevant literature.

Thesis format

The thesis should be organised in a rational manner to give a clear exposition of results, assessments, and conclusions. The text should be brief and to the point, with a clear language. Telegraphic language should be avoided.

The thesis shall contain the following elements: A text defining the scope, preface, list of contents, summary, main body of thesis, conclusions with recommendations for further work, list of symbols and acronyms, references and (optional) appendices. All figures, tables and equations shall be numerated.

The supervisors may require that the candidate, in an early stage of the work, presents a written plan for the completion of the work. The plan should include a budget for the use of computer and laboratory resources which will be charged to the department. Overruns shall be reported to the supervisors.

The original contribution of the candidate and material taken from other sources shall be clearly defined. Work from other sources shall be properly referenced using an acknowledged referencing system.

The report shall be submitted in two copies:

- Signed by the candidate
- The text defining the scope included
- In bound volume(s)
- Drawings and/or computer prints which cannot be bound should be organised in a separate folder.
- The report shall also be submitted in pdf format along with essential input files for computer analysis, spreadsheets, MATLAB files etc in digital format.

Ownership

NTNU has according to the present rules the ownership of the thesis. Any use of the thesis has to be approved by NTNU (or external partner when this applies). The department has the right to use the thesis as if the work was carried out by a NTNU employee, if nothing else has been agreed in advance.

Thesis supervisors

Prof. Jørgen Amdahl
Tore Holmås

Deadline: June 11, 2022

Trondheim, January 10, 2022

Jørgen Amdahl

Preface

This Master's Thesis is written as a final part of the Master of Science degree in Marine Technology and is a continuation of the Project Thesis written during autumn 2021. The thesis is composed by the Institute of Marine Technology at the Norwegian University of Science and Technology.

It has been decided, along with supervisor Professor Jørgen Amdahl, to modify the initial Master Thesis description. A more appropriate and relevant theme for this Thesis is designated *Fatigue Damage Assessment Of Floater Supported Offshore Wind Turbine Applying Equivalent Damping*.

The executive subject of this thesis is to optimize simulation time for an offshore wind turbine subjected to environmental loads. The design process and analysis are computed in USFOS.

The master thesis has been both challenging and time-consuming, mainly due to limited research on the subject and a newly introduced software program for me. Though rewarding and valuable to study the big picture of relations and also focus on a minor structure element.

I would thank my supervisor, Professor Jørgen Amdahl, for providing expert guidance, curiosity, and engagement in technical discussions. He has also contributed with great support and motivation throughout the semester. Additionally, I would like to thank Tore Holmås for the help and patients in considering modeling in USFOS, which applies as the primary analyzing program for this thesis. A great thanks to all my co-students for contributing to unforgettable five years.

Lucia Hanh Tran Vu
Trondheim, June 2022

Abstract

Improved renewable solutions are constantly investigated and evaluated to reduce the human-produced CO_2 footprint. One of the most promising renewable energy resources in the coming decades is floating wind energy. Design development of a wind turbine is an iterative process that employs time-consuming technical analysis, which requires great data storage. This thesis aims to design a simplified wind turbine model that corresponds to and operates as an ordinary full assembled wind turbine. It also includes an ambition of significantly reducing computational time and processing data yet obtaining reliable and precise results.

Establishing the modified structure in USFOS applies a mathematical simplification. This simplification implements an equivalent damper and a concentrated node mass that replaces and represents the rotor and blades of the full assembled wind turbine. The responses and forces for the simplified and assembled turbine are analyzed to calculate the fatigue life. The discussion of fatigue sensitivity identifies the quality level and accuracy of the wind turbine modification.

Computational time and cost of fatigue assessments are massive, and achieving a simulation time reduction while maintaining high accuracy is challenging. Although, the simplified model obtains similar fatigue results as the complete wind turbine by applying a damper equal to approximately 8 % of the critical damping of the structure. The damping magnitude appears somewhat sensitive and dependent on specific environmental conditions.

Norsk sammendrag

Forbedrede fornybare løsninger blir kontinuerlig studert og evaluert med fokus om å redusere det menneskeskapte CO_2-fotavtrykket. En av de mest lovende fornybare energiressursene de kommende tiårene er flytende vindkraft. Designutvikling av en vindturbin er en iterativ prosess som involverer tidkrevende teknisk analyser som betinger mye datalagring. Formålet med denne oppgaven er å designe en forenklet vindturbinmodell som tilsvarer og opererer som en ordinær fullmontert vindturbin. Oppgaven har en ambisjon om en betydelig reduksjon av beregningstid og behandlingsdata, og likevel oppnå pålitelige og presise resultater.

Etablering av simplifisert og modifisert struktur i USFOS baserer seg på en matematisk forenkling. Denne forenklingen implementerer en ekvivalent demper og konsentrert nodelast som erstatter og representerer rotoren og bladene på den ordinære fullmonterte vindturbinen. Responsene og kreftene for den forenklede og den sammensatte turbinen analyseres og sammenliknes for å kalkulere utmattelseslevetiden. Diskusjonen av utmattingssensitiviteten kartlegger kvalitetsnivået og nøyaktigheten til vindturbin-modifikasjonen.

Beregningstiden og kostnadene for utmattingsanalysene er omfattende. Å oppnå tidsreduksjon ved simulering og samtidig opprettholde høy nøyaktighet er utfordrende arbeid. Evaluering viser ar den forenklede modellen likevel oppnår lignende utmattingsresultater som den komplette vindturbinen ved å bruke en dempning som tilsvarer omtrent 8 % av konstruksjonens kritiske demping. Mengden demping er noe sensitiv og blir påvirket av de ulike omgivelsene.

Nomenclature

Abbreviations

ALS	Accidental Limit State
BEM	Blade Element Momentum
CF	Capacity Factor
DAF	Dynamic Amplification Factor
DFF	Design Fatigue Factor
DOF	Degrees Of Freedom
DTU	Danmarks Tekniske Universitet
FEM	Finite Element Method
FLS	Fatigue Limit States
FOWT	Floating Offshore Wind Turbine
GDW	Generalized Dynamic Wake
LSD	Limit State Design

NDT Non-Destructive Testing

OC4 Offshore Code Comparison Collaboration Continuation

RAO Response Amplitude Operator

ULS Ultimate Limit State

Contents

List of Figures

List of Tables

Chapter 1

Introduction

The climate on earth has changed through the last centuries because more greenhouse gases are emitted into the atmosphere than natural. The average temperature on earth has never been higher; the glaciers are melting, the oceans are rising, and the earth is experiencing more extreme weather than ever. The Paris Agreement will ensure that all countries can limit climate change, aiming to keep the average global temperature rise below 2 $°C$. To achieve this goal, it is necessary to increase the investment level in renewable energy and make the energy sector more sustainable [1].

Floating offshore wind turbines are considered one of the most promising renewable resources in the coming decades and greatly contribute to the green energy transition. The Norwegian government aims to use offshore wind power to generate an almost similar amount of new electricity as the total magnitude currently produced today [2].

If the offshore floating wind industry continues the development of knowledge and education, the ambition of building a leading offshore wind nation is bright. The onshore wind turbine technology is well matured and stands for about 80 % of newly installed wind power capacity in Europe. The largest share of offshore wind farms is bottom fixed turbines with monopile or jacket foundations in shallow water. For deeper water depths, floating offshore wind turbines have a tremendous energy potential and are highly preferred. Figure 1.0.1 illustrates how the capacity of onshore and offshore wind turbine installations has developed over the past four years in Europe and implies a gradual increase in total capacity. For two different scenarios, a prediction of total capacity for the next five years is also displayed. The realistic expectation presents a significant increase that expects Europe to install 116 GW of new wind farms over 2022-2026. It is expected to 60 % growth within five years compared to the capacity in 2021 [3].

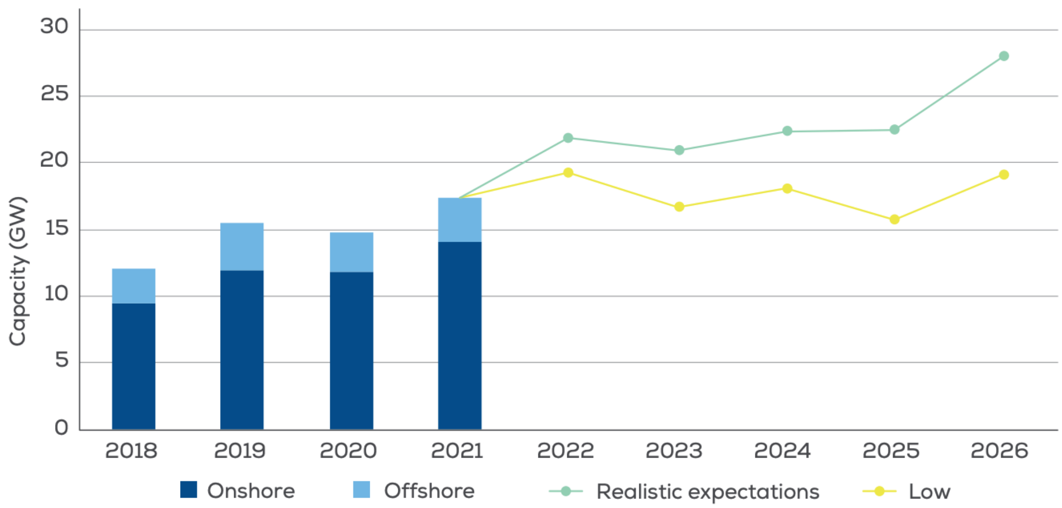

Figure 1.0.1: Power capacity development of onshore and offshore installations from 2018 to 2021, and the prediction until 2026

The installation location has statistically steadier and greater wind characteristics for a floating wind turbine than an onshore wind turbine. However, the variation in wind velocity and wave properties depends on several factors, including different areas, height above sea level, distance to shore, year's season, and environmental conditions. Figure 1.0.2 displays wind resource distribution onshore, up to 200 km offshore, at 100 m above sea surface [4]. Relatively high wind velocities are expected in the North Sea and The Norwegian Sea, with an annual average of about 10 m/s, which indicates the great potential to be converted into a large amount of energy.

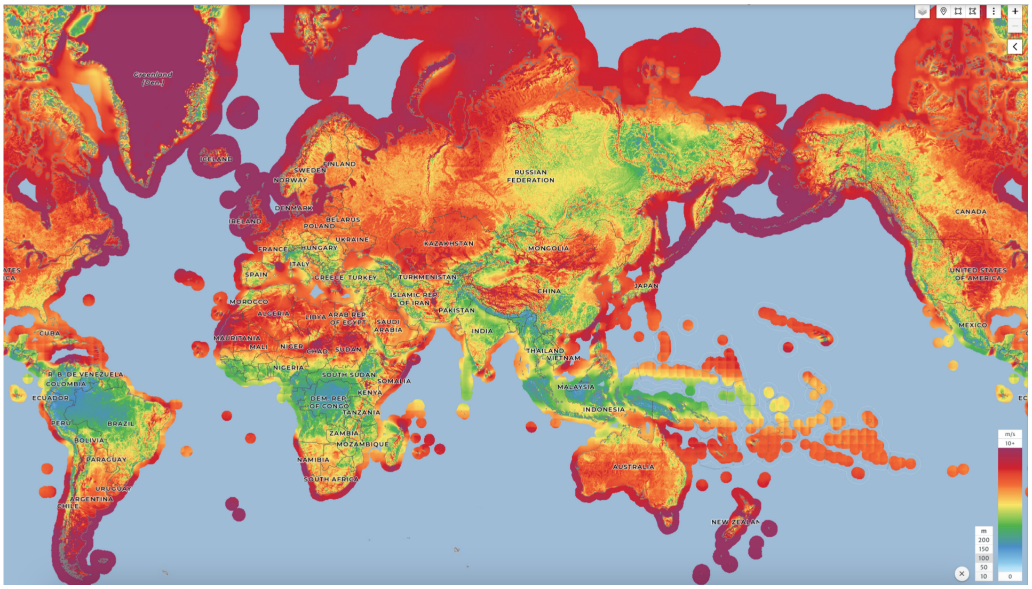

Figure 1.0.2: Wind velocity at 100 m above the sea surface. 250 m horizontal grid spacing, which simplifies the strategy and operation for a new project and installation developments

Wind turbines can experience significant and critical responses due to large forces from wind, waves, current, and other environmental loads. To avoid hazardous and dangerous situations, the calculations and computations of the aerodynamics, hydrodynamics, structural part, and the stability must be carefully and precisely conducted.

It is clear that offshore wind turbines are a discipline with new industrial opportunities and have a significant future potential for the Norwegian maritime industry. Our offshore experience from the North Sea and worldwide makes us uniquely qualified to lead the way and further develop floating offshore wind.

1.1 Background

Humans are constantly adding heat-trapping greenhouse gases to the atmosphere, and the effects of global warming are appearing right now. The primary aim of The Paris Agreement is to keep the average temperature rise below 2 $°C$ to avoid extreme weather scenarios, shifting precipitation patterns, and forcing animals on the move. The Energy Transition Outlook 2021 from DNV predicts that the global average temperature will increase to 2.3 $°C$ by the end of the century [5]. To avoid global warming and achieve the Paris Agreement goal, a dramatic cut in emissions and a considerable increase in investment in renewable energy and technology are required.

The Norwegian government acknowledges a major initiative to promote offshore wind electricity. Our offshore technology expertise and large sea areas may create about 52 000 new jobs and national economic growth.[6] The incentive to develop new offshore wind turbine designs will expand, making the industry compete and demand the best solutions. Additionally, various time-consuming analyses must be conducted and evaluated, which implies an incredible amount of computational time on a computer with a high level of performance that requires enormous data storage. Confronting the challenges and accomplishing better solutions implies that technical analysis becomes more time- and cost-effective.

Floating offshore wind turbines are exposed to environmental forces that cause fatigue damage to the structure, reducing service life. The dominating fatigue contributors should be investigated because a reduction of operational time is a highly costly affair.

1.2 Research Objectives

Designing and modeling a wind turbine is a highly time-consuming process. An ideal and optimal structure model goes through an iterative approach and several computations of technical analysis. Additionally, the simulations require computers with a high level of performance and great data storage, which may be considered inconvenient.

The primary objective of the master thesis is to design a wind turbine model which employs a simplified mathematical approach that replaces and represents the rotor and blades of a fully assembled wind turbine. The fundamental principle behind establishing the simplified structure is an implementation of a concentrated node load subjected at the tower top and employing an equivalent damper. The primary initiative of this simplification is to significantly reduce computational time and processing data, simultaneously obtaining high accuracy of fatigue life calculation.

Initially, a background study of offshore wind energy must be considered to gain further insight into governing parameters that drive the design of floating turbines. Main environmental characteristics are significant in the modeling phase, especially regarding resonance and large excitation, contributing to fatigue damage. Also, the cyclic axial stress and maximum thrust force form the framework of wind turbine design. The number of different environmental scenarios is enormous; hence, only a selection of conditions are considered. Simulation of typical mean wind velocities and associated turbulence intensities at the North Sea is necessary to evaluate responses and forces and locate and investigate critical points.

For the fatigue assessment, it is necessary to decide a representative weld class and determine an appropriate service life of the structure. Subsequently, apply the Rainflow-counting algorithm and Palmgren-Miner rule to quantify the fatigue damage. Analyzing the fatigue damage distribution is fundamental for determining the sensitivity of the fatigue assessment. And finally, a total evaluation of the overall obtained results must be conducted to determine the quality and accuracy of the modified wind turbine.

1.3 Organisation of thesis

Chapter 1 provides brief background information and a content overview of the master thesis. Chapter 2 describes the most essential theory that builds the foundation for software analysis in USFOS and fatigue calculations.

A floating offshore wind turbine is exposed to different loads, presented and explained in Chapter 3.

The modelling of tower structure with a mathematical simplification is described in Chapter 4, and corresponding eigenvalue analysis is discussed. The effect of dynamic simulation and the influence of damping is presented in Chapter 5.

Chapter 6 shows a global dynamic analysis simulated in USFOS-VpOne, where primary environmental loads are determined. The fatigue life assessment is presented and discussed in Chapter 7.

The overall work and results are considered and concluded in Chapter 8, including suggestions for further work.

Chapter 2

Theoretical Background

This section presents an essential underlying theory for applying for the software program USFOS-VpOne, and elementary floating wind turbine theory. The theory and methods are fundamental for conducting the following results and logical discussions in this master thesis. A brief explanation of the three limit states, Ultimate Limit State (ULS), Accidental Limit State (ALS), and Fatigue Limit State (FLS), is introduced. Elementary principles for fatigue life calculation of a cylinder are also included.

An introduction of several offshore wind turbines' designs and power capacity is also presented. Primary stability sources for each floating wind turbine are considered.

2.1 Limit states

Limit State Design (LSD) is a design method used to manage all activities that are likely to occur during the structure's life cycle. At the same time, maintaining the reliability level is relatively high for each limit state. A *limit state* is a condition beyond which the structure no longer satisfies the regulations and requirements introduced as limit states. The most relevant categories of states for this thesis are Ultimate Limit States, Fatigue Limit States, and the Accidental Limit States. Equation 2.1.1 shows the general safety format.

$$S_k \gamma_f \leq \frac{R_k}{\gamma_M} \tag{2.1.1}$$

The design action effect is expressed on the left side, where S_k represents the characteristic action effect and γ_f serves as a partial factor for actions. The right-hand side performs as the design resistance depends on characteristic resistance, R_k, and γ_M represent the resulting material factor. The design action effect must be less or equal to the design resistance to satisfy the safety level. According to regulations, there should be a low probability of failure, and in most cases, this indicates a conservatively estimated mean value. [7] [8]

2.1.1 Ultimate Limit States

Ultimate Limit State (ULS) considers the maximum load is carrying resistance for the rigid body or single components. The structure is restricted from exceeding the ultimate resistance; hence, the components' failure is further investigated to design for safety and security. The most critical conditions to evaluate for ULS are loss of structural resistance due to intense yielding and buckling, component failure due to brittle fracture, and loss of static equilibrium of the rigid body, which may lead to overturning, capsizing, excessive deformation, or collapse.

Rated wind speed and velocities close to generating the largest thrust forces at the turbine are the most interesting condition regarding ULS. In most cases, the operational condition during power production generates the most significant contribution of maximum loads. Nevertheless, the most extensive tower base bending moments may be caused by transients due to emergency stops. Storm conditions may also produce governing extreme loads due to wave motion in combination with high wind loads. Power production and parked condition need to be included for a complete long-term analysis of maximum loads. [9]

2.1.2 Accidental Limit States

Accidental Limit State (ALS) ensures the structure resists accidental loads. At the same time, maintaining the integrity and performance of the structure for a sufficient period under specified environmental conditions. An accidental event may cause local damage to the structure or flooding. The importance of determining ALS is high, especially for the design and operation regarding risk assessment and hazard identifications. Typical accidental loads are impacted by ship collisions, impact from dropped objects, fire, explosions, abnormal environmental conditions, and accidental flooding. [10]

2.1.3 Fatigue Limit States

Fatigue Limit State (FLS) considers stress concentration and damage accumulation under the action of cyclic loading. An infringement of this limit may initiate fatigue crack growth and associated failure of structural components. The structure's design is demanded to resist fatigue failure, and different S-N curves are applied based on the material of the floating wind turbine. For a turbine, the wind force is the fundamental part of the fatigue behavior with its significant contribution to bending stress in several structural components [9]. Following subsection 2.2 presents a detailed description of the fatigue damage calculation of the tower of a floating wind turbine.

2.2 Fatigue life calculation

The floating wind turbine is exposed to various environmental forces, and in order to determine fatigue damage to the structure, the procedure of calculations is presented in this section. Initially, the tower's main characteristics must be decided, including cross-section parameters and material composition. Figure 2.2.1 defines the coordinate system and parameters useful for fatigue calculation.

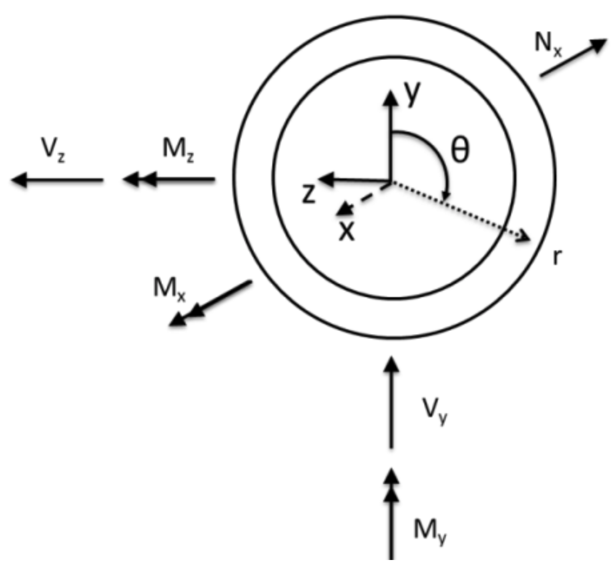

Figure 2.2.1: Cross-section of the tower with relevant variables and local coordinate system [11]

Thrust force produces large bending moments at the tower, and fatigue damage calculation must be considered. Fatigue occurs along with the whole tower height and around the circumference. Further evaluation will determine the critical location, which is particularly essential and relevant to be aware of. Due to the thrust force acting in the same direction as the incoming wind, it is reasonable to assume that the bending moment is greatest at the upwind position of the tower. This position is interesting to investigate, which, according to the coordinate system, implies $\theta = 270$ deg. Taking this into consideration, axial stress, σ, can be computed as in Equation 2.2.1. Axial stress is represented by axial force, N_x, and area of cross-section, determined as A. The bending moment is represented as M with a subscript which defines either the bending moment about Y- or Z-axis. The subscript also applies for the second moment of area I. [11]

$$\sigma = \frac{N_x}{A} + \frac{M_y}{I_y} r sin\theta + \frac{M_z}{I_z} r cos\theta \tag{2.2.1}$$

After computing a time history of stress at a given point, the number of stress cycles must be considered. The Rainflow-counting algorithm is introduced as a practical and adequate method. [12] An appropriate SN-curve must be determined and applied, and the selection is based on tower characteristics and environmental loading. Considering this, determining which design condition contributes the most to fatigue damage can be studied, and SN-curve is presented in Equation 2.2.2. The number of cycles to failure, N, depends on stress range, $\Delta\sigma$, material thickness, t, and material properties. The intercept of log N-axis by S–N curve, $log\bar{a}$, is also considered in the calculation.

$$logN = log\bar{a} - mlog\left(\Delta\sigma\left(\frac{t}{t_{ref}}\right)^k\right) \tag{2.2.2}$$

2.3 Offshore wind turbine solutions

In Norway, only a few adequate locations exist for bottom-fixed offshore wind because the structure is susceptible to water depth and soil conditions. Floating substructures have a higher potential for standardization and use more efficient and productive areas than bottom-fixed offshore wind. One of the greatest advantage of floating wind is that the installation locations statistically have steadier and greater wind characteristics with larger available power. Current technology development within wind turbines and the offshore industry drive turbines to operate at larger water depths than before. The most traditional fixed offshore wind turbines are monopile and jacket structures. For floating foundations, semi-submersible type, spar type, tension leg platform (TLP) type, and barge floaters are most common. Figure 2.3.1 illustrates the most typical offshore wind turbine solutions, with corresponding operating water depth and power capacity [13].

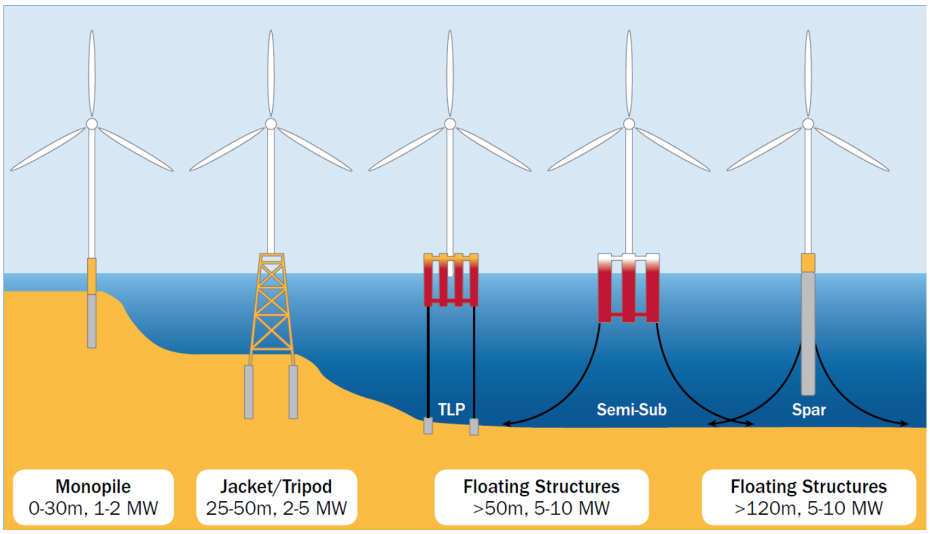

Figure 2.3.1: Different solutions of wind turbine floater foundation

Studying the stability criteria of a floating wind turbine is essential and highly coupled with the design process. Offshore floating solutions are connected to the seabed with mooring lines, and three primary sources of stabilizers are defined. A spar type's primary source of stability is ballast loaded in foundation compartments. The mooring lines are in tension to maintain the stability of a TLP. It is essential to obtain sufficient buoyancy to keep a semi-submersible floater stable.

2.3.1 Semi-submersible foundation

A semi-submersible floater is generally easier to install and more flexible with water depth than TLP and spar wind turbines. The catenary mooring lines and anchor foundations at the sea bed keep the semi-submersible floater in position. The majority of buoyancy stabilized floater solutions consist of large volume columns assembled with bracers and smaller columns. Figure 2.3.2 illustrates the concepts OO-Star Wind Floater and OC4-DeepCwind, with a floater manufactured in concrete and steel, respectively. [14] [16]

(a) OO-Star Wind Floater applies a concrete foundation [15]

(b) OC4-DeepCwind applies a steel foundation [16]

Figure 2.3.2: Examples of semi-submersible foundations

A common design challenge for a semi-submersible floater is obtaining enough pitch motion stability without gaining too much stiffness in heave. Designing too much stiffness in heave may lead to constructing a heave natural period in the similar range of wave frequencies, which is critical for the fatigue life of the structure. Expression of natural period, T_i, is found in Equation 2.3.1, that depends on mass of structure, M_{ii}, added mass, A_{ii}, and stiffness term, C_{ii}.

$$T_i = 2\pi\sqrt{\frac{M_{ii} + A_{ii}}{C_{ii}}} \tag{2.3.1}$$

Chapter 3

Environmental loads

Environmental condition varies from one location, influencing the determination of floater type, size, capacity, and loading of floating wind turbine. Design factors are therefore highly dependent on environmental conditions at the operating site. Meteorological conditions consider different variables: temperature, humidity, precipitation, wind, cloudiness, and atmospheric pressure. The oceanographic condition examines wave realizations, ocean currents, and ocean characteristics. Seismicity inspects plate tectonics and geology of both sea floor and soil mechanics.

When data and information about conditions in a specified area are collected, environmental loads acting on the floating wind turbine are closer investigated. Plenty of environmental loads are acting on a turbine, and in this section, a brief description of the primary underlying environmental loads are studied. Methods for estimating wind loads with corresponding turbulence intensity, wave loads, and current are presented.

Blade Element Momentum Theory (BEM) is introduced and shows the complexity of aerodynamics regarding blade calculation. Comprehensive analysis of blade elements is challenging and requires considerable computational time. This calculation method is included in USFOS-VpOne analysis of the fully assembled wind turbine.

3.1 Wind loads

Wind loads acting on a floating wind turbine produce both lift and drag forces, resulting in a positive torque that drives turbine rotation. This rotation represents mechanical power that is converted to electricity by a generator. The simulation of incoming wind is based on the environment in the North Sea, and this section introduces the characteristics of incoming wind and its different components.

Simulation of wind velocity consists of a slowly varying mean wind and a transient condition that includes wind gusts and wind with an orientation. Mean wind velocity strongly depends on the height above the sea surface, measured reference values, and shaping parameter, α, and the velocity profile, $U(z)$, is presented in Equation 3.1.1. Corresponding mean profile shape depends on atmospheric stability, considered natural for wind turbines at high wind speeds.

$$U(z) = U_{ref}(\frac{z}{z_{ref}})^{\alpha} \tag{3.1.1}$$

Turbulent wind operates as higher-frequency wind gusts, and total wind velocity for a three-dimensional problem is expressed in Equation 3.1.2. Gust components are given as u_1, u_2 and u_3, which represent x-, y- and z-direction, respectively.

$$U(x,y,z,t) = [U(z) + u_1(x,y,z,t)]\mathbf{i} + u_2(x,y,z,t)\mathbf{j} + u_3(x,y,z,t)\mathbf{k} \tag{3.1.2}$$

3.1.1 Turbulence intensity

A realistic wind simulation consists of a mean wind speed and corresponding turbulence for the considered area. *Turbulence* is defined as chaotic and capricious eddies of air, which are disturbed from a calmer state by different forces [17]. The intensity of turbulence may cause stress on both blades and structure and is therefore important to consider. Turbulence intensity, TI, is described by its statistical properties in Equation 3.1.3. It depends on turbulent fluctuations, σ_U, which describes the standard deviation of the longitudinal velocity component, U [18]. Higher wind velocities often have lower turbulent fluctuations than low wind speeds, which results in decreased turbulence intensity. Turbulence intensity caused by longitudinal speed component is, in general, greater than lateral and vertical turbulence intensity components [11].

$$TI = \frac{\sigma_U}{U} \tag{3.1.3}$$

The temporal variation must be implemented for an arbitrary point in the wind generation. Kaimal spectrum is an often used model to include temporal variation for a specific point in atmospheric turbulence. Equation 3.1.4 shows the spectrum for gust components in direction. $S_k(f)$ represents the autospectral density function for the longitudinal component as a function of frequency, f, measured in Hz. The standard deviation for the longitudinal component is noted as σ_k, and L_k is the length of a particular area [19].

$$\frac{fS_k(f)}{\sigma_k^2} = 4 \cdot \frac{\frac{fL_k}{U_{avg}}}{(1 + 6\frac{fL_k}{U_{avg}})^{5/3}} \tag{3.1.4}$$

Turbulence in space is also essential to include in wind simulations. Coherence describes the difference in the wind for two arbitrary points at a given time. Kaimal is a spatial coherence model often used and takes the distance between the specified points into account [20]. The model is expressed in Equation 3.1.5.

$$Coh_{i,jK}(r,f) = exp\left(-a_K\sqrt{\left(\frac{fr}{U_{avg}}\right)^2 + (rb_K)^2}\right) \tag{3.1.5}$$

3.1.2 Blade Element Momentum theory

A brief introduction of the Blade Element Momentum (BEM) theory, its assumptions, and corrections is presented in this section. BEM theory combines blade element theory and momentum theory to determine aerodynamic forces and induced velocities acting on the wind turbine rotor blades. Blade element theory separates the blade into infinitesimal sections, then determines the forces on each of these small blade elements. Momentum theory studies a mathematical model of an ideal actuator disk, represented as the blade rotor.

Governing equations related to BEM theory are the conservation of moment, conservation of mass, and Bernoulli equation, and corresponding assumptions are also established. The fluid flow is assumed to be homogeneous, incompressible, and steady state and is restricted from crossing stream tube boundaries. Assuming that the thrust force is uniformly distributed over the disk. Ambient pressure far from the disk must be equal to pressure upstream from the disk. Figure 3.1.1 illustrates how forces are distributed over the blade element and with the corresponding angle of attack. Relative velocity, V_{rel}, is effective velocity acting on the blade and is composed of mean wind velocity, axial- and angular induction factors, blade length, and rotational velocity.

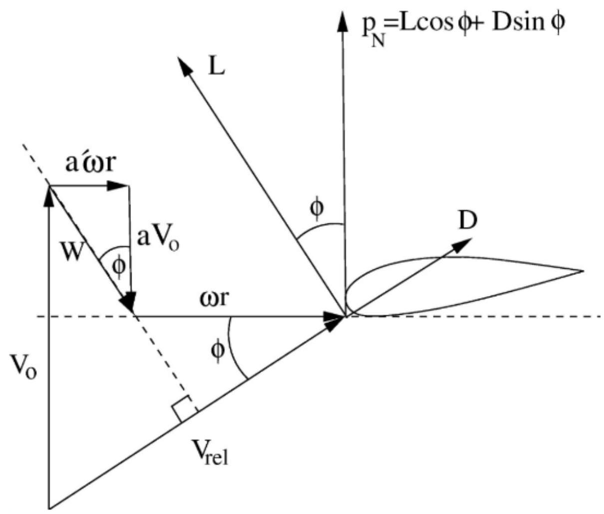

Figure 3.1.1: Forces with corresponding angles acting on blade element in 2D

In addition to establishing assumptions, several corrections must be taken into account, which is highlighted in this section. BEM theory does not consider the turbines' finite number of finite blades. The air tends to flow around the tip from the lower to the upper side, so tip-loss correction, Prandtl correction, is included. Gaulert correction is introduced when large axial induction factors ($a > \frac{1}{3}$) are implemented, giving two different empirical expressions for the thrust force coefficient. Dynamic wake correction is carried out due to the time-lag in induced velocities created by vorticity being shed and convected downstream. The dynamic wake can be implemented by introducing Stig Øyes filter for induced velocity. When the angle of attack changes, lift and drag coefficients need to be modified; hence the dynamic stall correction is established. Since inflow and rotor are not aligned, empirical correction for skewed wake is applied. This phenomenon often occurs when inflow is yawed, or the rotor is tilted by the platform pitch or built-in control algorithm.

An alternative method for calculating aerodynamic loads and induced velocities is the Generalized Dynamic Wake (GDW). The theory is based on the potential flow solution to Laplace's equation and was initially developed for computations of aerodynamic forces on helicopters. The GDW method is an inherent model of dynamic wake, tip loss, and skewed wake and is only valid for wind velocities above ~8 m/s. [21]

3.2 Wave loads

Boundary conditions and continuities are introduced for determining the characteristics of wave loads. Potential flow theory is initially assumed, implying that fluid is incompressible, inviscid, and irrotational motion. The continuity equation is then modified and may be expressed as the Laplace equation and is applied within an enclosed volume, Ω. The resulting Laplace equation is shown in Equation 3.2.1.

$$\nabla^2 \phi = 0 \tag{3.2.1}$$

The dynamic condition must be fulfilled to determine the velocity potential for fluid particles. This condition is satisfied by stating that Bernoulli's equation is valid along the sea surface, meaning that the pressure at a point on the sea surface equals atmospheric pressure. The equation is then expressed concerning pressure, p, as a function of velocity potential, and Equation 3.2.2 is obtained.

$$p = C(t) - \rho g z - \rho \frac{\partial \phi}{\partial t} - \frac{\rho}{2} \nabla \phi \cdot \nabla \phi \tag{3.2.2}$$

Kinematic conditions also restrict the behavior at the free surface. This condition requires that a fluid particle at the free surface of small waves always remains at the sea surface. Determination of velocity potential can be established when all requirements of boundary conditions and continuities are satisfied [22].

Elevation series of long-crested linear irregular waves are considered for a single wave. Each wave elevation component, ζ_n, has its own particular wave amplitude, ζ_{An}, frequency, ω_n, and phase angle, ϵ_n. Wave amplitude may be established based on the given wave spectrum, $S(\omega_n)$. By implementing this definition, the complete first-order surface elevation is expressed in Equation 3.2.3. For the computation of short crested wave elevation, directions of waves must be included [23].

$$\zeta_1(x,t) = \sum_{n=1}^{N} \sqrt{2S(\omega_n)\Delta\omega} cos(\omega_n t + k_n x + \epsilon_n) \tag{3.2.3}$$

Simulations that include second-order waves are more realistic than computation only considering first-order, implying steeper waves, wider thoughts, and narrower crests. The structure experiences nonlinear effects, so it is necessary to include second-order waves in the computation. This is expressed in Equation 3.2.4, where surface elevation quadratic transfer function is represented as $E_{ij}^{(\pm)}(\omega_i, \omega_j)$.

$$\begin{aligned} \zeta_2(t) = \zeta_1(t) + \textstyle\sum_{i=1}^{N}\sum_{j=1}^{N} \zeta_{Ai}\zeta_{Aj} E_{ij}^{(+)}(\omega_i,\omega_j) cos[(\omega_i+\omega_j)t + (\epsilon_i+\epsilon_j)] \\ + \textstyle\sum_{i=1}^{N}\sum_{j=1}^{N} \zeta_{Ai}\zeta_{Aj} E_{ij}^{(-)}(\omega_i,\omega_j) sin[(\omega_i-\omega_j)t + (\epsilon_i-\epsilon_j)] \end{aligned} \tag{3.2.4}$$

In addition to non-linear waves, the second-order non-linear problem also includes non-linear loads. Meaning that mean drift, sum-frequency, and difference frequency effects are acting on the structure. Slow drift motions may occur as a consequence of non-linear loads. These motions are resonance oscillations excited by non-linear interaction effects between waves and body motion and will occur in the surge, sway, and yaw of a moored system. A contribution from second-order potential is needed for the slow-drift excitation loads [24].

3.3 Current

Current loads may induce motions on a floating structure and is a significant load contributor for a floating wind turbine. Floater, mooring line, and electrical cable are directly subjected to current loads. Current velocities are decomposed into one component in the longitudinal direction and the other in the cross-flow direction of the slender structural part. Assuming that the longitudinal current velocity component causes only shear forces, cross-flow will cause flow separation. Drag and lift coefficients must be empirically determined before calculating mean force. $\bar{F_L}$ force acts as a mean force in the cross-flow plane, and F_D is orthogonal to this force and is the mean force in the same direction of the cross-flow component U_N of current velocity. Both forces are also dependent on the diameter of the structure, and the expression is shown in Equation 3.3.1 [24].

$$\begin{aligned} F_D &= \tfrac{\rho}{2} C_D D U_N^2 \\ \bar{F_L} &= \tfrac{\rho}{2} \bar{C}_L D U_N^2 \end{aligned} \tag{3.3.1}$$

Chapter 4

Modelling in USFOS

USFOS is a respected software program for nonlinear static and dynamic analysis of space frame structures. The computer program is an attractive helping aid for inspection planning, lifetime extension and integrity assessment of aging structures, and fire protection assessment for new designs. The conducted analysis is through the utility USFOS-VpOne, which is capable of and specializes in computing analyses for floating wind turbines. The analysis is conducted on a model inspired by DTU 10 MW Reference Wind Turbine (DTU 10 MW).

The appropriate assembly and production of the software program have implemented several theories, such as BEM theory with dynamic stall corrections for precise conduction of aerodynamic forces acting on blades and tower. Notice that the theory behind USFOS-VpOne only is valid for slender bodies or structures in long waves ($\frac{\lambda}{D} > 5$). Method of pressure integration estimates Froude-Krylov force by direct pressure integration using incident wave velocity potential. Airy theory with Wheeler stretching, Stokes' wave theory, Stream function theory and Morison's Equation, are implemented for hydrodynamic calculation. The structural dynamics are represented by The Finite Element Method (FEM).

This section's primary purpose is to gain further insight into the essential design parameters of a floating wind turbine. The construction is modeled in USFOS, excepted to restrain the characteristic magnitudes of environmental forces acting at the North Sea. There are made several assumptions to estimate and calculate the main parameters. Initial assumptions about dimensions and environmental forces are generally determined with a conservative view, which later will be modified to obtain the most optimal and feasible solution.

In order to model the wind turbine in USFOS the orientation of the coordinate system and degrees of freedom (DOF) are determined. Figure 4.0.1 illustrates an arbitrary floating wind turbine and the defined translation and rotation modes; surge, sway, heave, roll, pitch and yaw. Additionally, the turbine is subjected to wind loads, where the inflow wind velocity acts in the negative x-direction.

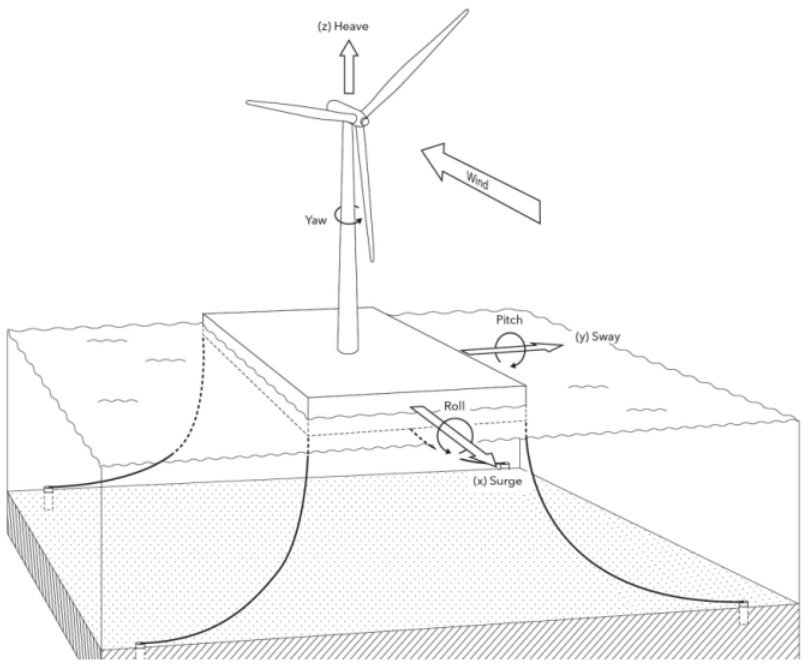

Figure 4.0.1: Degrees of freedom for a floating wind turbine

4.1 Modelling procedure

This section provides an overview of the wind turbine modeling procedure, from the beginning to the discussion and final results. The modeling process is illustrated in Figure 4.1.1 and starts by introducing the prestudy. The prestudy provides a robust theoretical foundation and framework considering environmental conditions and wind turbine theory. The tower design and dimensions may then be established. Together with the turbine controller, two different USFOS model files are constructed, the *simplified turbine model* and *the assembled model*. Analyses of these models are then conducted and compared. Iterations with the simplified model may be necessary to obtain good results.

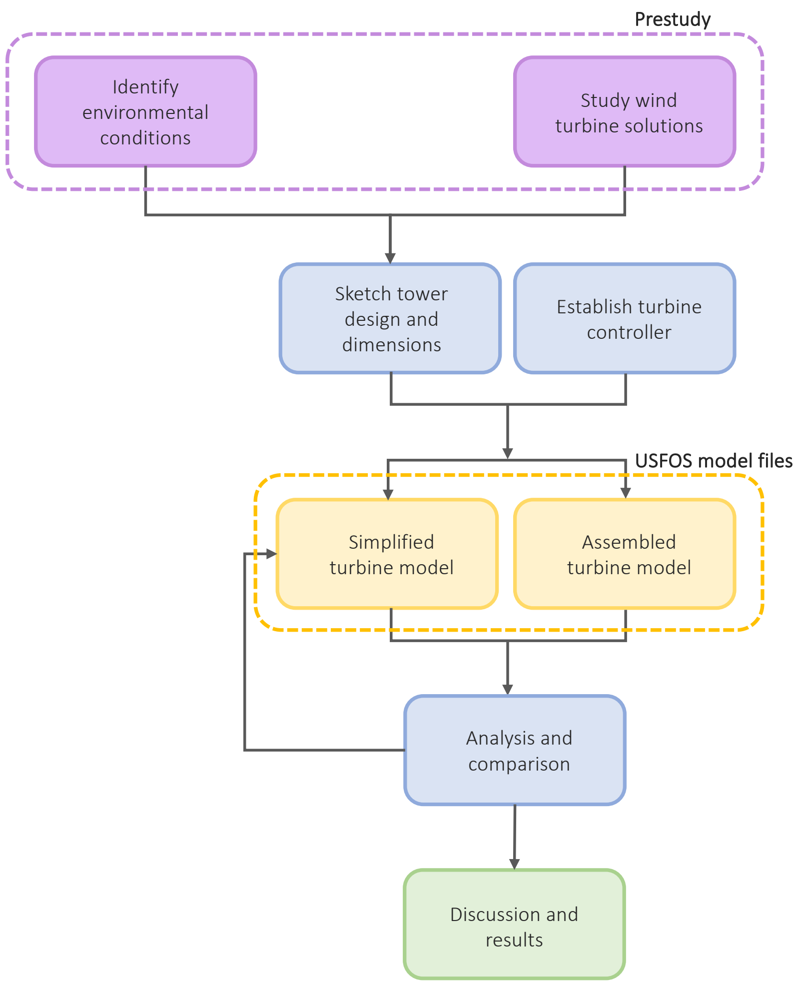

Figure 4.1.1: Executive modelling procedure of the simplified turbine and the assembled turbine

4.2 Simplified wind turbine applying equivalent damper

This section presents the establishment and construction of the simplified turbine, including the design process and the mathematical simplification. The tower is modelled in the software program USFOS, and the model code, model.fem, is attached in Appendix A.2.

4.2.1 Tower design and primary dimensions

The tower design and dimensions take inspiration from DTU 10 MW and other similar wind turbines with a capacity between 10-15 MW. The 101-meter high tower is divided into six beam elements, with the following seven nodes. The number of segments is determined based on the tower's level of detail regarding fatigue life. Seven nodes are implemented to represent forces and moments along with the tower. The later section shows that seven nodes are sufficient for presenting the distribution, hence satisfying fatigue damage calculation.

The main dimensions of the tower design are shown in Table 4.2.1, where heights, diameter, and wall thickness are presented at the different nodes. Both outer and inner diameters and wall thickness are linearly distributed along with the whole tower, and a calculation of the ratio between outer diameter and wall thickness is also conducted.

Table 4.2.1: Primary dimensions of the tower design

Node nr	**Distance from rotor** **H** [m]	**Outer diameter** **D** [m]	**Wall thickness** **t** [mm]	**D/t ratio** [-]
1	0	5	40	125
2	20	5.6	46	122
3	40	6.2	52	119
4	60	6,8	58	117
5	80	7.4	64	116
6	100	8	70	114
7	101	8	70	114

Following Figure 4.2.1 illustrates the tower where element- and node numbers are included. Each element is modeled as a cone for the first five segments, where the diameter at end 1 is unequal to the diameter at end 2. Furthermore, the joints between the elements will have a continuous transition. USFOS usually extracts forces, moments, and general characteristics in the transitions of the elements, accordingly end 1 and 2 with diameters 1 and 2, respectively. Therefore, element number six is implemented as a 1-meter-short cylinder structure to obtain the exact fatigue calculations at the tower bottom in the transition of the floating foundation.

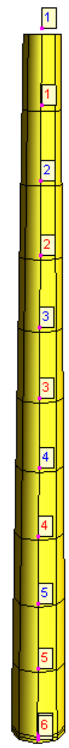

Figure 4.2.1: Model of simplified tower including element- and node numbers

Wind turbines in the capacity range of 10-15 MW exposed to similar environmental conditions have influenced the tower design and dimensions. Complete design and determination of a wind turbine's dimensions require several technical analyses, including ULS, ALS, and FLS. Modifications and adjustments are performed during processes of iterations and numbers of simulations. Conducted analysis has shown that tower thickness is a significant parameter, hence the ratio between outer diameter and wall thickness.

4.2.2 Mathematical simplification

A modification of the ordinary assembled wind turbine is conducted to simplify the technical analysis and hence reduce computational time. Dynamic analyses are compared for modified turbine and assembled reference turbine to identify the responses and determine the dynamic effects. The dynamic results are then considered and applied to calculate fatigue life. The fundamental perspective of responses and forces is required in order to conduct this simplification. Hence the equation of motion is introduced in Equation 4.2.1. The expression consists of a mass term, damping term, stiffness term, and force term, in order from left to right, respectively.

$$M\ddot{u}(t) + C\dot{u}(t) + Ku(t) = F(t) \tag{4.2.1}$$

Following Figure 4.2.2 illustrates how the environmental and structural elements for the assembled turbine are converted and replaced with mathematical components that represent the simplified turbine. [25]

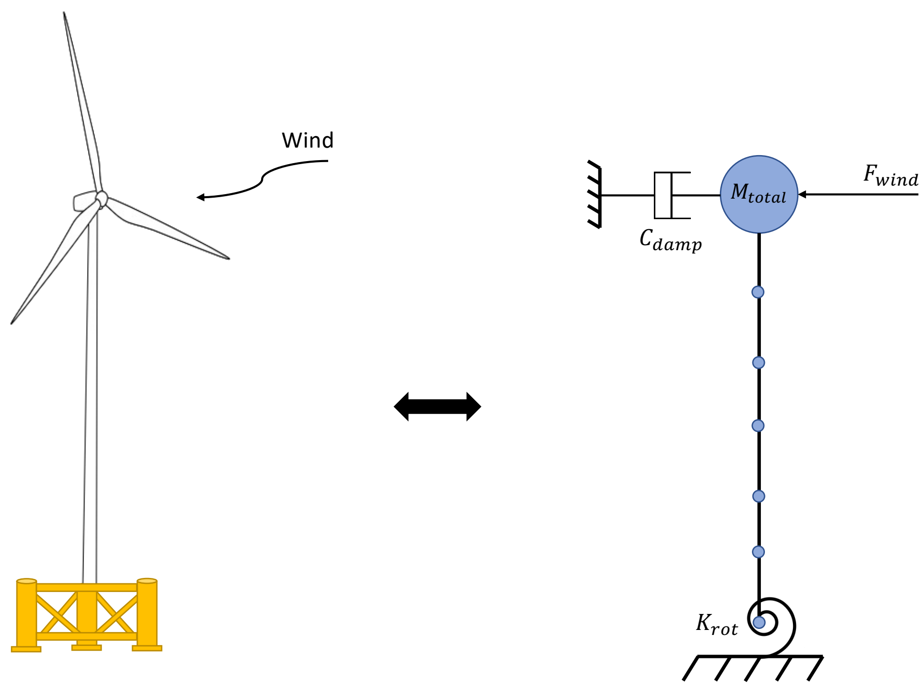

Figure 4.2.2: Model of mathematical simplification of the fully assembled wind turbine and environmental loads

By converting the wind turbine to simplify the technical analysis, the rotor and turbine elements must be replaced with a concentrated node mass to obtain a reasonable result. The variable M represents a lumped total mass and is multiplied with acceleration to achieve force. The total mass is subjected to the tower top at node 1, consisting of the mass of the hub, blades, nacelle, and drivetrain. Equation 4.2.2 expresses the lumped mass.

$$M_{Total} = \sum_{i=1}^{N} m_i = m_{nacelle} + m_{hub} + 3 \cdot m_{blade} + m_{drivetrain} \tag{4.2.2}$$

An equivalent damper is attached at the tower top, at node 1, and serves as the parameter C. This linear damper is implemented to represent the accumulated viscous damping from the rotor and blades of the assembled turbine. The magnitude of damping is multiplied by the velocity for obtaining the force. Several different damping coefficients must be investigated and compared to obtain a reliable result for fatigue calculation.

The rotational spring is defined as K and introduced at the bottom of the tower and represents the transition between the tower and the floating foundation. Different magnitudes of stiffness at node 6 are applied based on previous floating constructions. The structure will experience motions in roll and pitch when environmental forces are simulated. Hence, a rotational stiffness equal $1 \cdot 10^{11}$ Nm/rad is assumed and applied in DOF 4 and 5. The stiffness in DOF 4 and 5 are varying parameters while the remaining DOFs 1, 2, 3, and 6 are considered fixed, corresponding to neglected motions.

The environmental situation is evaluated and converted to quantified forces of wind and waves and designated as $F(t)$. This expression implies that the force is time-dependent throughout the simulation. The force history is based on realistic statistics from The North Sea. [26]

4.3 Blades and turbine

Along with supervisor, Professor Jørgen Amdahl, it was decided that modeling of blades and turbine should not be performed and instead use a model already designed and constructed. Figure 4.3.1 illustrates the establishment of blades and turbine in USFOS-VpOne.

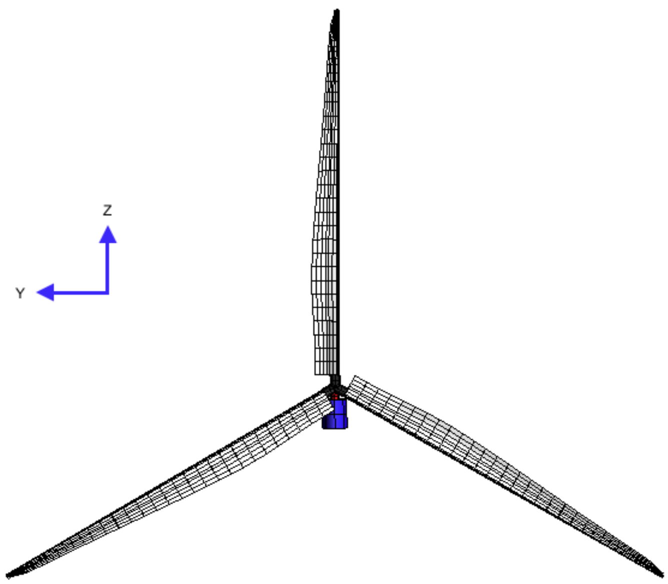

Figure 4.3.1: Model of turbine and blades in USFOS-VpOne

The coordinate system used in USFOS-VpOne defines coordinate origin at the hub, in the centre of blades. Z-axis is identified in the vertical direction, with positive values upwards, starting from the hub. When viewing the turbine in profile, Y-axis is orientated in the horizontal direction, with positive values on the left-hand side of the hub. Apart from the cone and shaft tilt, the rotational orientation acts only in YZ-plane. The positive X-axis is defined out of the plane, in the opposite direction of the incoming wind. An overview of the primary characteristics of blades and turbine are presented in Table 4.3.1 [27].

Table 4.3.1: Design Summary of DTU 10 MW Reference Wind Turbine for blades and turbine

Description	Magnitude	Unit
Rated power	10	MW
Rotor configuration	3	blades
Rotor diameter	178	m
Overhang	7.07	m
Shaft tilt	5	°
Precone	2.5	°
Drivetrain	Medium speed, multiple stage gearbox	

4.4 Turbine control algorithm

The wind turbine's control algorithm consists of several computers that continuously collect environmental conditions and statistics and determine turbine operation and situation. The controller manages hydraulic pumps, valves, motors and blade pitching. The primary characteristics of implemented parameters in the controller are presented in Table 4.4.1. The controller of the turbine, controller.fem, is implemented in the header file, and attached in Appendix B.3.

Table 4.4.1: Design Summary of DTU 10 MW Reference Wind Turbine for controller

Description	Magnitude	Unit
Control	Variable speed, collective pitch	
Cut-in wind speed	4	m/s
Rated wind speed	11.4	m/s
Cut-out wind speed	25	m/s
Cut-in rotor speed	6	RPM
Rated rotor speed	9.6	RPM

4.5 Eigenvalue analysis of wind turbine

An eigenvalue analysis is conducted in USFOS to evaluate if dimensions and design are compatible with the initial determined wind turbine characteristics, including the rotational frequency of the blades. Typical fluctuation frequencies of environmental forces at the North Sea are implemented in simulations to conduct a reasonable estimate. The analysis investigates if some frequencies will excite the tower and blades and perform significant responses of the structure.

Eigenperiods with associated vibration modes for the wind turbine is presented in Table 4.5.1. Each eigenmode excites in both x- and y-direction, which is consistent due to the circular symmetry of the tower. The analysis shows that for an increasing vibration mode, the eigenperiod decreases. The following section enlightens that eigenperiod number 1 is an important parameter when considering the environmental frequency spectrum.

Table 4.5.1: Eigenvalues of wind turbine and corresponding vibration mode

	Eigenmode 1	**Eigenmode 2**	**Eigenmode 3**	**Eigenmode 4**
Eigenperiod [s]	3.347	0.405	0.134	0.069
Vibration mode	1	2	3	4

Significant fatigue damages may occur when the tower is exposed to the combination of many fluctuations and great stress variations. The most significant fatigue damage contributor is when frequencies from environmental forces converge against the tower's natural frequency, which causes resonance.

Figure 4.5.1 illustrates two graphs representing an environmental spectrum of wind and waves. The wind and wave spectrum shows the typical magnitude of energy for the corresponding frequency in the North Sea. The shape of the wind spectrum implies that for minor frequencies, the amount of energy will be large, and for increasing frequencies, the energy decreases negatively exponentially. The purple graph shows the Pierson-Moskowitz wave spectrum, one of the most frequently used spectrums, and is based on data from the North Atlantic.

The illustration also displays the characteristic frequencies of the simplified turbine structure. The natural frequency of the tower and blade rotational frequency are compared to the wind and wave spectrum to investigate if a resonance may occur. The term *1p* describes the frequency of a blade rotating one whole rotation, while *3p* defines the frequency of a blade passing the tower, which occurs three times more often than *1p*. These illustrated frequency magnitudes apply for the operational condition and may vary for start-up and shut-down conditions.

By studying the graph, it can be seen that either the eigenfrequency or *1p* and *3p* do not overlap relevant load frequencies from considered environmental forces. The eigenfrequency of the tower is not close to any blade rotating frequencies, with a safety margin equal to approximately 1 rad/s in difference. A margin that large will not make the components excite each other.

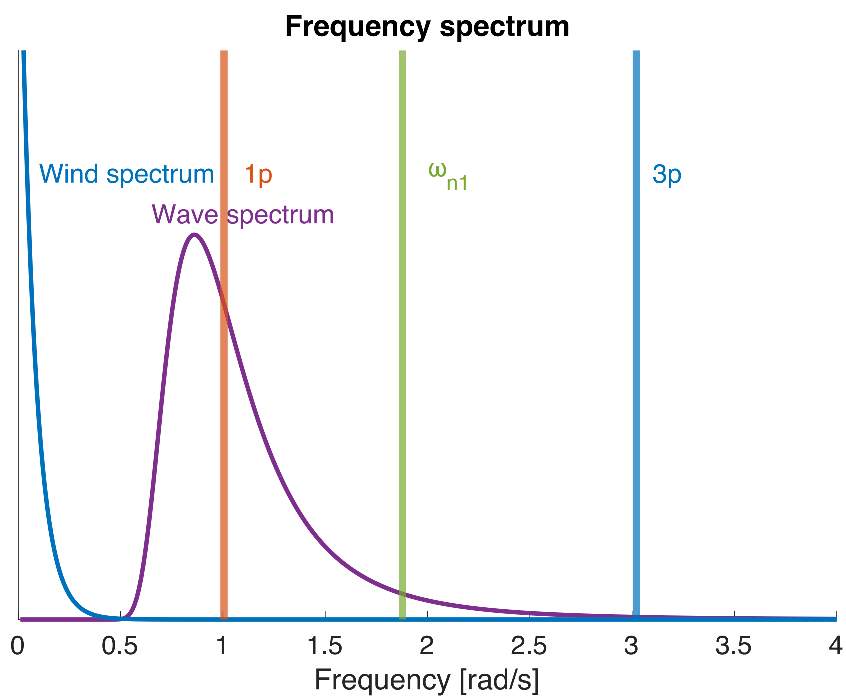

Figure 4.5.1: Frequency spectrum including typical wind and wave spectrum and characteristic load frequencies and eigenfrequency of the wind turbine

The presented eigenfrequency in the figure excludes structural and viscous damping. This frequency does not reflect the realistic picture of the floating structure; still, it indicates the main characteristics and foundation for further calculations.

Chapter 5

The effects of dynamics on structural response

Floating offshore marine structures are complex systems that bring significant risk in every condition; hence, the conduction of global dynamic analysis is fundamental. This section estimates essential characteristics for the dominant wind velocities in the North Sea, with mean wind speeds, equal 10, 12, 13 and 14 m/s. It is crucial to maximize operational lifetime for creating a cost-effective wind industry, but another central and leading parameter is an expansion of power production magnitude. Therefore, the wind turbine's efficiency is analyzed to present an overview of power capacity and the amount of energy production one operating turbine can generate.

The wind turbine's static and dynamic behavior are investigated, and a comparison is performed to review the influence of the environment and surroundings. In this way, the structural characteristics may be modified to reduce fatigue damage that the wind turbine is exposed to.

5.1 Static and dynamic loading

A static and dynamic history comparison is studied to investigate how dynamic behaviors influence fatigue damage and the ultimate limit state. The dynamic simulation load is applied dynamically, while the same force is applied statically for static analysis. The analysis simulates and considers primary environmental forces, which involve wave forces acting on the substructure and wind loads on blades and tower.

For this simulation, it is essential to note that the total computation time of 700 seconds also includes the start-up design situation for the wind turbine. A consequence is that an initial transient will occur at the beginning of the simulation. It is estimated that start-up time lasts for less than 100 seconds; hence, the operational condition is initiated, and the turbine will reach its steady-state condition. Figure 5.1.1-5.1.7 illustrates both forces and moments at tower bottom for respective DOF when a mean wind velocity of 10 m/s is applied and associated turbulence.

The reaction force in x-direction is illustrated in Figure 5.1.1. Observing that dynamic simulation presents relatively larger forces and variations than static calculation. However, the forces follow the same trends and achieve maximum and minimum values simultaneously during simulation. Both simulations obtain the same mean value for operating conditions and provide a magnitude of 1.46 MN.

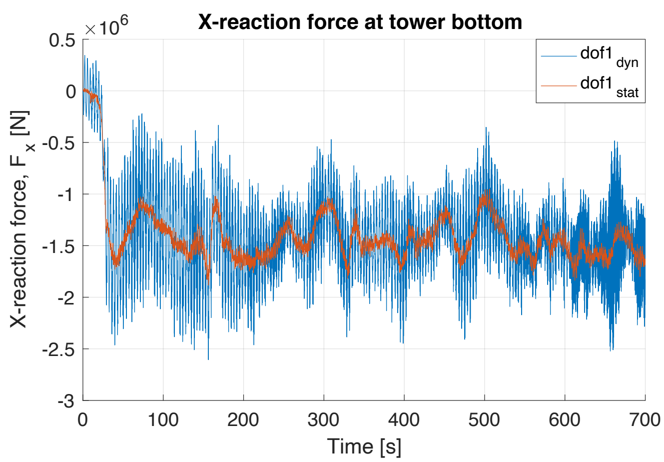

Figure 5.1.1: Force in x-direction at tower bottom with mean wind velocity, $U_{mean} = 10$ m/s

Figure 5.1.2 illustrates the reaction force at the tower bottom in the y-direction. Both static and dynamic analyses show that the force oscillates about zero throughout the simulation. The graphs follow more or less the same pattern, but the dynamic force varies considerably more than the static force. Between simulation times of 500 seconds and 600, the dynamic analysis decreases and obtains approximately the similar values as the static condition.

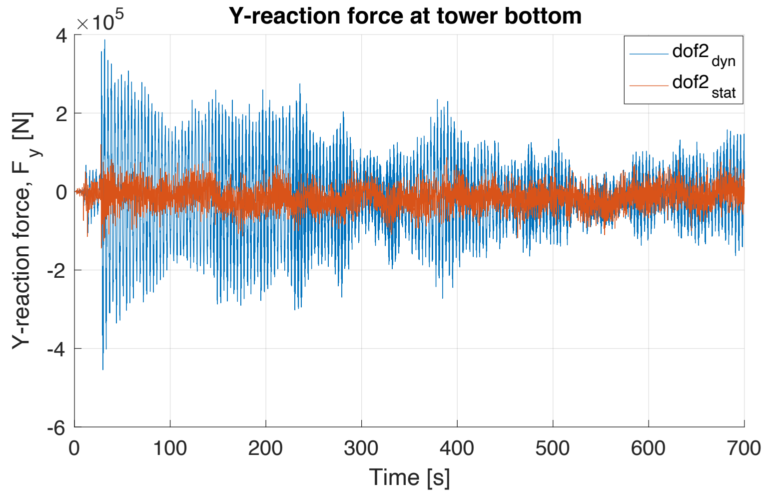

Figure 5.1.2: Force in y-direction at tower bottom with mean wind velocity, $U_{mean} = 10$ m/s

Reaction force in z-direction at tower bottom is presented in Figure 5.1.3. Right after initiating the analysis, the force increases instantly to 15.7 MN and is kept constant throughout the simulation. Small dynamic effects in the z-direction is expected due to mainly horizontal environmental forces and corresponds to the weight of the wind turbine.

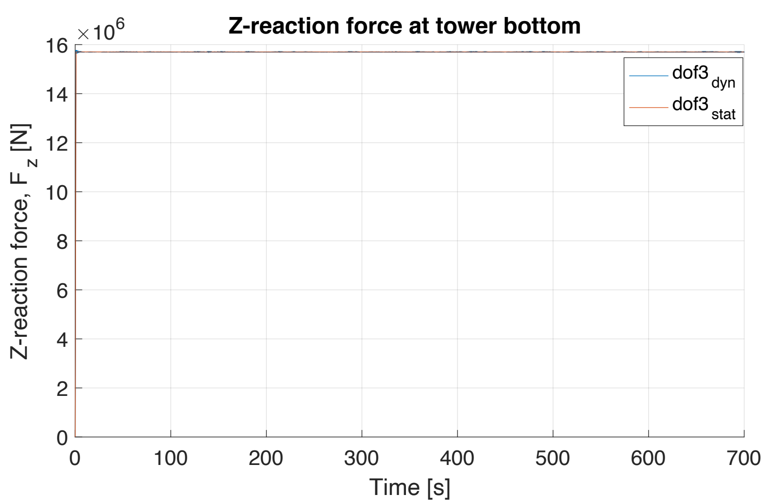

Figure 5.1.3: Force in z-direction at tower bottom with mean wind velocity, $U_{mean} = 10$ m/s

Moment about the x-axis at tower bottom appears in roll motion, displayed in Figure 5.1.4. The dynamic simulation produces a larger moment than the static simulation for the initiating start-up condition. For the dynamic operational conduction, X-moment is constantly decreasing and later following the same pattern as static analysis. The mean value for both simulations is calculated to be -10.3 MNm.

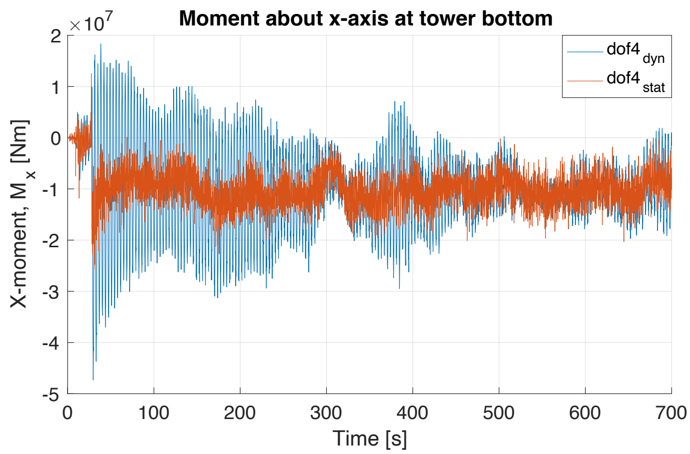

Figure 5.1.4: Moment about x-axis at tower bottom with mean wind velocity, $U_{mean} = 10$ m/s

Figure 5.1.5 presents the moment at tower bottom about y-axis that occurs in pitch motion. Both analyses follow the same tendency and pattern throughout the simulation, although the illustration shows considerable variations between the moments, especially in the initiating condition. The moment in pitch motion has a mean value of $1.4 \cdot 10^8$ Nm. It is a significant contributing parameter for fatigue life, where the number of cycles and variation in stress are highly relevant.

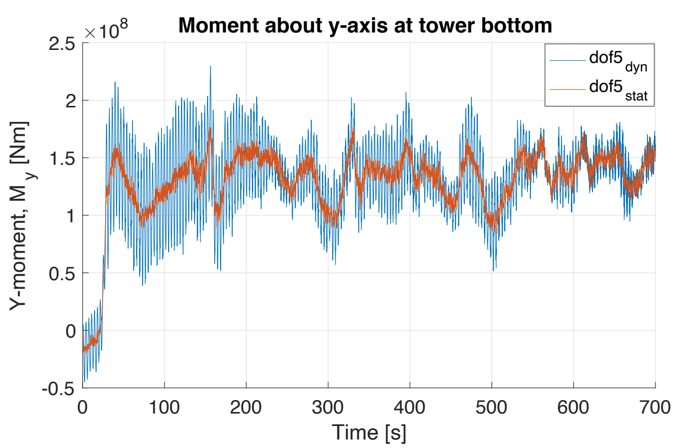

Figure 5.1.5: Moment about y-axis at tower bottom with mean wind velocity, $U_{mean} = 10$ m/s

The appearance of y-moment in pitch motion is significant for fatigue life calculation. A closer investigation of the fore-aft bending moment at the tower bottom is conducted, and a 50 seconds division of simulation time is illustrated in Figure 5.1.6. This moment is composed of thrust force and local turbulence from the environment, and as expected, the two graphs follow each other with similar mean values. The graphs form a sine curve with a roughly estimated period of 30 seconds. Analysis shows that during this time interval, the tower oscillates locally 14 times, representing the tower's flexible bending mode, oscillating with a period of 3.6 seconds. This mode can be characterized as a higher frequency component inside global pitch motion, which must be considered in a wind turbine's modification and design process.

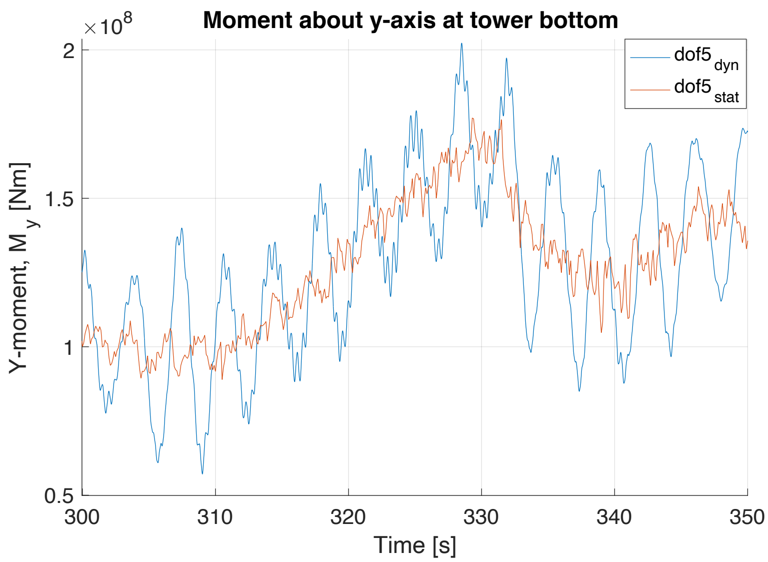

Figure 5.1.6: An inspection of the moment about y-axis at tower bottom with a mean wind velocity, U_{mean} = 10 m/s. Simulation time from 300 to 350 seconds.

The moment about the z-axis at tower bottom is presented in Figure 5.1.7. Both simulations follow the same pattern throughout the computational time and have a mean value of 1.3 MNm. This result implies that the dynamic effects are small and have a minor effect on the moment in yaw motion.

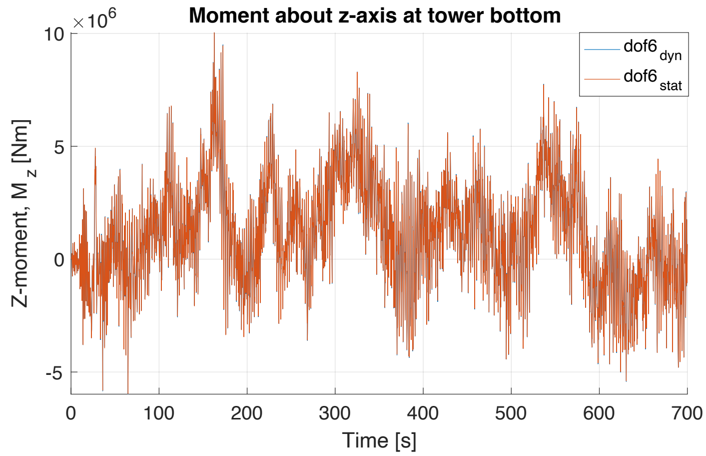

Figure 5.1.7: Moment about z-axis at tower bottom with mean wind velocity, $U_{mean} = 10$ m/s

A comparison of dynamic and static parameters for all DOF is presented in Table 5.1.1 to quantify the dynamic effect. Characteristics and statistics are obtained after the first 100 seconds have passed. The ratio between dynamic and static values is calculated for mean value, maximum, minimum, and standard deviation.

The simulations shows significant variations in forces and moments for different DOF. However, analysis conducted an identical mean value for both dynamic and static conditions. This implies that the mean value ratio is equal to one for all DOF.

The maximum value is the difference between the greatest positive value and the mean value itself. The conduction of the ratio between the maximum dynamic and static value is analogous to calculating the highest Dynamic Amplification Factor (DAF) above the mean value, which is expressed in Equation 5.1.1. Likewise, for the minimum value, the ratio between minimum dynamic and static value also represents the greatest DAF for an extreme point below the mean value. Most ratios between dynamic and static conditions for both maximum and minimum show a value equal to or greater than one. Implying that DAF magnitude is larger than one, the extreme statistics of forces and moments in the dynamic analysis are greater than the static condition.

$$DAF = \left|\frac{u_{dyn}}{u_{stat}}\right| = \frac{1}{\left[(1-\beta)^2 + (2\xi\beta)^2\right]^{1/2}} \tag{5.1.1}$$

A comparison between dynamic and static standard deviation is also conducted. This variation is an essential parameter when calculating the fatigue life of a fatigue exposed structure. Ratios for this parameter have the same tendency as the previous measurements, where the dynamic values are more significant than the static. Hence, the ratio for standard deviation is greater or equal to one.

Table 5.1.1: Ratios between static and dynamic forces and moments based on operational condition

Ratio $\frac{dyn}{stat}$	**Mean**	**Maximum**	**Minimum**	**St.dev.**
DOF 1	1.00	2.22	2.71	2.10
DOF 2	1.00	2.55	2.78	3.33
DOF 3	1.00	18.36	17.75	13.21
DOF 4	1.00	1.68	1.70	2.54
DOF 5	1.00	2.29	1.63	1.65
DOF 6	1.00	1.00	1.00	1.00

Conduction of static and dynamic simulation shows that forces and moments follow the same trends and have similar tendencies throughout the whole simulation time. Although, the analysis presents relatively large differences in force and moment magnitudes for all degrees of freedom, except moment about the z-axis. It is detected that the static analyses might underestimate the forces and moments, hence the structure's level of stress. The ratios for each individual DOF are associated and within an adequate range.

The dynamic analysis produces at least twice the forces magnitude in x- and y-direction than for static conditions. Considering forces in the z-direction, there are large variations for all the investigated parameters, with a significant ratios between 13 and 18. The resulting factor for the moment about the x- and the y-axis is estimated between 1.5 and 2.5. The conclusion is that forces and moments are larger when dynamics are implemented in the analysis, implying that tower response differences will occur.

The further intention is to study fatigue-causing forces for different magnitudes of damping. This study aims to reduce the most extensive and most damaging responses and modify the structure so that the tower fatigue life is approximately identical to the assembled wind turbine model.

5.2 Influence of damping

This section introduces structural damping and analyzes the effect of different equivalent dampers subjected to the simplified and modified tower. The damping factor is considered one of the primary characteristics for positive effect of fatigue life calculation for a structure. A comparison of simplified wind turbine and reference turbine is conducted to achieve a valid simplified model with integrity.

The order of damping magnitude is relative and depends on the type of marine constructions. Hence, it is convenient to introduce critical damping, c_{cr}. This variable is a characteristic quantity for the system and is determined by total mass, m, and undamped eigenfrequency, ω_0, which are presented in Equation 5.2.1.

$$\begin{aligned} c_{cr} &= 2m\omega_0 \\ &= 2 \cdot 1.62 \cdot 10^6 \text{ kg} \cdot 1.88 \text{ rad/s} = 6.09 \cdot 10^6 \text{ kg/s} \end{aligned} \tag{5.2.1}$$

The system damping term for an arbitrary construction is characterized as c and is determined as small or significant for an individual structure by comparing it to its critical damping. This introduces the damping ratio, ξ, which indicates if a damped system is categorized as either a critical, supercritical, or sub-critical damped system, as shown in Equation 5.2.2. For actual floating structures, the most common case is sub-critical damping, and the determination of system damping is further studied in this thesis.

$$\xi = \frac{c}{c_{cr}} = \begin{cases} 1 & \text{Critical damping} \\ > 1 & \text{Supercritical damping} \\ < 1 & \text{Sub-critical damping} \end{cases} \tag{5.2.2}$$

The damped eigenfrequency of a structure strongly depends on the system damping and its relation between mass and stiffness, which is presented in Equation 5.2.3. Considering the system as sub-critical damped, the expression shows that the damped natural frequency becomes smaller and will shift leftwards in Figure 4.5.1.

$$\omega_d = \sqrt{\frac{k}{m}(1-\xi^2)} \tag{5.2.3}$$

The magnitude of damping influences the damped eigenfrequency, and by increasing the damping and following damping ratio, the dynamic load factor will decrease for all load frequencies, especially in the resonance area. The eigenfrequency and different load frequencies should avoid each other to minimize the excitation and following fatigue consequences, which are further studied in chapter 7.

A simulated equivalent damping factor is considered a varying parameter for the simplified solution, and calculations show the variation of different damping influences damping and the resulting fatigue life. The oscillating axial stress at the turbine top is one of the primary contributors to causing fatigue, and hence bending moment at the tower bottom is considered for further study. Analysis of Y-moment is conducted to present the effect of different damping coefficients, and factors within the range of $5 \cdot 10^4$ to $1 \cdot 10^7$ kg/s are considered. In order to determine an appropriate and reasonable damping coefficient, a comparison of a fully assembled turbine and the modified turbine is performed with a mean wind velocity of 10 m/s. Figure 5.2.1 illustrates the analysis, where the bending moment for a fully assembled turbine is displayed as the orange graph, while graphs in shades of grey represent different damping coefficients. The curves follow the same tendency throughout the simulation time, although considerable deviations are observed for some of the damping coefficients.

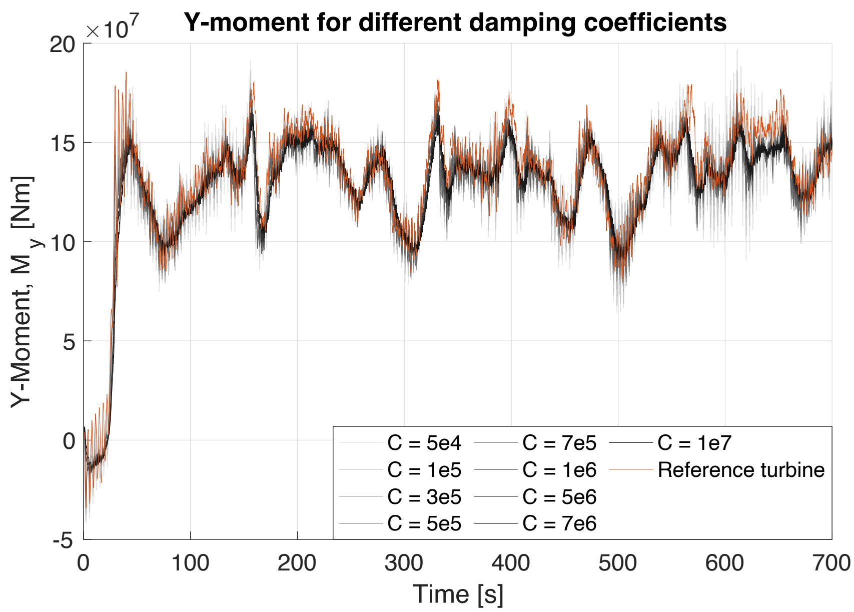

Figure 5.2.1: Analysis of bending moment are conducted for damping coefficients within the range $5 \cdot 10^4$ to 10^7 kg/s

5.3 Sources of errors

Determining an appropriate damping coefficient is challenging and depends on several influencing factors. Different approaches can be applied to evaluate and decide variables and provide the correct solution for an arbitrary condition. Although, a method may achieve incorrect and faulty results in other cases, which introduces sources of calculation errors.

A simulation division from 100 to 180 seconds is extracted, and the Y-moment for different damping coefficients and an assembled turbine are illustrated in Figure 5.3.1. The orange graph displays assembled turbine, and shades of grey represent different damping coefficients. By studying the figure, it is observed that the grey graphs are shifted leftwards, which is fairly notable by investigating the peaks of the curves. This analysis may indicate a lagging of the simplified turbine responses and that the graphs are slightly out of phase.

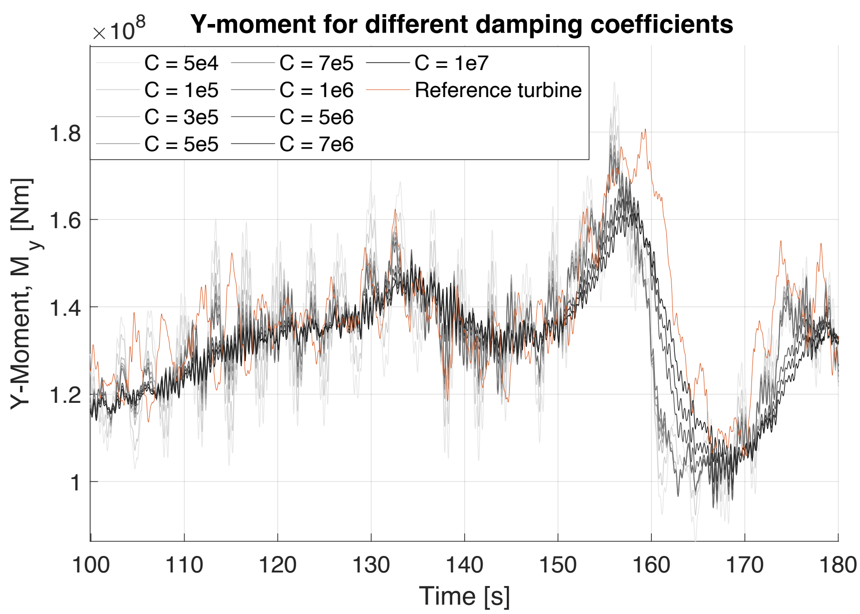

Figure 5.3.1: Analysis of bending moment for damping coefficients within the range 10^5 to 10^7 kg/s, where curves are out of phase

Other sources of errors may occur when determining a convenient damping factor. Figure 5.3.2 extracts the time series from 280 to 350 seconds and displays that the grey curves are approximately in phase with the orange graph. Although, the responses for the simplified model are represented both beneath and above the moment for the reference turbine.

This result indicates an over- and underestimating of values relative to the assembled turbine. This difference is essential to consider since the magnitude of fluctuation is a primary influencing factor for fatigue calculation.

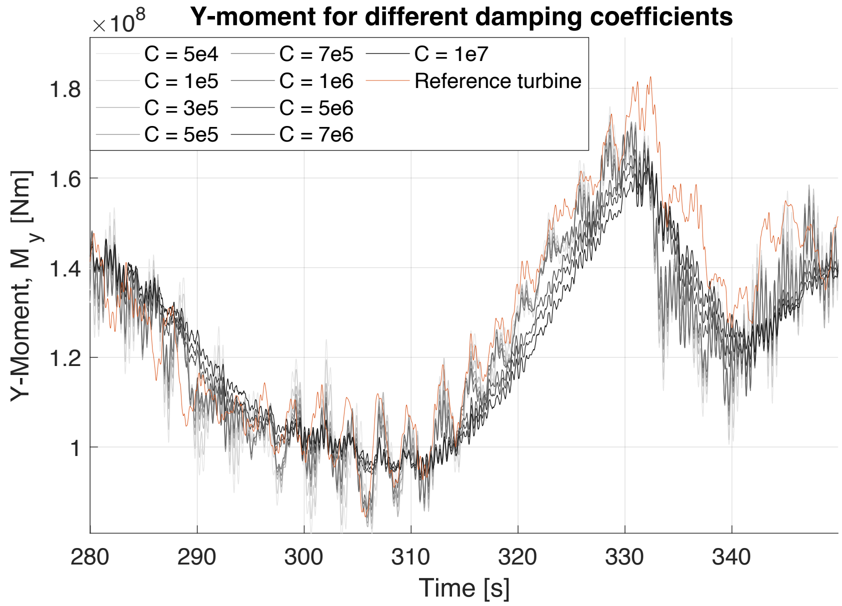

Figure 5.3.2: Analysis of bending moment for damping coefficients within the range 10^5 to 10^7 kg/s, where curves are both over and underestimating

These examples are some sources of errors that may occur when simplifications are considered. The analysis highlights that even though the spectra of damping coefficients are broad, the simplification of applying different damping factors may not present responses in identical phases or obtain exact moment variations.

Chapter 6

Global dynamic analysis in USFOS-VpOne

There are many influencing factors for calculating the fatigue life of a wind turbine; some are significant and have higher affection than others. Control of an assembled wind turbine is simulated, and analysis is conducted for mean wind speed at 10, 12, 13, and 14 m/s with associated turbulence intensities. The considered wind velocities are highly relevant and correspond well with typical conditions in the North Sea.

Loads that cause the greatest fatigue damage are primary contributors, represented by the mean and varying horizontal force component and bending moment. The magnitudes and variance of these parameters are investigated along the whole structure to analyze the most exposed position where fatigue damage is critical. Additionally, the amount of power extracted from incoming wind is defined as power capacity and is also investigated.

The estimated characteristics are based on simulations performed in USFOS-VpOne, considering only one condition at a time. This single implementation is not representative of a whole lifetime of a wind turbine and may be considered as an approximate result. Although, the simplified model indicates reasonable estimates that correspond well with the assembled reference structure.

The assembled reference turbine is modeled in USFOS-VpOne, and the model code is attached in Appendix B.2. Figure 6.0.1 illustrates the assembled structure with a global coordinate system. The origin is located at the turbine center where the two super elements, turbine and tower, are connected. The X-axis is defined from the turbine center with a positive orientation in the downstream direction relative to the rotor plane. The tower, hub, blades, drivetrain and yawbearing are the main components included in the assembled model. USFOS-VpOne employs BEM theory for calculating blade loads. By including these structure elements, the analysis needs extended time for computation due to more data processing and additional complex elements. This duration of computational time builds the foundation and reasoning for why a simplified wind turbine model is established.

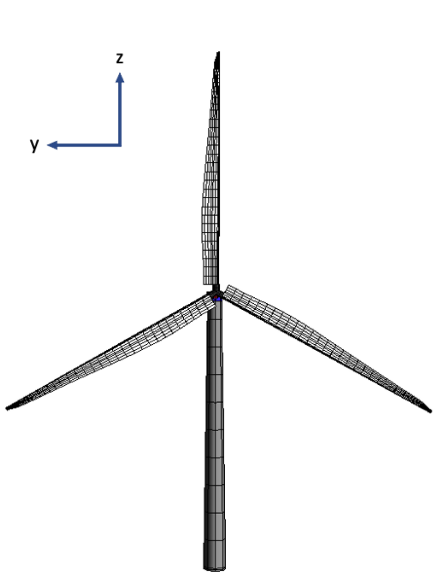

(a) Assembled reference turbine

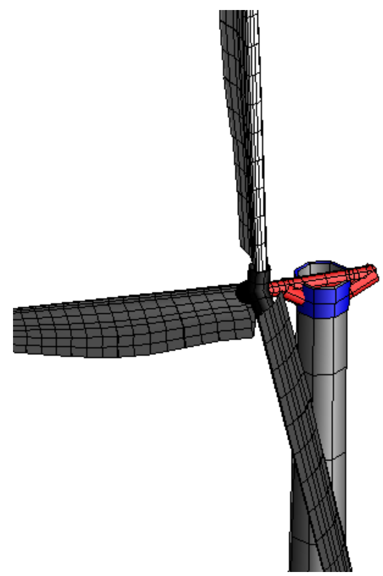

(b) Connection between main components of assembled turbine

Figure 6.0.1: Overview of components for an assembled turbine

The simulations are conducted for 700 seconds, where the first 100 seconds is reserved for initiating time to obtain steady-state condition. Primary characteristics are determined based on the operational time, and hence the start-up phase is omitted.

6.1 Thrust force at tower top

Several directions for incoming wind and associated turbulence generate forces with different orientations. The thrust force is achieved when the wind needs to slow down to extract kinetic energy from the incoming flow on the disk rotor. The resulting axial force is used to evaluate wind turbines' power production and fatigue life.

Thrust forces are analyzed for simulations with mean wind velocity at 10, 12, 13, and 14 m/s, displayed in Figure 6.1.1. The illustration shows that the thrust force graphs oscillate in the same order of magnitude, a region between -1 MN and -2 MN for the operational condition. The tendency of force variation is somewhat similar, especially for the three greatest mean wind velocities. For the same three mean wind velocities, an overshoot of thrust force is detected in the initiating phase, a force that exceeds the corresponding mean value. The graphs imply that greater thrust forces are obtained with lower wind velocity and that the force decreases for increased wind velocity. A reasonable explanation for this result is that the thrust force reaches the maximum value at the rated wind speed of 11.4 m/s. Past this velocity, the thrust force becomes lower due to the pitching of the blades for a constant rotor speed.

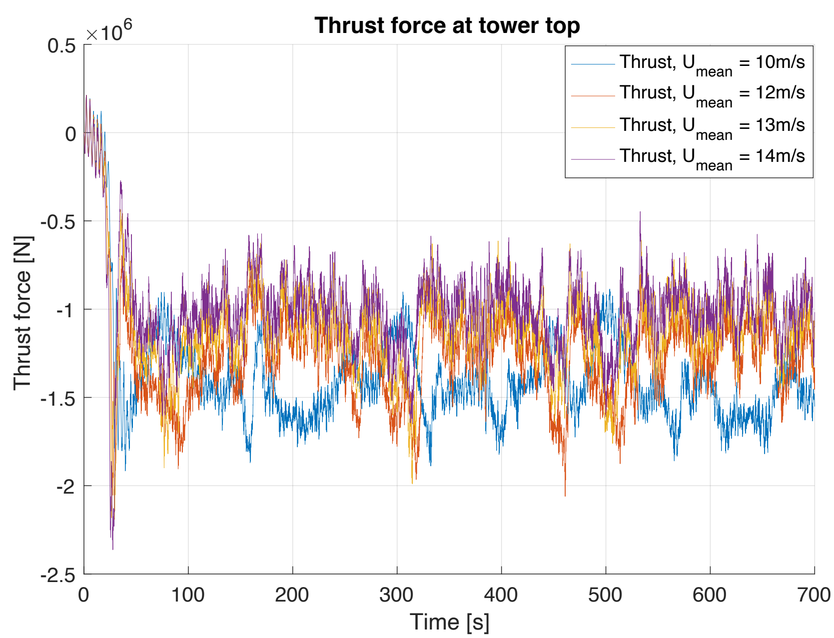

Figure 6.1.1: Thrust force during a simulation with mean wind velocity, U_{mean} = 10, 12, 13 and 14 m/s and associated turbulence

In order to estimate the fatigue life of a wind turbine, the variation in force is also an essential parameter that must be considered. Hence, the standard deviation of thrust force is conducted. Table 6.1.1 lists the mean thrust with standard deviation and calculates the corresponding ratio.

Table 6.1.1: Thrust force for various mean wind velocities

	Mean wind velocity			
Characteristics	**10 m/s**	**12 m/s**	**13 m/s**	**14 m/s**
Mean thrust [MN]	1.44	1.28	1.12	1.01
Standard deviation [MN]	0.18	0.20	0.19	0.17
Ratio	12.23 %	15.89 %	16.84 %	16.37 %

This table shows that the mean thrust force decreases with an increased mean wind velocity. The thrust force for a mean wind velocity of 10 m/s is reduced by 30 % when the wind velocity is increased to 14 m/s. The standard deviation for different wind velocities is within the same range, between 0.17 MN and 0.20 MN. By comparing standard deviation with the corresponding mean value thrust force, the tendency shows that the ratio is increasing for increased wind velocity. The variation in thrust force is a significant factor when calculating fatigue life.

6.2 Bending moment at various tower heights

A significant contributor to fatigue damage at the tower is the magnitude and variation of bending moment, which depends on several factors. Loads applied on the tower may cause bending moments, which are further investigated for different tower heights. Seven evaluated location points are equally distributed along with the tower, and the segments are assigned such that the tower top is segment 1. By following the tower top and downwards, the segment number is increasing until the tower bottom, which is defined as segment 7. A more detailed description and design are shown in Figure 4.2.1.

Figure 6.2.1 illustrates how bending moment varies during a simulation of 700 seconds. Computation of analysis for a mean wind velocity of 10, 12, 13 and 14 m/s with corresponding turbulence is conducted, and the figures show bending moments at different tower segments. The whole tower, from tower bottom to turbine location, is considered in this research. Observe that the curves for different heights follow the same pattern, with simultaneous progress throughout simulation time. As expected, analysis shows that magnitude of bending moment is decreasing for increasing tower segment. This result implies that the most extensive bending moment is located at the tower bottom and foundation transition, which applies to all considered wind velocities.

Furthermore, this may indicate that one of the most critical points is located at the tower base, close to the floater foundation. Figure 6.2.1a illustrates the bending moment for a mean wind speed of 10 m/s, and during the operational time, the mean value is measured to $14 \cdot 10^7$ Nm. This result is the most significant bending moment of considered segments and wind velocities.

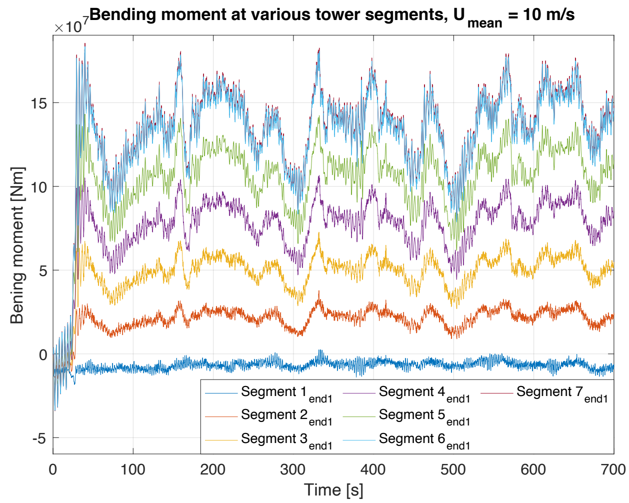

(a) Mean wind speed of 10 m/s

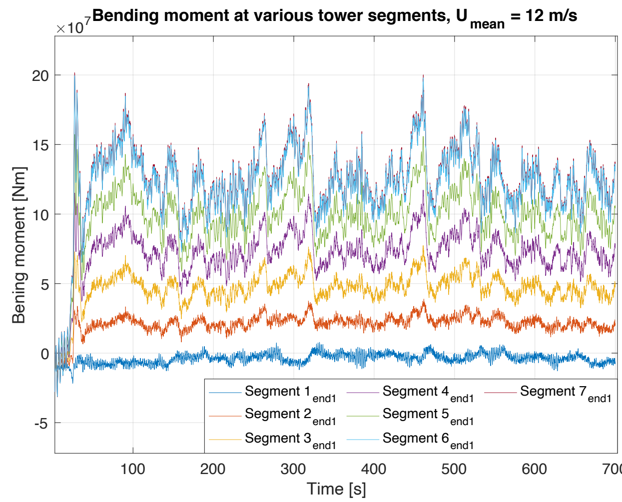

(b) Mean wind speed of 12 m/s

Following Figure 6.2.1c and Figure 6.2.1d illustrates the bending moment for a mean wind velocity of 13 and 14 m/s, respectively. By comparing the identical segment for several wind velocities, a decrease in the mean bending moment for an increased wind velocity is observed. Additionally, the difference in bending moment between the segments is decreasing. The smallest mean bending moment at segment 7 during operational time is registered for a wind velocity of 14 m/s and is measured to $10 \cdot 10^7$ Nm. As the thrust force, it is detected, an overshoot of bending moment in the initiating phase that exceeds the corresponding mean value.

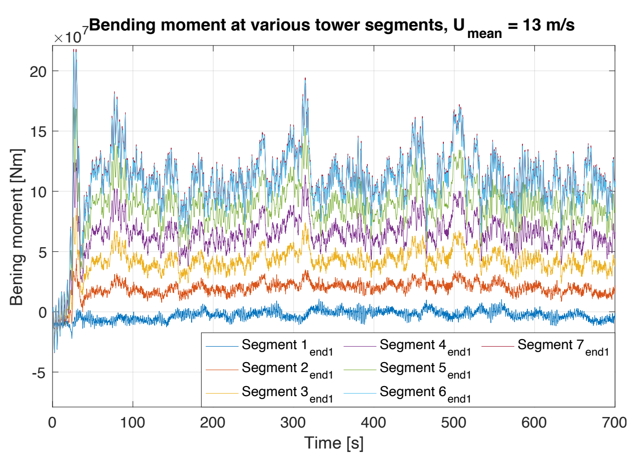

(c) Mean wind speed, $U_{mean} = 13$ m/s

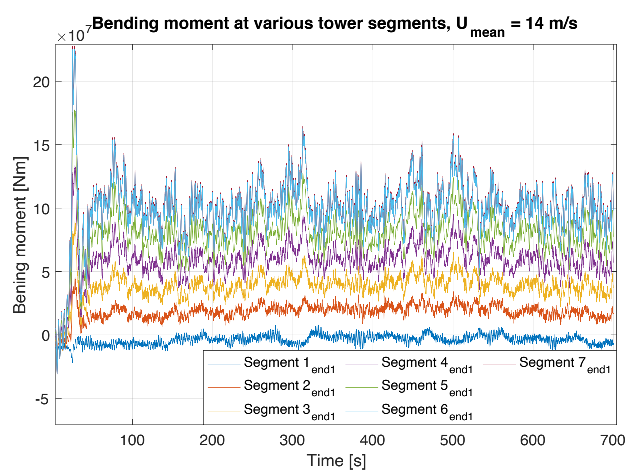

(d) Mean wind speed, $U_{mean} = 14$ m/s

Figure 6.2.1: Bending moment at various tower heights for several mean wind velocities

Curves for the mean wind speed of 10, 12, 13, and 14 m/s seem to operate in the exact order of magnitude. Hence, comparing the conditions is beneficial in defining the effect of increased wind velocity. Figure 6.2.2 displays the mean value and corresponding standard deviation for bending moments at considered segments. Since each distance between the segments is 20 meters, the result implies that the mean value increases linearly for all conditions, where the incline and magnitude for lower wind speed are generally more significant than for higher wind velocities.

Although the development of standard deviation is not that consistent, the most significant standard deviation at the tower bottom occurs for the wind velocity of 12 m/s and decreases for higher wind velocities. Inspecting the ratio between standard deviation and the corresponding mean value is valuable and relevant. The standard deviation at the tower bottom for a wind velocity of 10 m/s is measured at 13 % of the mean bending moment. The ratio for 12, 13, and 14 m/s are at 15 - 16 %.

For all wind speeds, the bending moment and standard deviation between segments 1 and 2 have similar results. The standard deviation measures approximately 19 % of the mean value for 10 and 12 m/s and 21 % for wind speed 13 and 14 m/s.

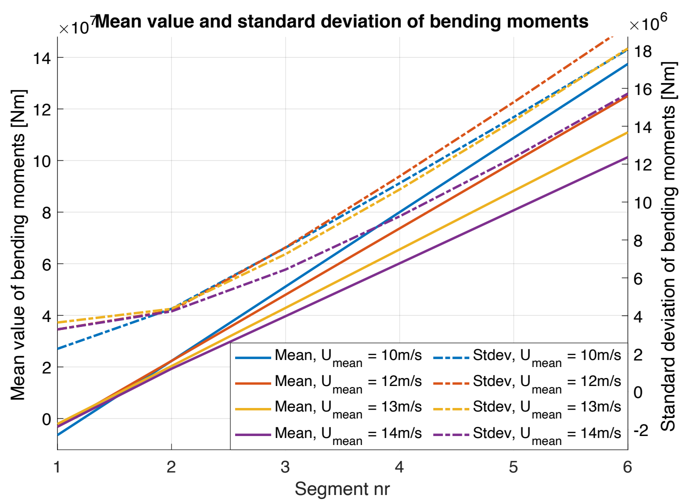

Figure 6.2.2: Mean value and standard deviation of bending moments for mean wind speed, U_{mean} = 10, 12, 13 and 14 m/s and associated turbulence

This analysis quantifies the most significant variations in bending moment at the tower bottom for all considered wind conditions. A further evaluation of this element, segment 7, is conducted.

6.3 Electrical power capacity

For wind velocities below the cut-in speed at 4 m/s, the rotor rotates but cannot extract any power. No power is generated for wind speed beyond cut-out wind speed at 25 m/s, where the blades are fully pitched, and no energy is produced. Power production depends on the environmental condition, where operating time, wind stability, and incoming wind velocity are crucial. Emergency shut-down, fault, maintenance, and repair situations limit operational time and total power production.

Power capacity indicates the magnitude of power generated by one wind turbine compared to total available power from incoming wind, expressed in Equation 6.3.1. Total available power, P_0, is proportional to the incoming wind velocity, V^3, which makes it highly sensitive to incoming wind velocity, and the area of the rotor disk is defined as the parameter, A. The capacity factor (CF) is generally more excellent offshore than onshore due to more stable wind forces and the environment. The typical capacity factor is 24 % and 38 % respectively for onshore, and offshore wind turbines [28].

$$CF = \frac{P_{eff}}{P_0}$$
$$P_0 = \frac{1}{2}\rho V^3 A \tag{6.3.1}$$

The effective electrical power generation for mean wind velocity 10, 12, 13, and 14 m/s is illustrated in Figure 6.3.1. Additionally, the mean power value for the operational condition is displayed. During the whole simulation, the production of electrical power for wind velocity 12, 13, and 14 m/s oscillates about 10 MW, which is the measured mean value of the operational condition. The variations are slight, which implies a more stabilized power generation. This result indicates greater extraction and a more stabilized amount of electrical power for higher mean wind speeds. The electrical power for the wind speed of 10 m/s varies and fluctuates about the mean power value, 7.65 MW.

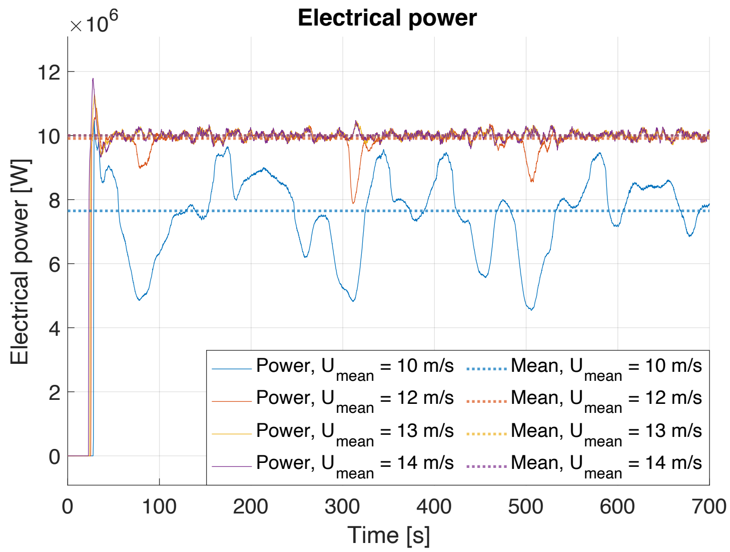

Figure 6.3.1: Power generation during one simulation for mean wind velocity, U_{mean} = 10, 12, 13 and 14 m/s

Various mean wind velocities affect the total available power, and subsequently, the capacity factor is calculated to determine if the resulting power generation is satisfying or not. Table 6.3.1 lists the mean power, total power, and corresponding capacity factor for the different wind velocities. Incoming wind velocity is the only parameter for total available power, resulting in increased total power for an increased wind velocity. Even with an increased mean power with increased velocity, it is calculated that the capacity factor decreases with increased wind speed. This result implies that the wind turbine extracts more of the available power for the lower wind velocity.

Table 6.3.1: Main characteristics of electrical power

	Mean wind velocity			
Characteristics	**10 m/s**	**12 m/s**	**13 m/s**	**14 m/s**
Mean power [MW]	7.65	9.91	10.00	10.00
Total power [MW]	15.30	26.44	33.61	41.98
Capacity factor	49.99 %	37.48 %	29.75 %	23.82 %

The wind turbine extracts an incredible amount of energy from the wind and will not exceed 10 MW. This result is the maximum power extracted, and the limit is reached for wind velocity at 13 m/s, implying that the capacity factor decreases with increasing wind velocity.

Chapter 7

Fatigue life assessment

In order to determine the reliability and quality of the simplified wind turbine, an analysis of fatigue life is performed. The structure design and environmental conditions lay the foundation for evaluating and electing a reasonable weld class. Rainflow-counting algorithm is introduced in this section to define how the cycles in force variations are counted for a corresponding stress range, which is later implemented into a SN-curve. Subsequently, the Palmgren-Miner linear damage hypothesis is presented. This approach is a cumulative method used to calculate a structure's fatigue life.

The majority of offshore structures today are projected to have a service life of about 20 to 30 years. Operational life for this wind turbine is estimated with a theoretical design age of 20 years; hence, fatigue damage for different equivalent dampers may be calculated. The resulting fatigue damage is presented to identify how the damping magnitude influences the fatigue life. A comparison of the fatigue life of the simplified wind turbine and the assembled structure is conducted and discussed.

As the simulation time is conducted for only 700 seconds, specific primary parameters may dominate the resulting fatigue damage life, and sensibility analysis of the damage contribution is conducted. This result is investigated to indicate the accuracy and validity of the simplified model.

7.1 Decision making of weld class

Initially, an appropriate and reasonable type of weld needs to be classified, and three main features are considered for the selection: Joint geometry, weld type (single/double-sided, grinding/as-welded, inspection, etc.), and load direction. The floating wind turbine is in a corrosive environment that may injure the material and structure strength. To reduce the corrosion rate to an acceptable level, selecting a curve within the class in seawater with cathodic protection is recommended. Figure 7.1.1 illustrates a SN-curve that shows DNV fatigue curves with relevant requirements and conditions and is found from regression analysis of test data.

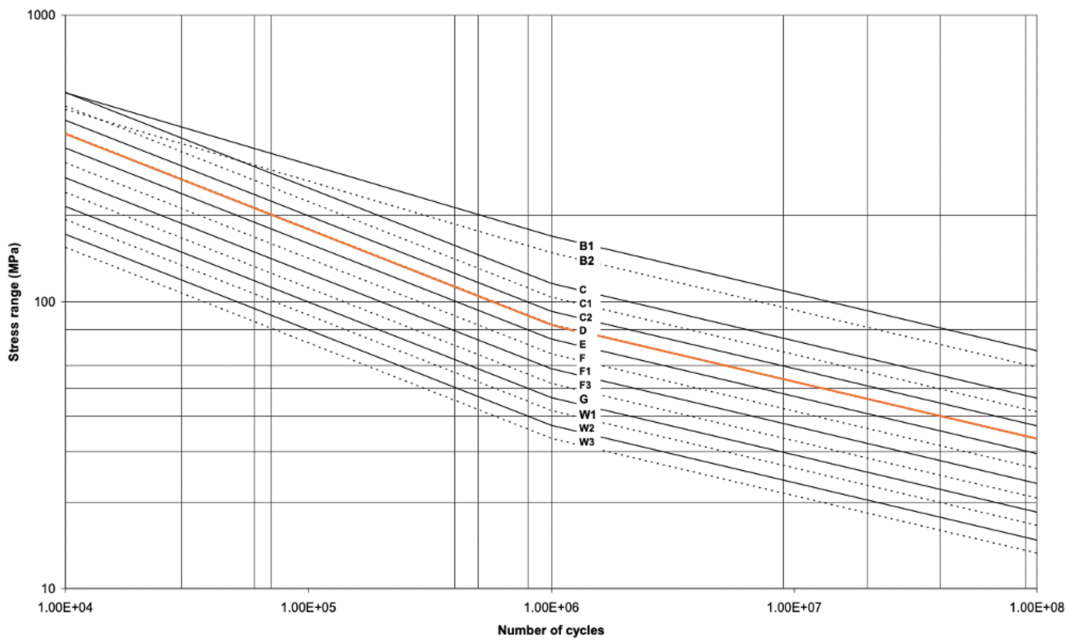

Figure 7.1.1: S-N curves for seawater environment with cathodic protection. The selected weld class, D, is highlighted [29]

Each tower section is seamed lengthwise to encircle every structure component and width-wise for connecting the next section. Typically these sections are butt welded both inside and outside, which is typical for classes C and D. Weld class C is the highest class for this type of weld and includes non-destructive testing (NDT), and particular welding practice increases the production costs. Based on these evaluations, weld class D is preferred as the initial selection and is highlighted in Figure 7.1.1. [30] [31]

An excerpt of parameters for relevant SN-curves is presented in Table 7.1.1, where weld class C, D, and E are considered. The determination of some variables depends on the predicted number of cycles to failure. These variables are introduced in section 2.2, and implemented in Equation 2.2.2 to calculate total stress.

Table 7.1.1: S-N curve in seawater with cathodic protection [29]

SN-curve	$N \leq 10^6$ m_1	$\log\bar{a}_1$	$N \geq 10^6$ $\log\bar{a}_2$ $m_2 = 5.0$	Fatigue limit at 10^7 cycles [MPa]	Thickness exponent k	Stress concentration in the S-N detail as derived by the hot spot method
C	3.0	12.192	16.320	73.10	0.05	
C1	3.0	12.049	16.081	65.50	0.10	
C2	3.0	11.901	15.835	58.48	0.15	
D	3.0	11.764	15.606	52.63	0.20	1.00
E	3.0	11.610	15.350	46.78	0.20	1.13

The total number of cycles before failure depends on the estimated number of cycles the structure is exposed for within service life and is expressed in Equation 7.1.1. During the operational condition, the controller system predicts 9.6 rotor rotations during one minute, introducing revolution per minute, rpm. Due to three blades passing within one revolution, this value is multiplied by three to calculate the total number of cycles. The number of cycles during service life is estimated to be $3 \cdot 10^8$. Hence $\log\bar{a}_2$ and m_2 are implemented in the computation. [32]

$$\begin{gathered} N_{total} = Y_{\text{service}} \cdot N_{\text{cycles, 1 year}} \\ N_{\text{cycles, 1 year}} = 3 \cdot rpm \cdot 60 \text{ min} \cdot 24 \text{ hours} \cdot 365 \text{ days} \end{gathered} \tag{7.1.1}$$

7.2 Rainflow-counting algorithm

A SN-curve defines a number of cycles to failure, N($\Delta\sigma$), for a material exposed for repeating cycles of a given stress range, $\Delta\sigma$. The curves depend on the shape of the applied load spectrum and hence wind turbine responses. Simulations in section 5.2 present how different damping coefficients influence responses, forces, and moments for the wind turbine. The affection and consequences of different damping coefficients are analyzed by calculating the resulting fatigue life.

The method used to count stress cycles from simulations is the Rainflow-counting algorithm, which is often applied when calculating the fatigue life of a structural member. The approach converts the loading sequence of varying stress into equivalent sets of constant amplitude stress reversals. The smaller cycles are also considered, representing the material memory effect seen with stress-strain hysteresis cycles.

The left side of Figure 7.2.1 illustrates the evolution and progress of strain and its turning points over a time series. The right side displays the corresponding hysteresis plot of stress-strain relation. By studying both graphs and applying Rainflow-counting, three full cycles and three half cycles are identified, respectively 2-3-2', 8-9-8', 5-6-5' and 1-2-4, 4-5-7, 7-8-10. [30]

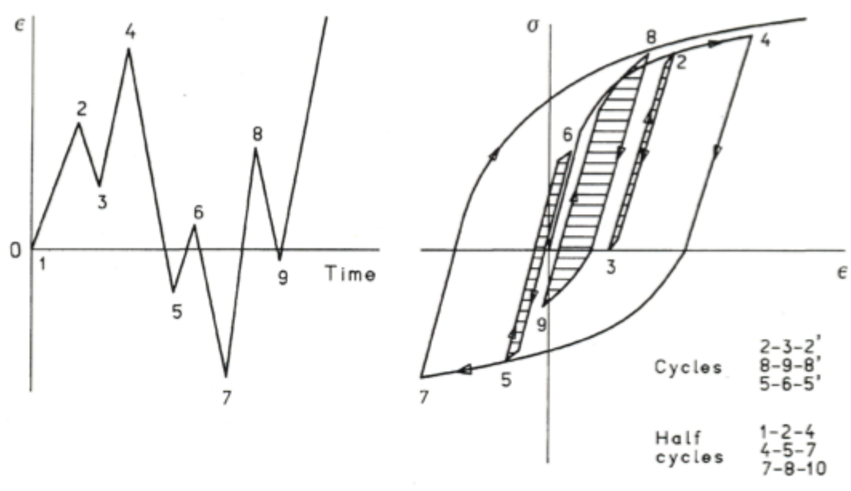

Figure 7.2.1: Rainflow counting that identifies closed cycles in a stress-strain curve [30]

7.3 Empiric SN-curve

Based on the performed simulations and employing the Rainflow-counting algorithm, an empiric SN-curve is conducted in MATLAB and is attached in Appendix C.1. Figure 7.3.1 illustrates stress range distribution for different damping coefficients and various mean wind velocities. Total moment variations and axial force variations at the tower bottom determine the presented stress ranges, where the bending moment dominates the total stress variations. These stress ranges are divided into 40 discrete and equal stress range blocks. The considered equivalent damping coefficients are within the range of $5 \cdot 10^4$ to $5 \cdot 10^6$ kg/s and conducted for mean wind velocities of 10, 12, 13, and 14 m/s. The vertical axis represents the magnitude of the stress range applied with the corresponding number of cycles horizontally on a logarithmic scale.

In order to compare the simulations, an identical load spectrum is applied for all computations with different implemented damping. Hence, an overview of stress distribution for a mean wind speed is provided. A central observation for Figure 7.3.1a-7.3.1d is observed that statistics follow a similar tendency and pattern, where the number of cycles decreases for an increasing stress range. Circular data points with darker colors indicate a more significant equivalent damper coefficient, and the yellow marking point determines statistics for the assembled turbine. The distribution of data points for different damping coefficients are seemingly clustered about similar values and spread within an acceptable range.

For each condition, it is recognized that data points for greater damping stay at a lower stress range level than less damping, implying that greater damping provides a reduced stress range. During 700 seconds of simulation time, 1300 to 1800 cycles are registered, depending on which condition is considered. Nevertheless, the number of cycles to corresponding stress ranges is a significant parameter to determine and calculate the exact fatigue life of a structure. A mean wind velocity of 10 m/s may generate a higher amount of cycles of smaller stress ranges than for wind velocity 12, 13, and 14 m/s.

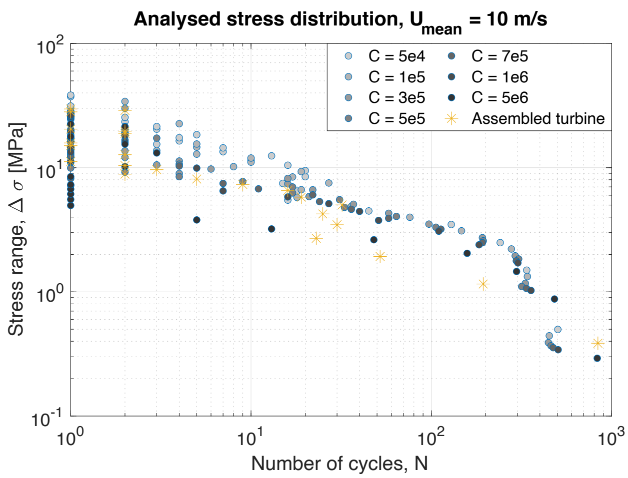

(a) Mean wind speed at $U_{mean} = 10m/s$

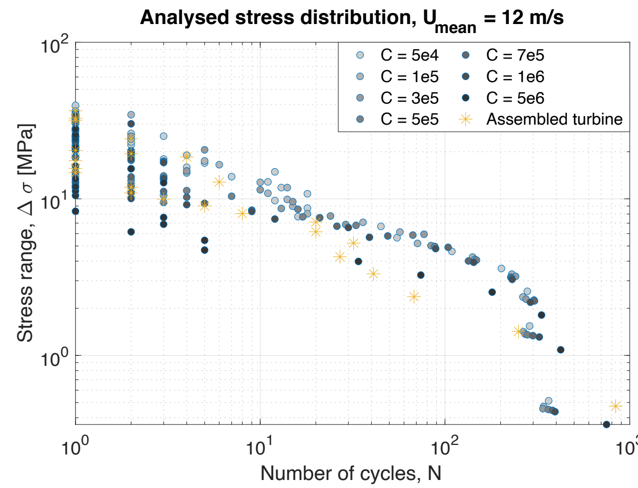

(b) Mean wind speed at $U_{mean} = 12m/s$

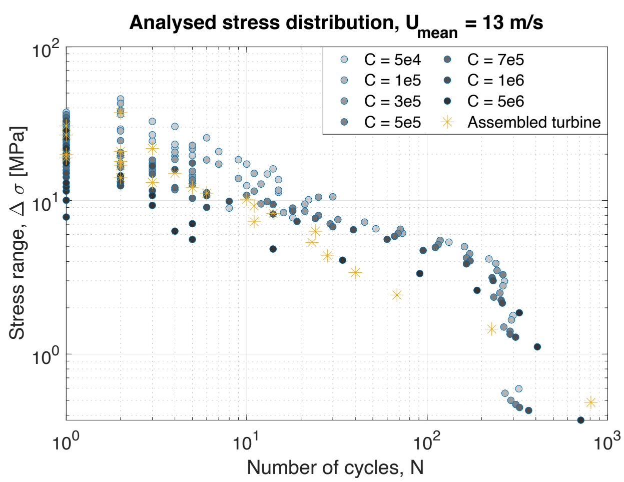

(c) Mean wind speed at $U_{mean} = 13m/s$

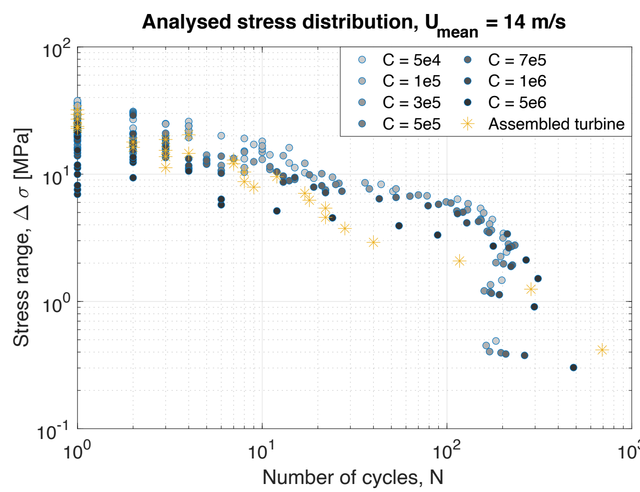

(d) Mean wind speed at $U_{mean} = 14m/s$

Figure 7.3.1: SN-curve for different damping coefficients and various mean wind velocities. Blue circular data points represent a simplified turbine with different equivalent damping coefficients. Yellow marking describes statistics for the assembled turbine.

To determine the simplification's quality, it is necessary to compare the statistics for the assembled turbine with an equivalent damper turbine. For greater stress ranges, data points for assembled and equivalent turbines have high correspondence with seemingly sufficient satisfaction. Measurements of the number of cycles for stress ranges below 10 MPa are more unpredictable and spread wider. For a greater number of cycles, the stress ranges for the assembled turbine are estimated to be smaller than for an equivalent damper. The different stress range distribution for wind conditions will affect the total fatigue damage.

Each analysis has a simulation time of 700 seconds and produces about 1500 cycles within this period. The time duration of the computation is defined as short-term simulation, where estimated values are obtained from considering only one single wind condition and sea state. Combining long-term and short-term simulations are preferred for obtaining ordinary operating conditions and detailed performance data for an absolute and total calculation of fatigue life. Hence, a short-time simulation will not be entirely representative of a lifetime for a floating wind turbine. However, an up-scaling of the simulation time will provide an indication of the expected statistics and characteristics of the wind turbine responses. After applying the Rainflow-counting algorithm and processing simulation data, the subsequent step of the procedure is to introduce Palmgren-Miner linear damage hypothesis to conduct fatigue life calculations.

7.4 Fatigue life estimation

Palmgren-Miner rule is a linear cumulative damage method supported by the SN-fatigue approach and is employed for estimating enduring damage and absolute fatigue life. The stress range distribution through the empiric SN-curve is established with a corresponding number of cycles. The method is accumulating fatigue damage ratios for k distinct stress blocks, $\Delta\sigma_i$. Each stress range block is assigned a corresponding number of stress repetitions n_i. Note that the number of distinct blocks k should be large enough to ensure reasonable numerical accuracy. Variables for weld curve D, shown in Table 7.1.1, are also considered in the fatigue computation. A fatigue failure is expected when the accumulated cumulative damage, D, reaches unity. Hence, it is necessary to introduce the usage factor, η, which is strongly dependent on the Design Fatigue Factor (DFF). A fatigue criterion requires that resulting fatigue damage is smaller or equal to the usage factor, which is mathematically expressed in Equation 7.4.1. [29] [33]

$$D = \sum_{i=1}^{k} \frac{n_i}{N_i} = \frac{1}{\bar{a}} \sum_{i=1}^{k} n_i \cdot (\Delta\sigma_i)^m \leq \eta \tag{7.4.1}$$

The conducted analysis are short-time simulations for 700 seconds with one single environmental condition at a time. Therefore, the calculation is up-scaled such that the wind turbine is designed for an average operating life of 20 years. Employing this up-scaling simplification and Palmgren-Miner rule, the fatigue damage is conducted for different damping coefficients, which is presented in Table 7.4.1.

For all considered wind velocity conditions, the calculations show that the resulting damage is definitively decreasing for an increasing equivalent damping factor. The response for the structure with higher damping is considerably smaller, implying smaller stress ranges than for models with less damping. An increase in damping coefficient from $5 \cdot 10^4$ to $1 \cdot 10^5$ kg/s reduces the fatigue damage by 40 - 50 % for all considered wind conditions. The magnitude between the smallest and largest equivalent damping is multiplied by a factor of 100, while the corresponding difference in fatigue damage varies from 3 - 13 %. This result may imply that fatigue damage does not decrease linearly with increased damping. In general, the fatigue damage increases when the mean wind velocity increases from 10 to 13 m/s. Fatigue damage, on the other hand, decreases when wind velocity increases from 13 to 14 m/s. This result may be related to the standard deviation of bending moment for 14 m/s, which had a minor magnitude of the considered wind conditions.

Table 7.4.1: Fatigue damage for equivalent damper and assembled turbine in various mean wind velocities, $U_{mean} = 10, 12, 13, 14$ m/s

	Equivalent damper, C [kg/s]							
Wind velocity	$\mathbf{5}\cdot10^4$	$\mathbf{1}\cdot10^5$	$\mathbf{3}\cdot10^5$	$\mathbf{5}\cdot10^5$	$\mathbf{7}\cdot10^5$	$\mathbf{1}\cdot10^6$	$\mathbf{5}\cdot10^6$	Assembled
10 m/s	0.0877	0.0445	0.0229	0.0172	0.0147	0.0120	0.0051	0.0259
12 m/s	0.1181	0.0713	0.0497	0.0435	0.0389	0.0336	0.0153	0.0461
13 m/s	0.3140	0.1566	0.0753	0.0519	0.0388	0.0313	0.0104	0.0601
14 m/s	0.1405	0.0880	0.0443	0.0358	0.0282	0.0221	0.0050	0.0329

The up-scaling simplification is also conducted for the assembled turbine with a mean wind velocity of 10, 12, 13, and 14 m/s. Based on the values from the table above, the following result are obtained; For the smallest wind velocity, the fatigue damage for assembled turbine compliance is greatest by applying an equivalent damper between $1 \cdot 10^5$ to $3 \cdot 10^5$ kg/s. Given the wind conditions of 12 and 13 m/s, an damping coefficient between $3 \cdot 10^5$ to $5 \cdot 10^5$ kg/s is preferred for the simplified wind turbine. An equivalent damper in the range of $5 \cdot 10^5$ to $7 \cdot 10^5$ kg/s is an appropriate value for the simplified turbine exposed for mean wind speed of 14 m/s.

The fatigue damage calculation shows that the assembled turbine corresponds well with the simplified turbine that applies an equivalent damper between $3 \cdot 10^5$ to $4 \cdot 10^5$ kg/s. Although, the determination of one specific equivalent damper magnitude is challenging which depends on wind condition the turbine is exposed for. An evaluation of the analysis indicated that increasing the damping coefficient for an increased mean wind velocity may be necessary to achieve sufficient fatigue damage.

The Palmgren-Miner linear damage hypothesis is an accumulated method, and inaccuracy and misunderstood interpretation of damage distribution may occur. Different damage distributions can obtain similar total fatigue damage by either being exposed to small stress ranges with many cycles or having few cycles for an extensive stress range. A factor that strengthens the validation of a simplified turbine is if the specific damage contribution is derived from a similar stress range with the corresponding number of cycles as the assembled turbine.

7.4.1 Damage contribution

Fatigue contributors affect the structure differently and may be classified as either primary or minor impacts. An analysis of damage contribution is considered to assure that the simplified equivalent damping turbine can conduct results with quality and accuracy. A closer investigation of the distribution of damage contribution is analyzed for a mean wind speed of 10, 12, 13, and 14 m/s with associated wind turbulence. Previous results have indicated that damping coefficients between $3 \cdot 10^5$ and $5 \cdot 10^5$ kg/s are especially relevant for these wind conditions. Figure 7.4.1 displays the damage contribution applied by the cycles within each discrete stress range for relevant dampers. Furthermore, the sensibility of the simulations is analyzed and discussed.

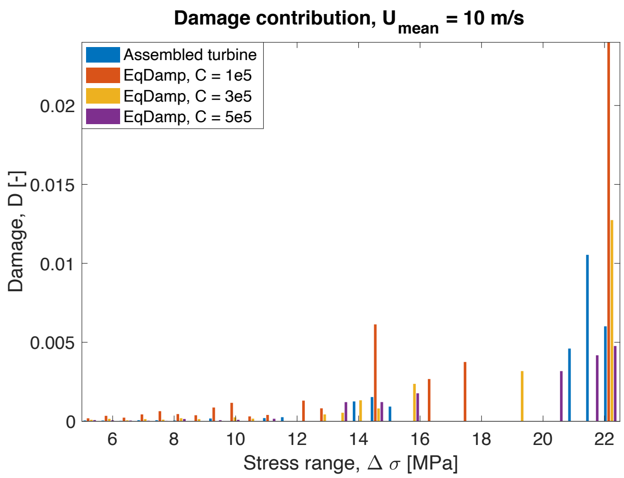

(a) Mean wind speed at $U_{mean} = 10$ m/s

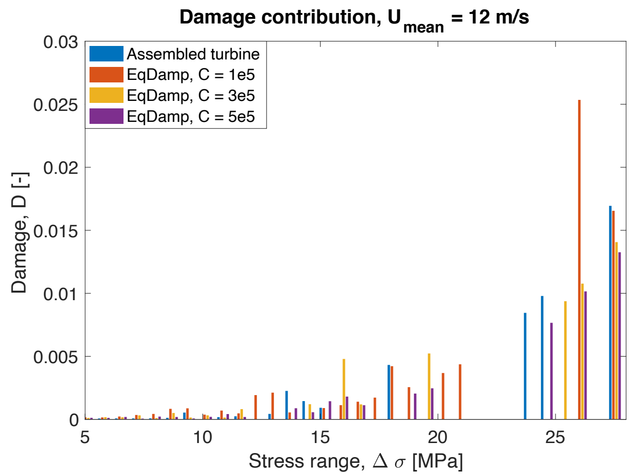

(b) Mean wind speed at $U_{mean} = 12$ m/s

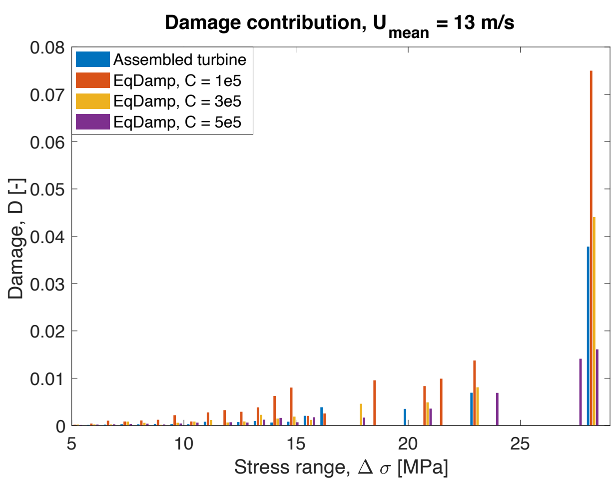

(c) Mean wind speed at $U_{mean} = 13$ m/s

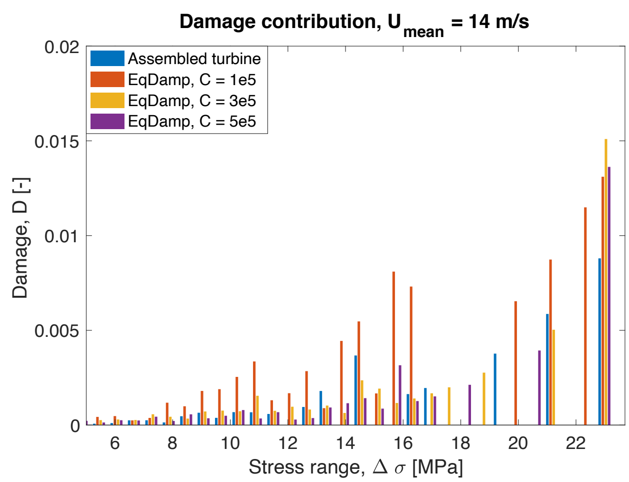

(d) Mean wind speed at $U_{mean} = 14$ m/s

Figure 7.4.1: Damage contribution is caused by stress ranges and the number of cycles with various mean wind velocities. The assembled turbine is represented as blue, and the equivalent damping turbine represents the remaining columns

Damage distribution for wind speed 10 m/s is considered in Figure 7.4.1a. The greatest damage contribution occurs for the highest stress ranges, and the impact from smaller stress ranges is less significant. Based on accumulated total fatigue damage, analysis implied that the damping factor of $3 \cdot 10^5$ kg/s had the greatest coincide with the assembled turbine. However, damage contribution for the simplified turbine is more concentrated for one stress range, while the distribution is wider for the assembled turbine. A damping factor of $5 \cdot 10^5$ kg/s obtains the same tendencies of stress range exposure as assembled turbine but without the exact contribution for each block.

Figure 7.4.1b illustrates the damage distribution for mean wind velocity of 12 m/s. Again, the illustration presents poor damage contribution for small stress ranges and significant affection for wider stress ranges. Total fatigue damage calculation implied that damping between $3 \cdot 10^5$ and $5 \cdot 10^5$ kg/s is most relevant, which is a reasonable and decent assumption for this condition.

Fatigue damage contributions for different stress ranges and mean wind velocity of 13 m/s are presented in Figure 7.4.1c. A significant damage contribution occurs for a more comprehensive stress range of 29 MPa. The most relevant equivalent damper is in the range of $3 \cdot 10^5$ and $5 \cdot 10^5$ kg/s, where both dampers represent an approximately similar number of cycles with a corresponding stress range.

Figure 7.4.1d displays damage contribution over a stress range for mean wind velocity at 14 m/s. In this case, the damage contributions are more evenly distributed over several stress ranges, which indicates minor domination of damage from wider stress ranges than for smaller wind conditions. The equivalent damper of magnitude $3 \cdot 10^5$ and $5 \cdot 10^5$ kg/s are both relevant for this simulation.

The analysis of fatigue damage distributions indicates if the equivalent damping turbine performs a reasonable model. In order to affirm appropriate damping coefficients and hence a valid simplification, it is necessary and preferred to conduct additional wind conditions with a longer simulation time.

7.4.2 Long-term fatigue damage

Four different wind conditions are considered in this thesis, where each short-term simulation was conducted for 700 seconds. Since the simulations only consider one single wind condition at a time implies that the individual fatigue life calculation is established based on one particular condition. The simplified scale-up method applies a similar condition for 20 years, which is unrealistic and may produce inaccurate values for fatigue damage calculation.

Although, this section introduces a more precise method to calculate fatigue damage for a structure. The long-term fatigue damage approach assumes a reasonable probability of occurrence for different environmental forces and magnitudes, p_{ij}. This probability depends on earlier environmental data and statistics for the specific location and hence multiplied by the corresponding fatigue damage, $D_{1\ \mathrm{hour},ij}$. The short-term fatigue damage is simulated for one hour in stationary conditions and goes through conditions for both wind and waves. The method for calculating long-term fatigue damage of an element is shown in Equation 7.4.2 and is conducted for a lifetime of N years.

$$D_{LT} = N \cdot 365 \text{ days} \cdot 24 \cdot \text{ hours} \sum_{i=1}^{N_{Hs}} \sum_{j=1}^{N_{Tp}} p_{ij} D_{1\ \mathrm{hour},ij} \tag{7.4.2}$$

Chapter 8

Conclusion

In order to achieve the aim of keeping the average global temperature rise below 2°C, the energy sector must be more sustainable. Offshore floating wind energy is characterized as a promising renewable energy resource by the Norwegian government and is a leading solution constantly improving and under development. Designing a wind turbine is time-consuming due to the iterative method and technical analysis. In addition to massive time consumption, simulations require computers with high-level performance and great data storage, which is considered challenging. The primary objective was to employ a mathematical simplification that replaces and represents the rotor and blades of a fully assembled turbine. The ambition of this modification was to obtain a significant reduction of computational time and processing data while performing high accuracy of fatigue life calculations.

Governing parameters that drive the design of a floating turbine were considered for determining primary characteristics. The wind turbine is designed such that the eigenfrequency is neither excited by the blade rotating frequencies nor typical environmental load frequencies at the North Sea. The basic principle behind establishing a simplified structure is an implementation of concentrated node load at the tower top, which is also subjected to an equivalent damper.

Thrust force variation is a significant contributor to causing fatigue damage due to cyclic axial stress. The largest thrust force is generated by a mean wind velocity of 10 m/s with associated turbulence. In comparison, a wind velocity of 13 m/s produces the most significant standard deviation relative to the corresponding thrust force. Maximal variations are located at the tower bottom, which is assumed as a critical point for further investigation of fatigue damage.

Weld class D is evaluated as an appropriate SN-curve for the wind turbine and its 20 years of service life. Rainflow-counting algorithm and Palmgren-Miner rule are employed for calculating the resulting fatigue damage. The structure with a simplified mathematical approach produces satisfying computational time reduction and reasonable fatigue results by analyzing damage distribution. This result is obtained by applying an equivalent damper equal to approximately 8 % of the critical damping of the structure. The damping magnitude appears somewhat sensitive to specific environmental conditions and must be modified and slightly increased for an increased mean wind velocity.

The constant development of floating wind technology and knowledge makes Norway a leading offshore wind nation promising.

8.1 Recommendations for Further Work

Studying and conducting this Master's Thesis has developed further insight and knowledge into the design process, software modeling and technical analysis. This section presents a bullet list of suggestions for several aspects that may be investigated for further work.

- Wind turbines with a capacity between 10-15 MW inspire the simplified model dimensions; hence, a realistic and reasonable structure is designed. Although, a more comprehensive iteration process of the design procedure may be investigated for optimizing and taking advantage of the whole service life.
- The most typical wind conditions in the North Sea are considered in this thesis, and an investigation of a broader wind spectrum and conditions would be fascinating regarding velocities from cut-in to cut-out speed. Analysis of forces and responses caused by extreme conditions is also of interest. The control algorithm produces high-quality results for wind speeds above rated wind speed and must be improved and modified for wind velocities below rated wind speed.
- A combination of several environmental conditions may be considered to achieve a more realistic long-term fatigue result and determine a specific pattern for damping magnitude.
- Due to limited time constraints it was decided along with supervisor, Professor Jørgen Amdahl, to reduce the objective regarding floating foundation design. Although, several types of offshore floating solutions are evaluated, and concepts are presented in this thesis. A recommendation for further work is to determine a floater type, conduct design iteration, and modeling process with appropriate dimensions and characteristics.

Bibliography

[1] FN (2020) *Paris agreement.*
Available at: https://www.fn.no/om-fn/avtaler/miljoe-og-klima/parisavtalen
(Accessed: 05. January 2022)

[2] NOU 2022: 83 (2022). *Kraftfull satsing på havvind.*
Press release: https://www.regjeringen.no/no/aktuelt/kraftfull-satsing
-pa-havvind/id2912297/

[3] Komusanac, I., Brindley, G., Fraile, D. and Ramirez L. (2022) *Wind energy in Europe 2021 Statistics and the outlook for 2022-2026.* Brussels: Wind Europe.
Available at: https://windeurope.org/intelligence-platform/product/wind-energy-in-europe-2021-statistics-and-the-outlook-for-2022-2026/ (Accessed: 02. June 2022)

[4] Global Wind Atlas (2022) *Wind velocity, 100m above sea surface.*
Available at: https://globalwindatlas.info/ (Accessed: 07. January 2022)

[5] DNV (2021) *Energy Transition Outlook 2021 A global and regional forecast to 2050.*
Available at: https://eto.dnv.com/2021/about-energy-transition-outlook
(Accessed: 27. January 2022)

[6] Aslesen, S., Basso, M., Erraia, J., Foseid, H., Hernes, S., Jakobsen, E. and Winje, E. (2022) *Flytende havvind analyse av markedet og norske aktørers omsetningspotensial.* (Menon-publikasjon nr. 53/2022). Oslo: Menon.
Available at: https://rederi.no/rapporter/ (Accessed: 30. May 2022)

[7] NORSOK (2004) *Design of steel structures.*
Available at: https://www.standard.no/pagefiles/1145/n-004.pdf
(Accessed: 03. February 2022)

[8] Moan, T. and Karimirad M. (2011) *Extreme Dynamic Structural Response Analysis of Catenary Moored Spar Wind Turbine in Harsh Environmental Conditions*. Paper. Norwegian University of Science and Technology.
Available at: https://asmedigitalcollection.asme.org/offshoremechanics/article /133/4/041103/468282/Extreme-Dynamic-Structural-Response-Analysis-of
(Accessed: 22. January 2022)

[9] DNV (2018) *DNVGL-ST-0119: Floating wind turbine structures.*
Available at: https://rules.dnv.com/docs/pdf/DNV/ST/2018-07/DNVGL-ST-0119.pdf
(Accessed: 06. March 2022)

[10] DNV (2015) *DNVGL-OS-C101: Design of offshore steel structures, general - LRFD method.*
Available at: https://rules.dnv.com/docs/pdf/DNV/os/2015-07/DNVGL-OS-C101.pdf
(Accessed: 01. February 2022)

[11] Bachynski, E. (2021) *Course Project: Integrated Dynamic Analysis of Wind Turbines.* Trondeheim.
Available at: https://ntnu.blackboard.com (Accessed: 09. February 2022)

[12] Lee Y., Tjhung T. (2012) *Metal Fatigue Analysis Handbook: Practical Problem-Solving Techniquesfor Computer-Aided Engineering*. Oxford: Elsevier

[13] DNV (2018) *Integrated Analysis of Floating Wind Turbines*. Oslo.
Available at: https://www.dnv.com/Images/Sesam-Wind-Integrated-analysis-of-floating-wind-turbine-whitepaper_tcm8-124150.pdf (Accessed: 26. March 2022)

[14] Olav Olsen (2021). *OO-Star Wind Floater*.
Available at: https://www.olavolsen.no/en/business-areas/renewable-energy
(Accessed: 16. January 2022)

[15] The Explorer (2021). *Floating offshore wind turbines: OO-Star Wind Floater*.
Available at: https://www.theexplorer.no/solutions/offshore-floating-wind-turbines/
(Accessed: 16. January 2022)

[16] OC4-DeepCwind (2021) *OC4-DeepCwind.*
Available at: https://www.researchgate.net/figure/OC4-DeepCwind-Semisubmersible -Floating-System-Author_fig7_265795516 (Accessed: 18. January 2022)

[17] Donahue, M. (2019) *What is turbulence—and how can you calm down about it?* Available at: https://www.nationalgeographic.com/travel/article/what-is-turbulence-explained (Accessed: 20. Mars 2022)

[18] S. Caires, J. Schouten (2019) *Uncertainties in offshore wind turbulence intensity.* Available at: https://www.sintef.no/globalassets/project/eera-deepwind-2019 /presentations/c1_caires_deltaresfugro.pdf (Accessed: 20. April 2022)

[19] Burton, T. and Sharpe, D. (2011) *Wind Energy Handbook*. Chichester: John Wiley & Sons

[20] Bachynski, E. 2021. Introduction to offshore wind power and technology. *TMR03 Integrated dynamic analysis of wind turbines.* Available at: https://ntnu.blackboard.com (Accessed: 20. January 2022)

[21] Bachynski, E. 2021. Basic Aerodynamics for Wind Turbines. *TMR03 Integrated dynamic analysis of wind turbines.*
Available at: https://ntnu.blackboard.com (Accessed: 20. January 2022)

[22] Pettersen, B. (2014) *Marin Teknikk 3: Hydrodynamikk*. Trondheim: Akademika forlag

[23] Larsen, C., Bachynski, E., Kristiansen, T. and Myrhaug, D. (2019) *Marine Dynamics.* Available at: https://ntnu.blackboard.com (Accessed: 25. January 2022)

[24] Faltinsen, O. M. (1990) *Sea Loads on Ships and Offshore Structures*. Cambridge: Cambridge University Press

[25] *Wind turbine sketch* (2017)
Available at: https://freesvg.org/wind-turbine-sketch (Accessed: 05. June 2022)

[26] Katsikogiannis, G., Sørum, S., Bachynski E. and Amdahl J. (2021)
Environmental lumping for efficient fatigue assessment of large-diameter monopile wind turbines. Paper. Norwegian University of Science and Technology.
Available at: https://ntnuopen.ntnu.no/ntnu-xmlui/bitstream/handle/11250/2733559/1-s2.0-S0951833921000071-main%2b%25285%2529.pdf?sequence=2&isAllowed=y
(Accessed: 03. February 2022)

[27] Bak, C, Zahle, F, Bitsche, R, Kim, T, Yde, A, Henriksen, LC, Hansen, MH, Blasques, JPAA, Gaunaa, M and Natarajan, A. (2013) *The DTU 10-MW Reference Wind Turbine* Danish Wind Power Research 28. May 2013.

Available at: https://backend.orbit.dtu.dk/ws/portalfiles/portal/55645274/The_DTU_10MW_Reference_Turbine_Christian_Bak.pdf (Accessed: 28. January 2022)

[28] WindEurope (2019) *Wind Energy in Europe 2019 - Key trends and statistics.*
Available from: https://windeurope.org/about-wind/statistics/european/wind-energy-in-europe-in-2019/ (Accessed: 02. March 2022)

[29] DNV (2012) *DNV-RP-C203: Fatigue Design of Offshore Steel Structures - Fatigue Analysis Based on S-N Data.*
Available at: https://rules.dnv.com/docs/pdf/dnvpm/codes/docs/2012-10/RP-C203.pdf (Accessed: 04. March 2022)

[30] Berge S., Ås S. (2017) *Fatigue and Fracture Design of Marine Structures* Trondheim.
Available at: https://ntnu.blackboard.com (Accessed: 11. April 2022)

[31] Bureau Veritas (2019) *NI 572: Classification and Certification of Floating Offshore Wind Turbines.*
Available at: https://erules.veristar.com/dy/data/bv/pdf/572-NI_2019-01.pdf (Accessed: 06. March 2022)

[32] American Bureau of Shipping (2020) *Guide for fatigue Assessment of Offshore Structures.*
Available at: https://ww2.eagle.org/content/dam/eagle/rules-and-guides/current/offshore/115_fatigueassessmentofoffshorestructures/offshore-fatigue-guide-jun20.pdf (Accessed: 10. April 2022)

[33] DNV (2018) *DNVGL-OS-C101: Design of offshore steel structures, general - LRFD method.*
Available at: https://rules.dnv.com/docs/pdf/DNV/OS/2018-07/DNVGL-OS-C101.pdf (Accessed: 11. April 2022)

Appendices

Appendix A

USFOS source codes

A.1 headA.fem

```
HEAD          WindLoad from Turbine. 12 m/s. damp = 1.0e5
                                  2022
                                     .
'
'               End_Time    Delta_T    Dt_Res   Dt_Pri
 DYNAMIC          700.0       0.010       1          1
'
'                KeyWord   Value
EigenVal           Time       1.0
EigenVal           Numberof10        10
EigenVal           ModeScale         10
'
'                Ratio1     Ratio2     Freq1 [Hz]   Freq1 [Hz]
 DampRatio      0.01        0.01          0.1          10.0
'
 Liter
'
 CNODES 1           1     1     1
'
 TimeHist   1     S_Curve 0 1
```

```
 LoadHist     1       1
'
 Chg_Boun   0 0 0    0 0 0    Node 6   ! Release fixation
'
 SpriDiag   1000 1e12 1e12  1e12       1e11  1e11  1e12
'
'              elm     nod   mat
 Sprng2Gr    1006     6     1000
'
'            LCase    Node     Fx    Fy    Fz       Mx    My    Mz
 NodeLoad     101        1      1     0     0        0     0     0
 NodeLoad     102        1      0     1     0        0     0     0
 NodeLoad     104        1      0     0     0        1     0     0
 NodeLoad     105        1      0     0     0        0     1     0
 NodeLoad     106        1      0     0     0        0     0     1
'
'            LoadCase   TimeHist
 LoadHist       101          101
 LoadHist       102          102
 LoadHist       104          104
 LoadHist       105          105
 LoadHist       106          106
'
 Dynres_X     TimeHist   101
 Dynres_X     TimeHist   102
 Dynres_X     TimeHist   104
 Dynres_X     TimeHist   105
 Dynres_X     TimeHist   106
'
'            Type      Node     Dof
 Dynres_N    Disp        1         1
'
'
'              Type       Elem_ID  End        Dof
 Dynres_E            Force       1006       1            1
 Dynres_E            Force       1006       1            2
 Dynres_E            Force       1006       1            4
```

```
 Dynres_E            Force       1006       1             5
 Dynres_E            Force       1006       1             6
'
'
'                  MatID       s11  s22  s33  s44  s55  s66
 Spridiag      9999  0  0  0  0  0  0
'
'                  ElemID            Nod1     Mat    [LCorr  Ecc1]
 Sprng2Gr      9999                1     9999
'
'                  DoF         C            Elem_1       Elem_2 ........
 Spridamp      1           1.0e5       9999
'   ——————————— e o f ————————————
```

A.2 modelA.fem

```
'
' NodeID  X  Y  Z  [Boundary   Code]
 NODE  1  0  0  0  !  Tower  top
 NODE  2  0  0  -20
 NODE  3  0  0  -40
 NODE  4  0  0  -60
 NODE  5  0  0  -80
 NODE  6  0  0  -100
 NODE  7  0  0  -101   !  1  1  1  1  1  1  !  Fixed  tower  bottom
'
' ElemID  Nod1  Nod2  Mat  Geo  [LCorr  Ecc1  Ecc2]
 BEAM  1  1  2  1  1
 BEAM  2  2  3  1  2
 BEAM  3  3  4  1  3
 BEAM  4  4  5  1  4
 BEAM  5  5  6  1  5
 BEAM  6  6  7  1  6
'
'      GeoID     Do     Thick    Sy  Sz    D2
 PIPE    1       5.0     0.040     0    0    5.6  !  Conial  shape
```

```
PIPE   2      5.6     0.046    0   0   6.2
PIPE   3      6.2     0.052    0   0   6.8
PIPE   4      6.8     0.058    0   0   7.4
PIPE   5      7.4     0.064    0   0   8.0
PIPE   6      8.0     0.064
'
'   MatID E-mod poiss yield density term.exp
MISOIEP   1 210000e6 0.3 355e6 7850
' LCase aX aY aZ
GRAVITY   1 0 0 -9.81
' NodeID Mass
NODEMASS   1 750E3
'
Illegal BeamLength    Accept   0.1
Illegal BeamLength    Elem    6
'
' ------------------------------------------------------------------------
'
```

Appendix B

USFOS-VpOne source codes

B.1 headB.fem

```
HEAD            Full tower. U = 10 m/s . Normal Turbulence
                                 VP
                                2022
'
'
'             End_Time    Delta_T    Dt_Res   Dt_Pri
 DYNAMIC        700.0      0.010       1        1
'
' ------------------------------------------------------------------------
'   Definition of Basic Loads :
' ------------------------------------------------------------------------
'
'   Load Case 1   :   Gravity
'   Load Case 2   :   Wind
'   Load Case 3   :   Wave
'
' ------------------------------------------------------------------------
'     Time histories and loads to apply
' ------------------------------------------------------------------------
'
```

```
'              ID       Type       T1       T2      Fac     Pow
 TimeHist       1      S_Curve      0        1       1       2      ! Gravity
 TimeHist      21      S_Curve      0       15       1       2      ! WindHist
'
'               ID    <type>   dTime    factor    Tstart
 TIMEHIST       2     Switch      0        1          0             ! Wind
 TIMEHIST       3     Switch      0        1          0             ! Wave
'
'
'             Ildcs    Tim  Hist
 LoadHist       1          1        !   Gravity
 LoadHist       2          2        !   Wind
#LoadHist       3          3        !   Wave
'
'             Dof  Hist
 WindHist      X     21
 WindHist      Y     21
 WindHist      Z     21
'
'           LC   GWF_Typ     Ux        Uy        Uz       Z_0       Z_Bott   RhoAir
 WindField     2  GWF_3        12       0.0       0.0     -135       0.0      1.260
#
 FileName    Wind   GWF_06_1101.w33
#FileName    Wind   $(WIND_HOME)/GWF_06_1101.w33
'
'
'             Ildcs   <type>    H     Period    Direction  Phase   Surf_Lev
    Depth
 WAVEDATA         3     Airy      0      10          0          0      -135       150
'
'
'           Type
 Control  External
 FileName    Control   control.inp
'
```

——

```
'   Result  files
'
  *------------------------------------------------------------------------------*
'
'              Type       End   DofCode      Elem_Id
 Dynres_E   MultForce   1      123456     101  102  103
                                          104  105  106     770100
'
'
' ---------------------------------------------------------------------------
```

B.2 modelB.fem

```
'
' ----------------------------------------------------------------------------
'      General  Options.
' ----------------------------------------------------------------------------
'
'
 ElmTrans    Loc   999  All        !  Replace  Usfos  TROT  with  TNROT.  Use  both
      ends.
'
 Switches   NodeData  Doubly  ON  !  Accept  Doubly  Definie  nodes  with  same
    Coord.
'
'
 BeamType   Riser    All           !  Use  large  rot  elements

 CNODES     1       500    4    1   !  Rotation  of  Hub
'
 REL_VELO                          !  Relative  Velocity
'
'
 GRAVITY           1    0  0      -9.81
'
```

```
'             mass    stiff
RaylDamp   0.00    3E-3          ! Gives 0.5% damp at 0.5Hz !3E-3
'
LITER  1                         ! One Iteration
DeterOff                         ! Switch off determinant crit due to springs
Sysdamp 1                        ! System Damping
'
'
'
' ------------------------------------------------------------------
'      Options related to the Turbine
' ------------------------------------------------------------------
'
'
'
' *----------------------------------------------------------------------*
'      Aerodynamic coefficients
' *----------------------------------------------------------------------*
'
W_Coeffs   11   Drag       0    0.7    ! Constant (Circular)
'
'                                      - Combine Drag/Lift coeffs
W_Coeffs    1   Combine    11          ! Drag Only
'
'             Coeff ID    List Type    ID's
ElmCoeff       1            Pipe
'
'
' *----------------------------------------------------------------------*
'      Generator element properties
```

```
'
 *------------------------------------------------------------------------------*

'               DOF     C           ElemID
SpriDamp         4      1             707
'
'             DepType   ID   DOF    ListType    IDs
DampDep      Control     1    4        Elem      707      !  Controlled
'
'
'
' ---------------------------------------------------------------------------*
'       Tower  parameters
' ---------------------------------------------------------------------------*
'                          top  btm
TowerPar    TowerNod       100  101    !  Top  and  bottom  nodes  of  tower
TowerPar    Diam           8.000       !  Diameter  used  for  wake
TowerPar    TowerElm       100         !  Upper  tower  element
TowerPar    RotorNorm       708        !  Axle  of  drivetrain
TowerPar    ConeAngle       0.62
TowerPar    SyrupGWF       0.5
TowerPar    Cd    0.7
TowerPar    iDynStall       +1         !  Dynamic  stall  ON  (-1  means  OFF)
TowerPar    IndWinSW        +1         !  Induced  wind  ON
'
'
'
DynRes_G     Hub_Wind
DynRes_G     ElPower
DynRes_G     RotSpeed
'
Dynres_G     DemGTorq
DynRes_G     DemPtch1
DynRes_G     DemPtch2
DynRes_G     DemPtch3
DynRes_G     MeaPtch1
DynRes_G     MeaPtch2
```

```
 DynRes_G     MeaPtch3
#DynRes_G     TipClear
'
 Dynres_G     Bl1_Lift
#Dynres_G     Bl1TipCl
'

' ------------------------------------------------------------------------
'      Upper Part of  Tower (Yaw bearing section )
' ------------------------------------------------------------------------
'
'
'           MatID     E-mod     poiss    yield    density    term.exp.
 MISOIEP  8001      2.100e+11  0.3      3.550e+08  7855.0       0.0
'
'
   *-------------------------------------------------------------------------------*
'         Pipe  Yaw
'
   *-------------------------------------------------------------------------------*
'      GeoID    D1    Thick   Shear_y   Shear_z   D2
 Pipe  8100   5.500  0.020      0          0      5.750
'
' ------------------------------------------------------------------------------*
'      NODE   interface to tower
' ------------------------------------------------------------------------------*
'
'             Node ID       X             Y            Z      Boundary code
 NODE            101       7.1000       0.0000       0.000   ! 1 1 1 1 1 1
#NODE            101       7.1000       0.0000     -10.000   ! 1 1 1 1 1 1
'
'    Elem ID   Node1  Node2  MatID  GeoID
 Beam     100     100     101   8001   8100
'
' ------------------ e o f  ----------------
```

```
'
'                    PartID      Transp      Red     Green     Blue    Fringe    Smooth
 PartData            14               0         0         0      200         1         1   ! YawBearing
'
'                              PartID       name
 Name          Part             14          YawBearing
'
 PartElem            14        Mat     8001     !  Yawbearing
'



'
' *----------------------------------------------------------------------------*
'        Drivetrain
' *----------------------------------------------------------------------------*
'        Node  ID        X       Y       Z     Boundary  code
 NODE            100        7.1000        0.0000       -3.3700  !   1  1  1  1  1  1  !  To tower
 NODE              1        1.3500        0.0000       -0.1180  !
 NODE             21        2.7000        0.0000       -0.2360  !  Main  bearing
 NODE             22        2.7000        0.0000       -0.2360  !  Bearing
 NODE             31        4.7000        0.0000       -0.4110  !  Spring  interface gear
 NODE             32        4.7000        0.0000       -0.4110  !  Spring  interface gear
 NODE              4        9.7870        0.0000       -0.8560  !  CM  Nacelle , approximately  on  shaft
 NODE             51       10.7870        0.0000       -0.9440  !  Generator
 NODE             52       10.7870        0.0000       -0.9440  !  Generator
 NODE              6       12.7870        0.0000       -1.1190  !  Rear  point
'
```

```
'      Elem ID    Node1  Node2     MatID      GeoID
 BEAM       601     100      21       601         601   ! Support front
 BEAM       602     100       6       602         602   ! Support back
 BEAM       603      21       6       603         603   ! Horizontal brace
 BEAM       604      21      22       604         604   ! NL spring, bearing
 BEAM       605      21      22       605         605   ! NL spring, brake
'
'      Elem ID    Node1  Node2     MatID     GeoID
 BEAM       701       1     500       701         701   ! Outer axle, points upwind
 BEAM       702       1      22       702         702   ! Axle interface bearing
 BEAM       703      22      31       703         703   ! Axle
 BEAM       704      31      32       7040        704   ! NL spring torsion
        stiffness
 BEAM       705      32       4       705         705   ! Axle
 BEAM       706       4      51       706         706   ! Axle
 BEAM       707      52      51       7070        707   ! NL spring generator
 BEAM       708       6      52       708         708   ! Support of generator
#BEAM       708      52       6       708         708   ! Support of generator
'
'
    *------------------------------------------------------------------------*
'      Define Local Transformations
'
    *------------------------------------------------------------------------*
 ElmTrans   Loc 2   Elem      604 ! Bearing
 ElmTrans   Loc 2   Elem      605 ! Brake
 ElmTrans   Loc 1   Elem      704 ! Spring
 ElmTrans   Loc 2   Elem      707 ! Generator
'
'
    *------------------------------------------------------------------------*
'      Bearing
'
    *------------------------------------------------------------------------*
```

```
'
MATERIAL    604  Bear  Lin  1e12  1e12  1e12    0     0     0
'
'
  *------------------------------------------------------------------------*
'       Brake
'
  *------------------------------------------------------------------------*
MATERIAL    605  Bear  Lin  1e12  1e12  1e12    0     0     0
'
'
  *------------------------------------------------------------------------*
'       Gear
'
  *------------------------------------------------------------------------*
'
MREF      7040  7041  7042  7043  7044  7045  7046
'
 HypElast   7041   -1.00e+12   -1.00e+00  1.00e+12  1.00e+00  !
 HypElast   7042   -1.00e+12   -1.00e+00  1.00e+12  1.00e+00  !
 HypElast   7043   -1.00e+12   -1.00e+00  1.00e+12  1.00e+00  !
 HypElast   7044   -2.32e+08   -1.00e+00  2.32e+08  1.00e+00  !
 HypElast   7045   -1.00e+12   -1.00e+00  1.00e+12  1.00e+00  !
 HypElast   7046   -1.00e+12   -1.00e+00  1.00e+12  1.00e+00  !
'
' ----------------------------------------------------------------------*
'       Generator  Torsion  free ,  else  fixed .
' -----------------------------------------------------------------------*
'                                                rX
MREF      7070       7071       7072       7073        0       7075       7076
'
 HypElast        7071    -1.00e+12    -1.00e+00  1.00e+12  1.00e+00  !
```

```
HypElast      7072   -1.00e+12   -1.00e+00  1.00e+12  1.00e+00  !
HypElast      7073   -1.00e+12   -1.00e+00  1.00e+12  1.00e+00  !
HypElast      7075   -1.00e+12   -1.00e+00  1.00e+12  1.00e+00  !
HypElast      7076   -1.00e+12   -1.00e+00  1.00e+12  1.00e+00  !
'
'
*--------------------------------------------------------------------------*
'      Drivetrain  pipes
'
*--------------------------------------------------------------------------*
PIPE       601   2.000   0.100
PIPE       602   2.000   0.100
PIPE       603   1.500   0.100
PIPE       604   2.000   0.100
PIPE       605   2.000   0.100
'
PIPE       701   1.500   0.100
PIPE       702   1.500   0.100
PIPE       703   1.500   0.100
PIPE       704   1.500   0.100
PIPE       705   1.500   0.100
PIPE       706   1.500   0.100
PIPE       707   1.500   0.100
PIPE       708   1.500   0.100
'
SURFPIPE      603  0.010  0.001
'
'
*--------------------------------------------------------------------------*
'      Translation  masses
'
*--------------------------------------------------------------------------*
'           Node        Mass
```

```
NodeMass   4        4.460e+05 !  Nacelle mass
NodeMass 500      105.5e+03    ! Hub mass
'
'   *------------------------------------------------------------------------*
'       Rotation masses
'   *------------------------------------------------------------------------*
'                                              Yaw
NodeMass 100   0 0 0     0        0 7.326e+06  ! Nacelle inertia about tower top element
NodeMass    1   0 0 0   3.260e+05 0   0            ! Hub rotation mass about rotor axis
NodeMass   51   0 0 0   1.500e+03 0   0            ! Generator rotation mass
'
'                   nod      elm
LocNMass Node    1       701
LocNMass Node   51       708
LocNMass Node   100      100   ! Nacelle rotation mass about top element
'
'   *------------------------------------------------------------------------*
'       Materials
'   *------------------------------------------------------------------------*
MATERIAL      601    Elastic  2.100e+11  0.30  0.000e+00  10.000  1.200e-05
MATERIAL      602    Elastic  2.100e+11  0.30  0.000e+00  10.000  1.200e-05
MATERIAL      603    Elastic  2.100e+11  0.30  0.000e+00  10.000  1.200e-05
MATERIAL      701    Elastic  2.100e+11  0.30  0.000e+00  10.000  1.200e-05
MATERIAL      702    Elastic  2.100e+11  0.30  0.000e+00  10.000  1.200e-05
MATERIAL      703    Elastic  2.100e+11  0.30  0.000e+00  10.000  1.200e-05
MATERIAL      705    Elastic  2.100e+11  0.30  0.000e+00  10.000  1.200e-05
MATERIAL      706    Elastic  2.100e+11  0.30  0.000e+00  10.000  1.200e-05
```

```
MATERIAL      708   Elastic  2.100e+11  0.30  0.000e+00  10.000  1.200e-05
'
'
'
'                 PartID     Transp    Red    Green    Blue   Fringe   Smooth
 PartData           12            0    255       0       0        1        1   !
    DriveTrain
'
'                           PartID     name
 Name         Part            12        DriveTrain
'

 PartElem           12      Mat
'
                601     701     602    603     702
                703     705     706     708
'
'
    *------------------------------------------------------------------------*

'      End  drivetrain
'
    *------------------------------------------------------------------------*

'
'
'
'
'                Node  ID              X                Y                Z
   Boundary  code
NODE              500          0.00000          0.00000          0.00000
NODE              501          0.24400          0.00000          2.67800
NODE              502         -0.10750         -2.32880         -1.34030
NODE              503         -0.10750          2.32880         -1.34020
'
'                Elem  ID      np1        np2    material    geom      lcoor
BEAM              501         500        501      8000        8000       501  !  Hub
```

```
BEAM              502        500        502       8000       8000       502  !  Hub
BEAM              503        500        503       8000       8000       503  !  Hub

'                Loc-Coo           dx              dy              dz
UNITVEC             501          0.00000        -1.00000         0.00000     !  Hub
UNITVEC             502         -0.07548         0.50000        -0.86273     !  Hub
UNITVEC             503          0.07548         0.50000         0.86273     !  Hub


PIPE              8000          2.200         0.150
'                 Mat   ID      E-mod          Poiss        Yield         Density      ThermX
MISOIEP           8000    2.100E+11    3.000E-01    3.550E+08    6.531E+03    0.000E+00


'                  PartID   Transp   Red   Green   Blue  Fringe  Smooth
 PartData            13        0       0      0       0      1       1

'                     PartID        name
Name      Part          13    HUB

'
'                  PartID     ListType     ElemID  .....
 PartElem            13         Elem
                    501         502         503


'
'
'                  PartID   Transp   Red   Green   Blue  Fringe  Smooth
 PartData            11        0     255    255     255      1       1
'
'                     PartID        name
```

```
 Name      Part          11    BLADES
'
'                  PartID     ListType    ElemID  .....
 PartElem            11        Elem
                    61004      61005      61006      61007      61008      61009
                    61010      61011      61012      61013      61014      61015
                    61016      61017      61018      61019      61020      61021
                    61022      61023      62004      62005      62006      62007
                    62008      62009      62010      62011      62012      62013
                    62014      62015      62016      62017      62018      62019
                    62020      62021      62022      62023      63004      63005
                    63006      63007      63008      63009      63010      63011
                    63012      63013      63014      63015      63016      63017
                    63018      63019      63020      63021      63022      63023
'
'  ----------------------------------------------------------------------------
       Pitch  elements
'  ----------------------------------------------------------------------------
'
'                 Node  ID           X              Y              Z      Boundary  code
#NODE              501          0.24400        0.00000        2.67800
#NODE              502         -0.10750       -2.32880       -1.34030
#NODE              503         -0.10750        2.32880       -1.34020
'
'                 Elem  ID      np1      np2    material    geom     lcoor   ecc1    ecc2
 BEAM              6010        501      6011      6000      6000
 BEAM              6020        502      6021      6000      6000
 BEAM              6030        503      6031      6000      6000

'                 Type       Node     ListType         ID
 ElmTrans     LocNode          1    Elem            6010
```

```
 ElmTrans    LocNode          1   Elem          6020
 ElmTrans    LocNode          1   Elem          6030
'
'
' *------------------------------------------------------------------------------*
'       Blade pitch mechanism
' *------------------------------------------------------------------------------*
MATERIAL 6000 Bear Lin 1e12 1e12 1e12 5e9 1e12 1e12

'
'                Node ID          X            Y            Z     Boundary code
NODE             6011       0.24400      0.00000      2.67800
NODE             6012      -3.64500      0.00000     85.11200
NODE             6021      -0.10750     -2.32880     -1.34030
NODE             6022     -14.68810    -73.15350    -41.11150
NODE             6031      -0.10750      2.32880     -1.34020
NODE             6032     -14.68810     73.15350    -41.11150
NODE            61011      -0.04770      0.00000      8.86060
NODE            61012      -0.33940      0.00000     15.04310
NODE            61013      -0.63100      0.00000     21.22570
NODE            61014      -0.92270      0.00000     27.40820
NODE            61015      -1.21440      0.00000     33.59080
NODE            61016      -1.50610      0.00000     39.77330
NODE            61017      -1.79770      0.00000     45.95580
NODE            61018      -2.08940      0.00000     52.13840
NODE            61019      -2.38110      0.00000     58.32100
NODE            61020      -2.67280      0.00000     64.50350
NODE            61021      -2.89060      0.00000     69.12100
NODE            61022      -3.06490      0.00000     72.81500
NODE            61023      -3.20430      0.00000     75.77020
NODE            61024      -3.31580      0.00000     78.13440
NODE            61025      -3.40500      0.00000     80.02570
```

```
NODE        61026      -3.47640      0.00000     81.53870
NODE        61027      -3.53350      0.00000     82.74910
NODE        61028      -3.57910      0.00000     83.71760
NODE        61029      -3.61580      0.00000     84.49230
NODE        62011      -1.20120     -7.64070     -4.32320
NODE        62012      -2.29470    -12.95250     -7.30600
NODE        62013      -3.38810    -18.26440    -10.28890
NODE        62014      -4.48180    -23.57620    -13.27170
NODE        62015      -5.57530    -28.88810    -16.25450
NODE        62016      -6.66880    -34.19990    -19.23740
NODE        62017      -7.76230    -39.51170    -22.22010
NODE        62018      -8.85590    -44.82370    -25.20310
NODE        62019      -9.94940    -50.13550    -28.18590
NODE        62020     -11.04310    -55.44740    -31.16870
NODE        62021     -11.85970    -59.41450    -33.39640
NODE        62022     -12.51310    -62.58830    -35.17870
NODE        62023     -13.03580    -65.12740    -36.60440
NODE        62024     -13.45390    -67.15860    -37.74510
NODE        62025     -13.78840    -68.78350    -38.65760
NODE        62026     -14.05600    -70.08350    -39.38750
NODE        62027     -14.27020    -71.12350    -39.97160
NODE        62028     -14.44140    -71.95550    -40.43880
NODE        62029     -14.57850    -72.62110    -40.81250
NODE        63011      -1.20120      7.64070     -4.32310
NODE        63012      -2.29470     12.95250     -7.30590
NODE        63013      -3.38810     18.26440    -10.28880
NODE        63014      -4.48170     23.57620    -13.27160
NODE        63015      -5.57530     28.88810    -16.25440
NODE        63016      -6.66880     34.19990    -19.23730
NODE        63017      -7.76230     39.51170    -22.22010
NODE        63018      -8.85590     44.82370    -25.20300
NODE        63019      -9.94940     50.13550    -28.18580
NODE        63020     -11.04300     55.44740    -31.16860
NODE        63021     -11.85970     59.41450    -33.39640
NODE        63022     -12.51310     62.58830    -35.17870
NODE        63023     -13.03580     65.12740    -36.60440
NODE        63024     -13.45390     67.15860    -37.74500
```

```
NODE        63025     -13.78840     68.78350     -38.65760
NODE        63026     -14.05600     70.08350     -39.38750
NODE        63027     -14.27010     71.12350     -39.97150
NODE        63028     -14.44140     71.95550     -40.43870
NODE        63029     -14.57850     72.62110     -40.81250
'
'           Elem ID    np1     np2     material   geom    lcoor   ecc1   ecc2
BEAM        61004     6011    61011    61004     61002    61004
BEAM        61005    61011    61012    61005     61003    61005
BEAM        61006    61012    61013    61006     61004    61006
BEAM        61007    61013    61014    61007     61005    61007
BEAM        61008    61014    61015    61008     61006    61008
BEAM        61009    61015    61016    61009     61007    61009
BEAM        61010    61016    61017    61010     61008    61010
BEAM        61011    61017    61018    61011     61009    61011
BEAM        61012    61018    61019    61012     61010    61012
BEAM        61013    61019    61020    61013     61011    61013
BEAM        61014    61020    61021    61014     61012    61014
BEAM        61015    61021    61022    61015     61013    61015
BEAM        61016    61022    61023    61016     61014    61016
BEAM        61017    61023    61024    61017     61015    61017
BEAM        61018    61024    61025    61018     61016    61018
BEAM        61019    61025    61026    61019     61017    61019
BEAM        61020    61026    61027    61020     61018    61020
BEAM        61021    61027    61028    61021     61019    61021
BEAM        61022    61028    61029    61022     61020    61022
BEAM        61023    61029     6012    61023     61021    61023
BEAM        62004     6021    62011    62004     62002    62004
BEAM        62005    62011    62012    62005     62003    62005
BEAM        62006    62012    62013    62006     62004    62006
BEAM        62007    62013    62014    62007     62005    62007
BEAM        62008    62014    62015    62008     62006    62008
BEAM        62009    62015    62016    62009     62007    62009
BEAM        62010    62016    62017    62010     62008    62010
BEAM        62011    62017    62018    62011     62009    62011
BEAM        62012    62018    62019    62012     62010    62012
```

```
BEAM        62013   62019   62020   62013   62011   62013
BEAM        62014   62020   62021   62014   62012   62014
BEAM        62015   62021   62022   62015   62013   62015
BEAM        62016   62022   62023   62016   62014   62016
BEAM        62017   62023   62024   62017   62015   62017
BEAM        62018   62024   62025   62018   62016   62018
BEAM        62019   62025   62026   62019   62017   62019
BEAM        62020   62026   62027   62020   62018   62020
BEAM        62021   62027   62028   62021   62019   62021
BEAM        62022   62028   62029   62022   62020   62022
BEAM        62023   62029    6022   62023   62021   62023
BEAM        63004    6031   63011   63004   63002   63004
BEAM        63005   63011   63012   63005   63003   63005
BEAM        63006   63012   63013   63006   63004   63006
BEAM        63007   63013   63014   63007   63005   63007
BEAM        63008   63014   63015   63008   63006   63008
BEAM        63009   63015   63016   63009   63007   63009
BEAM        63010   63016   63017   63010   63008   63010
BEAM        63011   63017   63018   63011   63009   63011
BEAM        63012   63018   63019   63012   63010   63012
BEAM        63013   63019   63020   63013   63011   63013
BEAM        63014   63020   63021   63014   63012   63014
BEAM        63015   63021   63022   63015   63013   63015
BEAM        63016   63022   63023   63016   63014   63016
BEAM        63017   63023   63024   63017   63015   63017
BEAM        63018   63024   63025   63018   63016   63018
BEAM        63019   63025   63026   63019   63017   63019
BEAM        63020   63026   63027   63020   63018   63020
BEAM        63021   63027   63028   63021   63019   63021
BEAM        63022   63028   63029   63022   63020   63022
BEAM        63023   63029    6032   63023   63021   63023
'
'
'          Geom ID      Do        Thick    (Shear_y   Shear_z
   Diam2 )
 PIPE         6000      2.200     0.150
'
```

```
'               Geom ID       Type     B1      dBdL     HoB     Thick    Twist    AeroOffs YDisNose
 WINGPROF     61002 Shaped       5.380    0.008    0.300    0.982    0.010       0.000    1.000
            8.947E−01 1.344E+00 3.098E+00 3.014E+00 1.344E+00 1.344E+00 1.344E+00 1.344E+00 1.344E+00
'
'               Geom ID       Type     B1      dBdL     HoB     Thick    Twist    AeroOffs YDisNose
 WINGPROF     61003 Shaped       5.428    0.056    0.300    0.797    0.211       0.000    1.000
            7.750E−01 8.288E−01 2.045E+00 2.384E+00 8.288E−01 8.288E−01 8.288E−01 8.288E−01 8.288E−01
'
'               Geom ID       Type     B1      dBdL     HoB     Thick    Twist    AeroOffs YDisNose
 WINGPROF     61004 Shaped       5.777    0.059    0.300    0.540    0.599       0.000    1.000
            6.172E−01 2.827E−01 9.204E−01 1.519E+00 2.827E−01 2.827E−01 2.827E−01 2.827E−01 2.827E−01
'
'               Geom ID       Type     B1      dBdL     HoB     Thick    Twist    AeroOffs YDisNose
 WINGPROF     61005 Shaped       6.140    0.002    0.300    0.393    0.370       0.000    1.000
            4.898E−01 1.127E−01 4.817E−01 1.072E+00 1.127E−01 1.127E−01 1.127E−01 1.127E−01 1.127E−01
'
'               Geom ID       Type     B1      dBdL     HoB     Thick    Twist    AeroOffs YDisNose
 WINGPROF     61006 Shaped       6.154   −0.048    0.300    0.328    0.207       0.000    1.000
            4.226E−01 5.858E−02 2.877E−01 8.412E−01 5.858E−02 5.858E−02 5.858E−02 5.858E−02 5.858E−02
'
'               Geom ID       Type     B1      dBdL     HoB     Thick    Twist    AeroOffs YDisNose
```

```
WINGPROF      61007 Shaped      5.857   -0.072    0.300    0.290    0.194    0.000    1.000
        3.838E-01 3.560E-02 1.818E-01 6.022E-01 3.560E-02 3.560E-02 3.560E-02 3.560E-02 3.560E-02
'
'            Geom ID      Type     B1      dBdL     HoB     Thick     Twist   AeroOffs YDisNose
WINGPROF      61008 Shaped      5.412   -0.084    0.300    0.266    0.209    0.000    1.000
        3.409E-01 2.200E-02 1.135E-01 4.223E-01 2.200E-02 2.200E-02 2.200E-02 2.200E-02 2.200E-02
'
'            Geom ID      Type     B1      dBdL     HoB     Thick     Twist   AeroOffs YDisNose
WINGPROF      61009 Shaped      4.889   -0.089    0.300    0.251    0.219    0.000    1.000
        2.915E-01 1.335E-02 6.845E-02 2.689E-01 1.335E-02 1.335E-02 1.335E-02 1.335E-02 1.335E-02
'
'            Geom ID      Type     B1      dBdL     HoB     Thick     Twist   AeroOffs YDisNose
WINGPROF      61010 Shaped      4.336   -0.089    0.300    0.243    0.205    0.000    1.000
        2.413E-01 8.120E-03 4.125E-02 1.622E-01 8.120E-03 8.120E-03 8.120E-03 8.120E-03 8.120E-03
'
'            Geom ID      Type     B1      dBdL     HoB     Thick     Twist   AeroOffs YDisNose
WINGPROF      61011 Shaped      3.786   -0.086    0.300    0.241    0.184    0.000    1.000
        1.900E-01 4.852E-03 2.378E-02 9.156E-02 4.852E-03 4.852E-03 4.852E-03 4.852E-03 4.852E-03
'
'            Geom ID      Type     B1      dBdL     HoB     Thick     Twist   AeroOffs YDisNose
WINGPROF      61012 Shaped      3.257   -0.082    0.300    0.241    0.169    0.000    1.000
```

```
             1.433E-01 3.022E-03 1.377E-02 5.349E-02 3.022E-03 3.022E-03 3.022E-03 3.022E-03 3.022E-03
'
'              Geom ID       Type     B1       dBdL     HoB      Thick      Twist   AeroOffs YDisNose
WINGPROF       61013 Shaped        2.877   -0.076    0.300    0.241    0.154    0.000    1.000
             1.092E-01 2.023E-03 8.387E-03 3.347E-02 2.023E-03 2.023E-03 2.023E-03 2.023E-03 2.023E-03
'
'              Geom ID       Type     B1       dBdL     HoB      Thick      Twist   AeroOffs YDisNose
WINGPROF       61014 Shaped        2.598   -0.073    0.300    0.241    0.146    0.000    1.000
             8.385E-02 1.433E-03 5.288E-03 2.231E-02 1.433E-03 1.433E-03 1.433E-03 1.433E-03 1.433E-03
'
'              Geom ID       Type     B1       dBdL     HoB      Thick      Twist   AeroOffs YDisNose
WINGPROF       61015 Shaped        2.381   -0.081    0.300    0.241    0.142    0.000    1.000
             6.472E-02 1.057E-03 3.414E-03 1.563E-02 1.057E-03 1.057E-03 1.057E-03 1.057E-03 1.057E-03
'
'              Geom ID       Type     B1       dBdL     HoB      Thick      Twist   AeroOffs YDisNose
WINGPROF       61016 Shaped        2.190   -0.105    0.300    0.241    0.136    0.000    1.000
             4.966E-02 7.712E-04 2.238E-03 1.109E-02 7.712E-04 7.712E-04 7.712E-04 7.712E-04 7.712E-04
'
'              Geom ID       Type     B1       dBdL     HoB      Thick      Twist   AeroOffs YDisNose
WINGPROF       61017 Shaped        1.991   -0.105    0.300    0.241    0.136    0.000    1.000
             3.768E-02 5.470E-04 1.396E-03 7.702E-03 5.470E-04 5.470E-04 5.470E-04 5.470E-04 5.470E-04
```

```
'
'                Geom ID       Type     B1      dBdL     HoB     Thick      Twist    AeroOffs  YDisNose
 WINGPROF        61018  Shaped        1.833   -0.316    0.300    0.241    0.132        0.000     1.000
            2.825E-02  3.751E-04  8.212E-04  5.182E-03  3.751E-04  3.751E-04  3.751E-04  3.751E-04  3.751E-04
'
'                Geom ID       Type     B1      dBdL     HoB     Thick      Twist    AeroOffs  YDisNose
 WINGPROF        61019  Shaped        1.449   -0.351    0.300    0.241    0.131        0.000     1.000
            2.097E-02  2.503E-04  5.309E-04  3.490E-03  2.503E-04  2.503E-04  2.503E-04  2.503E-04  2.503E-04
'
'                Geom ID       Type     B1      dBdL     HoB     Thick      Twist    AeroOffs  YDisNose
 WINGPROF        61020  Shaped        1.109   -0.351    0.300    0.241    0.131        0.000     1.000
            1.514E-02  1.504E-04  2.985E-04  2.137E-03  1.504E-04  1.504E-04  1.504E-04  1.504E-04  1.504E-04
'
'                Geom ID       Type     B1      dBdL     HoB     Thick      Twist    AeroOffs  YDisNose
 WINGPROF        61021  Shaped        0.837   -0.351    0.300    0.241    0.131        0.000     1.000
            1.048E-02  7.055E-05  1.127E-04  1.054E-03  7.055E-05  7.055E-05  7.055E-05  7.055E-05  7.055E-05
'
'                Geom ID       Type     B1      dBdL     HoB     Thick      Twist    AeroOffs  YDisNose
 WINGPROF        62002  Shaped        5.380    0.008    0.300    0.982    0.010        0.000     1.000
            8.947E-01  1.344E+00  3.098E+00  3.014E+00  1.344E+00  1.344E+00  1.344E+00  1.344E+00  1.344E+00
'
'                Geom ID       Type     B1      dBdL     HoB     Thick      Twist
```

```
     AeroOffs  YDisNose
WINGPROF        62003  Shaped        5.428     0.056     0.300     0.797     0.211     0.000     1.000
             7.750E-01  8.288E-01  2.045E+00  2.384E+00  8.288E-01  8.288E-01  8.288E-01  8.288E-01  8.288E-01
'
'                 Geom  ID        Type      B1       dBdL      HoB      Thick       Twist     AeroOffs  YDisNose
WINGPROF        62004  Shaped        5.777     0.059     0.300     0.540     0.599     0.000     1.000
             6.172E-01  2.827E-01  9.204E-01  1.519E+00  2.827E-01  2.827E-01  2.827E-01  2.827E-01  2.827E-01
'
'                 Geom  ID        Type      B1       dBdL      HoB      Thick       Twist     AeroOffs  YDisNose
WINGPROF        62005  Shaped        6.140     0.002     0.300     0.393     0.370     0.000     1.000
             4.898E-01  1.127E-01  4.817E-01  1.072E+00  1.127E-01  1.127E-01  1.127E-01  1.127E-01  1.127E-01
'
'                 Geom  ID        Type      B1       dBdL      HoB      Thick       Twist     AeroOffs  YDisNose
WINGPROF        62006  Shaped        6.154    -0.048     0.300     0.328     0.207     0.000     1.000
             4.226E-01  5.858E-02  2.877E-01  8.412E-01  5.858E-02  5.858E-02  5.858E-02  5.858E-02  5.858E-02
'
'                 Geom  ID        Type      B1       dBdL      HoB      Thick       Twist     AeroOffs  YDisNose
WINGPROF        62007  Shaped        5.857    -0.072     0.300     0.290     0.194     0.000     1.000
             3.838E-01  3.560E-02  1.818E-01  6.022E-01  3.560E-02  3.560E-02  3.560E-02  3.560E-02  3.560E-02
'
'                 Geom  ID        Type      B1       dBdL      HoB      Thick       Twist     AeroOffs  YDisNose
WINGPROF        62008  Shaped        5.412    -0.084     0.300     0.266     0.209
```

```
      0.000     1.000
            3.409E-01 2.200E-02 1.135E-01 4.223E-01 2.200E-02 2.200E-02
               2.200E-02 2.200E-02 2.200E-02
'
'              Geom ID       Type     B1       dBdL     HoB      Thick      Twist
   AeroOffs YDisNose
WINGPROF        62009 Shaped        4.889   -0.089    0.300    0.251     0.219
      0.000     1.000
            2.915E-01 1.335E-02 6.845E-02 2.689E-01 1.335E-02 1.335E-02
               1.335E-02 1.335E-02 1.335E-02
'
'              Geom ID       Type     B1       dBdL     HoB      Thick      Twist
   AeroOffs YDisNose
WINGPROF        62010 Shaped        4.336   -0.089    0.300    0.243     0.205
      0.000     1.000
            2.413E-01 8.120E-03 4.125E-02 1.622E-01 8.120E-03 8.120E-03
               8.120E-03 8.120E-03 8.120E-03
'
'              Geom ID       Type     B1       dBdL     HoB      Thick      Twist
   AeroOffs YDisNose
WINGPROF        62011 Shaped        3.786   -0.086    0.300    0.241     0.184
      0.000     1.000
            1.900E-01 4.852E-03 2.378E-02 9.156E-02 4.852E-03 4.852E-03
               4.852E-03 4.852E-03 4.852E-03
'
'              Geom ID       Type     B1       dBdL     HoB      Thick      Twist
   AeroOffs YDisNose
WINGPROF        62012 Shaped        3.257   -0.082    0.300    0.241     0.169
      0.000     1.000
            1.433E-01 3.022E-03 1.377E-02 5.349E-02 3.022E-03 3.022E-03
               3.022E-03 3.022E-03 3.022E-03
'
'              Geom ID       Type     B1       dBdL     HoB      Thick      Twist
   AeroOffs YDisNose
WINGPROF        62013 Shaped        2.877   -0.076    0.300    0.241     0.154
      0.000     1.000
            1.092E-01 2.023E-03 8.387E-03 3.347E-02 2.023E-03 2.023E-03
```

```
            2.023E-03 2.023E-03 2.023E-03
'
'           Geom ID      Type     B1      dBdL     HoB     Thick     Twist   AeroOffs YDisNose
 WINGPROF     62014  Shaped      2.598   -0.073   0.300   0.241   0.146    0.000   1.000
          8.385E-02 1.433E-03 5.288E-03 2.231E-02 1.433E-03 1.433E-03 1.433E-03 1.433E-03 1.433E-03
'
'           Geom ID      Type     B1      dBdL     HoB     Thick     Twist   AeroOffs YDisNose
 WINGPROF     62015  Shaped      2.381   -0.081   0.300   0.241   0.142    0.000   1.000
          6.472E-02 1.057E-03 3.414E-03 1.563E-02 1.057E-03 1.057E-03 1.057E-03 1.057E-03 1.057E-03
'
'           Geom ID      Type     B1      dBdL     HoB     Thick     Twist   AeroOffs YDisNose
 WINGPROF     62016  Shaped      2.190   -0.105   0.300   0.241   0.136    0.000   1.000
          4.966E-02 7.712E-04 2.238E-03 1.109E-02 7.712E-04 7.712E-04 7.712E-04 7.712E-04 7.712E-04
'
'           Geom ID      Type     B1      dBdL     HoB     Thick     Twist   AeroOffs YDisNose
 WINGPROF     62017  Shaped      1.991   -0.105   0.300   0.241   0.136    0.000   1.000
          3.768E-02 5.470E-04 1.396E-03 7.702E-03 5.470E-04 5.470E-04 5.470E-04 5.470E-04 5.470E-04
'
'           Geom ID      Type     B1      dBdL     HoB     Thick     Twist   AeroOffs YDisNose
 WINGPROF     62018  Shaped      1.833   -0.316   0.300   0.241   0.132    0.000   1.000
          2.825E-02 3.751E-04 8.212E-04 5.182E-03 3.751E-04 3.751E-04 3.751E-04 3.751E-04 3.751E-04
'
```

```
'                Geom  ID       Type     B1       dBdL     HoB      Thick      Twist
   AeroOffs  YDisNose
 WINGPROF        62019  Shaped        1.449   −0.351    0.300     0.241     0.131
       0.000     1.000
             2.097E−02  2.503E−04  5.309E−04  3.490E−03  2.503E−04  2.503E−04
                 2.503E−04  2.503E−04  2.503E−04
'
'                Geom  ID       Type     B1       dBdL     HoB      Thick      Twist
   AeroOffs  YDisNose
 WINGPROF        62020  Shaped        1.109   −0.351    0.300     0.241     0.131
       0.000     1.000
             1.514E−02  1.504E−04  2.985E−04  2.137E−03  1.504E−04  1.504E−04
                 1.504E−04  1.504E−04  1.504E−04
'
'                Geom  ID       Type     B1       dBdL     HoB      Thick      Twist
   AeroOffs  YDisNose
 WINGPROF        62021  Shaped        0.837   −0.351    0.300     0.241     0.131
       0.000     1.000
             1.048E−02  7.055E−05  1.127E−04  1.054E−03  7.055E−05  7.055E−05
                 7.055E−05  7.055E−05  7.055E−05
'
'                Geom  ID       Type     B1       dBdL     HoB      Thick      Twist
   AeroOffs  YDisNose
 WINGPROF        63002  Shaped        5.380    0.008    0.300     0.982     0.010
       0.000     1.000
             8.947E−01  1.344E+00  3.098E+00  3.014E+00  1.344E+00  1.344E+00
                 1.344E+00  1.344E+00  1.344E+00
'
'                Geom  ID       Type     B1       dBdL     HoB      Thick      Twist
   AeroOffs  YDisNose
 WINGPROF        63003  Shaped        5.428    0.056    0.300     0.797     0.211
       0.000     1.000
             7.750E−01  8.288E−01  2.045E+00  2.384E+00  8.288E−01  8.288E−01
                 8.288E−01  8.288E−01  8.288E−01
'
'                Geom  ID       Type     B1       dBdL     HoB      Thick      Twist
   AeroOffs  YDisNose
```

```
WINGPROF      63004  Shaped      5.777    0.059    0.300    0.540    0.599
    0.000    1.000
          6.172E-01  2.827E-01  9.204E-01  1.519E+00  2.827E-01  2.827E-01
             2.827E-01  2.827E-01  2.827E-01
'
'              Geom  ID      Type    B1      dBdL    HoB     Thick    Twist
   AeroOffs  YDisNose
WINGPROF      63005  Shaped      6.140    0.002    0.300    0.393    0.370
    0.000    1.000
          4.898E-01  1.127E-01  4.817E-01  1.072E+00  1.127E-01  1.127E-01
             1.127E-01  1.127E-01  1.127E-01
'
'              Geom  ID      Type    B1      dBdL    HoB     Thick    Twist
   AeroOffs  YDisNose
WINGPROF      63006  Shaped      6.154   -0.048    0.300    0.328    0.207
    0.000    1.000
          4.226E-01  5.858E-02  2.877E-01  8.412E-01  5.858E-02  5.858E-02
             5.858E-02  5.858E-02  5.858E-02
'
'              Geom  ID      Type    B1      dBdL    HoB     Thick    Twist
   AeroOffs  YDisNose
WINGPROF      63007  Shaped      5.857   -0.072    0.300    0.290    0.194
    0.000    1.000
          3.838E-01  3.560E-02  1.818E-01  6.022E-01  3.560E-02  3.560E-02
             3.560E-02  3.560E-02  3.560E-02
'
'              Geom  ID      Type    B1      dBdL    HoB     Thick    Twist
   AeroOffs  YDisNose
WINGPROF      63008  Shaped      5.412   -0.084    0.300    0.266    0.209
    0.000    1.000
          3.409E-01  2.200E-02  1.135E-01  4.223E-01  2.200E-02  2.200E-02
             2.200E-02  2.200E-02  2.200E-02
'
'              Geom  ID      Type    B1      dBdL    HoB     Thick    Twist
   AeroOffs  YDisNose
WINGPROF      63009  Shaped      4.889   -0.089    0.300    0.251    0.219
    0.000    1.000
```

```
          2.915E-01 1.335E-02 6.845E-02 2.689E-01 1.335E-02 1.335E-02 1.335E-02 1.335E-02 1.335E-02
'
'          Geom ID     Type     B1     dBdL    HoB    Thick    Twist AeroOffs YDisNose
WINGPROF    63010 Shaped    4.336  -0.089   0.300   0.243   0.205    0.000    1.000
          2.413E-01 8.120E-03 4.125E-02 1.622E-01 8.120E-03 8.120E-03 8.120E-03 8.120E-03 8.120E-03
'
'          Geom ID     Type     B1     dBdL    HoB    Thick    Twist AeroOffs YDisNose
WINGPROF    63011 Shaped    3.786  -0.086   0.300   0.241   0.184    0.000    1.000
          1.900E-01 4.852E-03 2.378E-02 9.156E-02 4.852E-03 4.852E-03 4.852E-03 4.852E-03 4.852E-03
'
'          Geom ID     Type     B1     dBdL    HoB    Thick    Twist AeroOffs YDisNose
WINGPROF    63012 Shaped    3.257  -0.082   0.300   0.241   0.169    0.000    1.000
          1.433E-01 3.022E-03 1.377E-02 5.349E-02 3.022E-03 3.022E-03 3.022E-03 3.022E-03 3.022E-03
'
'          Geom ID     Type     B1     dBdL    HoB    Thick    Twist AeroOffs YDisNose
WINGPROF    63013 Shaped    2.877  -0.076   0.300   0.241   0.154    0.000    1.000
          1.092E-01 2.023E-03 8.387E-03 3.347E-02 2.023E-03 2.023E-03 2.023E-03 2.023E-03 2.023E-03
'
'          Geom ID     Type     B1     dBdL    HoB    Thick    Twist AeroOffs YDisNose
WINGPROF    63014 Shaped    2.598  -0.073   0.300   0.241   0.146    0.000    1.000
          8.385E-02 1.433E-03 5.288E-03 2.231E-02 1.433E-03 1.433E-03 1.433E-03 1.433E-03 1.433E-03
```

```
'
'                Geom ID        Type      B1       dBdL     HoB      Thick      Twist
    AeroOffs  YDisNose
WINGPROF       63015  Shaped        2.381    -0.081     0.300     0.241     0.142
        0.000     1.000
            6.472E-02  1.057E-03  3.414E-03  1.563E-02  1.057E-03  1.057E-03
                1.057E-03  1.057E-03  1.057E-03
'
'                Geom ID        Type      B1       dBdL     HoB      Thick      Twist
    AeroOffs  YDisNose
WINGPROF       63016  Shaped        2.190    -0.105     0.300     0.241     0.136
        0.000     1.000
            4.966E-02  7.712E-04  2.238E-03  1.109E-02  7.712E-04  7.712E-04
                7.712E-04  7.712E-04  7.712E-04
'
'                Geom ID        Type      B1       dBdL     HoB      Thick      Twist
    AeroOffs  YDisNose
WINGPROF       63017  Shaped        1.991    -0.105     0.300     0.241     0.136
        0.000     1.000
            3.768E-02  5.470E-04  1.396E-03  7.702E-03  5.470E-04  5.470E-04
                5.470E-04  5.470E-04  5.470E-04
'
'                Geom ID        Type      B1       dBdL     HoB      Thick      Twist
    AeroOffs  YDisNose
WINGPROF       63018  Shaped        1.833    -0.316     0.300     0.241     0.132
        0.000     1.000
            2.825E-02  3.751E-04  8.212E-04  5.182E-03  3.751E-04  3.751E-04
                3.751E-04  3.751E-04  3.751E-04
'
'                Geom ID        Type      B1       dBdL     HoB      Thick      Twist
    AeroOffs  YDisNose
WINGPROF       63019  Shaped        1.449    -0.351     0.300     0.241     0.131
        0.000     1.000
            2.097E-02  2.503E-04  5.309E-04  3.490E-03  2.503E-04  2.503E-04
                2.503E-04  2.503E-04  2.503E-04
'
'                Geom ID        Type      B1       dBdL     HoB      Thick      Twist
```

```
    AeroOffs  YDisNose
WINGPROF        63020  Shaped        1.109   −0.351    0.300    0.241    0.131
        0.000    1.000
            1.514E−02  1.504E−04  2.985E−04  2.137E−03  1.504E−04  1.504E−04
                1.504E−04  1.504E−04  1.504E−04
'
'                Geom  ID        Type      B1       dBdL      HoB      Thick       Twist
    AeroOffs  YDisNose
WINGPROF        63021  Shaped        0.837   −0.351    0.300    0.241    0.131
        0.000    1.000
            1.048E−02  7.055E−05  1.127E−04  1.054E−03  7.055E−05  7.055E−05
                7.055E−05  7.055E−05  7.055E−05
'
'                Elem  ID  iBlade  Radius     R_Elem     XiMean     Twist     PA_to_AC
      StruOffZ
BLADEELEM    61004          1     89.166      5.775       0.068    −14.469       0.000
        0.000
BLADEELEM    61005          1     89.166     11.954       0.140    −13.784       0.000
        0.000
BLADEELEM    61006          1     89.166     18.141       0.213    −11.276       0.000
        0.000
BLADEELEM    61007          1     89.166     24.329       0.286     −8.278       0.000
        0.000
BLADEELEM    61008          1     89.166     30.518       0.358     −6.492       0.000
        0.000
BLADEELEM    61009          1     89.166     36.707       0.431     −5.249       0.000
        0.000
BLADEELEM    61010          1     89.166     42.896       0.504     −4.001       0.000
        0.000
BLADEELEM    61011          1     89.166     49.086       0.576     −2.676       0.000
        0.000
BLADEELEM    61012          1     89.166     55.275       0.649     −1.364       0.000
        0.000
BLADEELEM    61013          1     89.166     61.464       0.721     −0.161       0.000
        0.000
BLADEELEM    61014          1     89.166     66.870       0.785      0.798       0.000
        0.000
```

```
BLADELEM    61015    1    89.166    71.030    0.834    1.473    0.000
    0.000
BLADELEM    61016    1    89.166    74.359    0.873    1.972    0.000
    0.000
BLADELEM    61017    1    89.166    77.021    0.904    2.355    0.000
    0.000
BLADELEM    61018    1    89.166    79.151    0.929    2.652    0.000
    0.000
BLADELEM    61019    1    89.166    80.855    0.949    2.884    0.000
    0.000
BLADELEM    61020    1    89.166    82.219    0.965    3.067    0.000
    0.000
BLADELEM    61021    1    89.166    83.309    0.978    3.210    0.000
    0.000
BLADELEM    61022    1    89.166    84.182    0.988    3.325    0.000
    0.000
BLADELEM    61023    1    89.166    84.880    0.996    3.417    0.000
    0.000
BLADELEM    62004    2    89.166     5.775    0.068  -14.469    0.000
    0.000
BLADELEM    62005    2    89.166    11.954    0.140  -13.784    0.000
    0.000
BLADELEM    62006    2    89.166    18.141    0.213  -11.276    0.000
    0.000
BLADELEM    62007    2    89.166    24.330    0.286   -8.278    0.000
    0.000
BLADELEM    62008    2    89.166    30.519    0.358   -6.492    0.000
    0.000
BLADELEM    62009    2    89.166    36.708    0.431   -5.249    0.000
    0.000
BLADELEM    62010    2    89.166    42.898    0.504   -4.001    0.000
    0.000
BLADELEM    62011    2    89.166    49.087    0.576   -2.676    0.000
    0.000
BLADELEM    62012    2    89.166    55.277    0.649   -1.364    0.000
    0.000
BLADELEM    62013    2    89.166    61.466    0.721   -0.161    0.000
```

```
      0.000
BLADELEM  62014     2   89.166   66.872    0.785    0.798    0.000
      0.000
BLADELEM  62015     2   89.166   71.033    0.834    1.473    0.000
      0.000
BLADELEM  62016     2   89.166   74.361    0.873    1.972    0.000
      0.000
BLADELEM  62017     2   89.166   77.024    0.904    2.355    0.000
      0.000
BLADELEM  62018     2   89.166   79.154    0.929    2.652    0.000
      0.000
BLADELEM  62019     2   89.166   80.858    0.949    2.884    0.000
      0.000
BLADELEM  62020     2   89.166   82.221    0.965    3.067    0.000
      0.000
BLADELEM  62021     2   89.166   83.312    0.978    3.210    0.000
      0.000
BLADELEM  62022     2   89.166   84.185    0.988    3.325    0.000
      0.000
BLADELEM  62023     2   89.166   84.883    0.996    3.417    0.000
      0.000
BLADELEM  63004     3   89.166    5.775    0.068  -14.469    0.000
      0.000
BLADELEM  63005     3   89.166   11.954    0.140  -13.784    0.000
      0.000
BLADELEM  63006     3   89.166   18.141    0.213  -11.276    0.000
      0.000
BLADELEM  63007     3   89.166   24.330    0.286   -8.278    0.000
      0.000
BLADELEM  63008     3   89.166   30.519    0.358   -6.492    0.000
      0.000
BLADELEM  63009     3   89.166   36.708    0.431   -5.249    0.000
      0.000
BLADELEM  63010     3   89.166   42.898    0.504   -4.001    0.000
      0.000
BLADELEM  63011     3   89.166   49.087    0.576   -2.676    0.000
      0.000
```

```
BLADELEM    63012    3    89.166    55.277    0.649    -1.364    0.000
        0.000
BLADELEM    63013    3    89.166    61.466    0.721    -0.161    0.000
        0.000
BLADELEM    63014    3    89.166    66.872    0.785     0.798    0.000
        0.000
BLADELEM    63015    3    89.166    71.033    0.834     1.473    0.000
        0.000
BLADELEM    63016    3    89.166    74.361    0.873     1.972    0.000
        0.000
BLADELEM    63017    3    89.166    77.024    0.904     2.355    0.000
        0.000
BLADELEM    63018    3    89.166    79.154    0.929     2.652    0.000
        0.000
BLADELEM    63019    3    89.166    80.858    0.949     2.884    0.000
        0.000
BLADELEM    63020    3    89.166    82.221    0.965     3.067    0.000
        0.000
BLADELEM    63021    3    89.166    83.312    0.978     3.210    0.000
        0.000
BLADELEM    63022    3    89.166    84.185    0.988     3.325    0.000
        0.000
BLADELEM    63023    3    89.166    84.883    0.996     3.417    0.000
        0.000
'
'            Loc-Coo         dx            dy            dz
UNITVEC        6011      0.00000      -1.00000       0.00000
UNITVEC        6021     -0.07548       0.50000      -0.86273
UNITVEC        6031      0.07548       0.50000       0.86273
UNITVEC       61004      0.97884      -0.19937       0.04618
UNITVEC       61005      0.98028      -0.19213       0.04625
UNITVEC       61006      0.98875      -0.14213       0.04665
UNITVEC       61007      0.99506      -0.08745       0.04694
UNITVEC       61008      0.99705      -0.06057       0.04704
UNITVEC       61009      0.99812      -0.03917       0.04709
UNITVEC       61010      0.99873      -0.01768       0.04712
UNITVEC       61011      0.99887       0.00564       0.04712
```

```
UNITVEC    61012    0.99847     0.02880     0.04711
UNITVEC    61013    0.99765     0.04986     0.04707
UNITVEC    61014    0.99669     0.06629     0.04702
UNITVEC    61015    0.99585     0.07800     0.04698
UNITVEC    61016    0.99513     0.08672     0.04695
UNITVEC    61017    0.99453     0.09337     0.04692
UNITVEC    61018    0.99403     0.09848     0.04690
UNITVEC    61019    0.99363     0.10251     0.04688
UNITVEC    61020    0.99329     0.10569     0.04686
UNITVEC    61021    0.99303     0.10818     0.04685
UNITVEC    61022    0.99281     0.11017     0.04684
UNITVEC    61023    0.99263     0.11176     0.04683
UNITVEC    62004    0.94662    -0.01404    -0.32205
UNITVEC    62005    0.94859    -0.01783    -0.31602
UNITVEC    62006    0.96068    -0.04381    -0.27418
UNITVEC    62007    0.97101    -0.07188    -0.22798
UNITVEC    62008    0.97499    -0.08555    -0.20510
UNITVEC    62009    0.97766    -0.09638    -0.18679
UNITVEC    62010    0.97988    -0.10720    -0.16835
UNITVEC    62011    0.98177    -0.11887    -0.14825
UNITVEC    62012    0.98313    -0.13040    -0.12820
UNITVEC    62013    0.98391    -0.14084    -0.10991
UNITVEC    62014    0.98421    -0.14894    -0.09559
UNITVEC    62015    0.98428    -0.15470    -0.08536
UNITVEC    62016    0.98422    -0.15897    -0.07773
UNITVEC    62017    0.98414    -0.16223    -0.07190
UNITVEC    62018    0.98403    -0.16473    -0.06741
UNITVEC    62019    0.98394    -0.16670    -0.06387
UNITVEC    62020    0.98385    -0.16824    -0.06107
UNITVEC    62021    0.98378    -0.16946    -0.05889
UNITVEC    62022    0.98371    -0.17043    -0.05713
UNITVEC    62023    0.98365    -0.17121    -0.05574
UNITVEC    63004    0.97672     0.21341     0.02196
UNITVEC    63005    0.97759     0.20996     0.01549
UNITVEC    63006    0.98213     0.18594    -0.02895
UNITVEC    63007    0.98421     0.15933    -0.07708
UNITVEC    63008    0.98414     0.14612    -0.10058
```

```
UNITVEC    63009    0.98357    0.13555    −0.11921
UNITVEC    63010    0.98255    0.12488    −0.13784
UNITVEC    63011    0.98092    0.11323    −0.15797
UNITVEC    63012    0.97878    0.10160    −0.17790
UNITVEC    63013    0.97639    0.09098    −0.19594
UNITVEC    63014    0.97421    0.08265    −0.20997
UNITVEC    63015    0.97250    0.07670    −0.21995
UNITVEC    63016    0.97113    0.07225    −0.22735
UNITVEC    63017    0.97004    0.06886    −0.23300
UNITVEC    63018    0.96916    0.06625    −0.23734
UNITVEC    63019    0.96846    0.06419    −0.24075
UNITVEC    63020    0.96790    0.06255    −0.24344
UNITVEC    63021    0.96745    0.06128    −0.24555
UNITVEC    63022    0.96708    0.06026    −0.24724
UNITVEC    63023    0.96678    0.05945    −0.24858
'
'          Ecc−ID          Ex          Ey          Ez
'
'          Mat    ID    E−mod    Poiss    Yield    Density    ThermX
MISOIEP    61004    2.000E+10    3.000E−01    5.000E+10    1.332E+03    1.000E−06
MISOIEP    61005    2.000E+10    3.000E−01    5.000E+10    1.315E+03    1.000E−06
MISOIEP    61006    2.000E+10    3.000E−01    5.000E+10    1.321E+03    1.000E−06
MISOIEP    61007    2.000E+10    3.000E−01    5.000E+10    1.352E+03    1.000E−06
MISOIEP    61008    2.000E+10    3.000E−01    5.000E+10    1.351E+03    1.000E−06
MISOIEP    61009    2.000E+10    3.000E−01    5.000E+10    1.313E+03    1.000E−06
MISOIEP    61010    2.000E+10    3.000E−01    5.000E+10    1.290E+03    1.000E−06
MISOIEP    61011    2.000E+10    3.000E−01    5.000E+10    1.260E+03    1.000E−06
MISOIEP    61012    2.000E+10    3.000E−01    5.000E+10    1.234E+03
```

```
        1.000E-06
MISOIEP      61013   2.000E+10   3.000E-01   5.000E+10   1.219E+03
        1.000E-06
MISOIEP      61014   2.000E+10   3.000E-01   5.000E+10   1.227E+03
        1.000E-06
MISOIEP      61015   2.000E+10   3.000E-01   5.000E+10   1.246E+03
        1.000E-06
MISOIEP      61016   2.000E+10   3.000E-01   5.000E+10   1.272E+03
        1.000E-06
MISOIEP      61017   2.000E+10   3.000E-01   5.000E+10   1.311E+03
        1.000E-06
MISOIEP      61018   2.000E+10   3.000E-01   5.000E+10   1.350E+03
        1.000E-06
MISOIEP      61019   2.000E+10   3.000E-01   5.000E+10   1.399E+03
        1.000E-06
MISOIEP      61020   2.000E+10   3.000E-01   5.000E+10   1.455E+03
        1.000E-06
MISOIEP      61021   2.000E+10   3.000E-01   5.000E+10   1.509E+03
        1.000E-06
MISOIEP      61022   2.000E+10   3.000E-01   5.000E+10   1.589E+03
        1.000E-06
MISOIEP      61023   2.000E+10   3.000E-01   5.000E+10   1.717E+03
        1.000E-06
MISOIEP      62004   2.000E+10   3.000E-01   5.000E+10   1.332E+03
        1.000E-06
MISOIEP      62005   2.000E+10   3.000E-01   5.000E+10   1.315E+03
        1.000E-06
MISOIEP      62006   2.000E+10   3.000E-01   5.000E+10   1.321E+03
        1.000E-06
MISOIEP      62007   2.000E+10   3.000E-01   5.000E+10   1.352E+03
        1.000E-06
MISOIEP      62008   2.000E+10   3.000E-01   5.000E+10   1.351E+03
        1.000E-06
MISOIEP      62009   2.000E+10   3.000E-01   5.000E+10   1.313E+03
        1.000E-06
MISOIEP      62010   2.000E+10   3.000E-01   5.000E+10   1.290E+03
        1.000E-06
```

```
MISOIEP    62011   2.000E+10   3.000E-01   5.000E+10   1.260E+03   1.000E-06
MISOIEP    62012   2.000E+10   3.000E-01   5.000E+10   1.234E+03   1.000E-06
MISOIEP    62013   2.000E+10   3.000E-01   5.000E+10   1.219E+03   1.000E-06
MISOIEP    62014   2.000E+10   3.000E-01   5.000E+10   1.227E+03   1.000E-06
MISOIEP    62015   2.000E+10   3.000E-01   5.000E+10   1.246E+03   1.000E-06
MISOIEP    62016   2.000E+10   3.000E-01   5.000E+10   1.272E+03   1.000E-06
MISOIEP    62017   2.000E+10   3.000E-01   5.000E+10   1.311E+03   1.000E-06
MISOIEP    62018   2.000E+10   3.000E-01   5.000E+10   1.350E+03   1.000E-06
MISOIEP    62019   2.000E+10   3.000E-01   5.000E+10   1.399E+03   1.000E-06
MISOIEP    62020   2.000E+10   3.000E-01   5.000E+10   1.455E+03   1.000E-06
MISOIEP    62021   2.000E+10   3.000E-01   5.000E+10   1.509E+03   1.000E-06
MISOIEP    62022   2.000E+10   3.000E-01   5.000E+10   1.589E+03   1.000E-06
MISOIEP    62023   2.000E+10   3.000E-01   5.000E+10   1.717E+03   1.000E-06
MISOIEP    63004   2.000E+10   3.000E-01   5.000E+10   1.332E+03   1.000E-06
MISOIEP    63005   2.000E+10   3.000E-01   5.000E+10   1.315E+03   1.000E-06
MISOIEP    63006   2.000E+10   3.000E-01   5.000E+10   1.321E+03   1.000E-06
MISOIEP    63007   2.000E+10   3.000E-01   5.000E+10   1.352E+03   1.000E-06
MISOIEP    63008   2.000E+10   3.000E-01   5.000E+10   1.351E+03   1.000E-06
MISOIEP    63009   2.000E+10   3.000E-01   5.000E+10   1.313E+03
```

```
    1.000E-06
MISOIEP    63010   2.000E+10   3.000E-01   5.000E+10   1.290E+03
    1.000E-06
MISOIEP    63011   2.000E+10   3.000E-01   5.000E+10   1.260E+03
    1.000E-06
MISOIEP    63012   2.000E+10   3.000E-01   5.000E+10   1.234E+03
    1.000E-06
MISOIEP    63013   2.000E+10   3.000E-01   5.000E+10   1.219E+03
    1.000E-06
MISOIEP    63014   2.000E+10   3.000E-01   5.000E+10   1.227E+03
    1.000E-06
MISOIEP    63015   2.000E+10   3.000E-01   5.000E+10   1.246E+03
    1.000E-06
MISOIEP    63016   2.000E+10   3.000E-01   5.000E+10   1.272E+03
    1.000E-06
MISOIEP    63017   2.000E+10   3.000E-01   5.000E+10   1.311E+03
    1.000E-06
MISOIEP    63018   2.000E+10   3.000E-01   5.000E+10   1.350E+03
    1.000E-06
MISOIEP    63019   2.000E+10   3.000E-01   5.000E+10   1.399E+03
    1.000E-06
MISOIEP    63020   2.000E+10   3.000E-01   5.000E+10   1.455E+03
    1.000E-06
MISOIEP    63021   2.000E+10   3.000E-01   5.000E+10   1.509E+03
    1.000E-06
MISOIEP    63022   2.000E+10   3.000E-01   5.000E+10   1.589E+03
    1.000E-06
MISOIEP    63023   2.000E+10   3.000E-01   5.000E+10   1.717E+03
    1.000E-06
'
'
'
   *-----------------------------------------------------------------------*
'      Aerodynamic  coefficients
'
   *-----------------------------------------------------------------------*
```

```
 W_Coeffs   100   ClCdCmPack   6   105
'Ri/R
 0.2480
 'alfa   Cl    Cd   Cm
 -180.0  0.0000  0.0000  0.0000
 -175.0  0.1736  0.0099  0.0218
 -170.0  0.3420  0.0392  0.0434
 -165.0  0.5000  0.0871  0.0647
 -160.0  0.6428  0.1521  0.0855
 -155.0  0.7660  0.2322  0.1057
 -150.0  0.8660  0.3250  0.1250
 -145.0  0.9397  0.4277  0.1434
 -140.0  0.9848  0.5371  0.1607
 -135.0  1.0000  0.6500  0.1768
 -130.0  0.9848  0.7629  0.1915
 -125.0  0.9397  0.8723  0.2048
 -120.0  0.8660  0.9750  0.2165
 -115.0  0.7660  1.0678  0.2266
 -110.0  0.6428  1.1479  0.2349
 -105.0  0.5000  1.2129  0.2415
 -100.0  0.3420  1.2608  0.2462
 -95.0  0.1736  1.2901  0.2490
 -90.0  0.0000  1.3000  0.2500
 -85.0  -0.1736  1.2901  0.2490
 -80.0  -0.3420  1.2608  0.2462
 -75.0  -0.5000  1.2129  0.2415
 -70.0  -0.6428  1.1479  0.2349
 -65.0  -0.7660  1.0678  0.2266
 -60.0  -0.8660  0.9750  0.2165
 -55.0  -0.9397  0.8723  0.1978
 -50.0  -0.9848  0.7629  0.1775
 -45.0  -1.0000  0.6500  0.1488
 -40.0  -0.9516  0.5282  0.1176
 -39.0  -0.9039  0.5026  0.1076
 -38.0  -0.8262  0.4671  0.0906
 -37.0  -0.7185  0.4345  0.0805
```

```
-36.0 -0.6208 0.3989 0.0665
-35.0 -0.5231 0.3634 0.0595
-34.0 -0.4454 0.3278 0.0524
-33.0 -0.3477 0.3013 0.0454
-32.0 -0.2571 0.2729 0.0470
-30.0 -0.1574 0.2332 0.0606
-28.0 -0.0776 0.2034 0.0742
-26.0 0.0115 0.1858 0.0875
-24.0 0.1007 0.1681 0.1008
-22.0 0.1962 0.1526 0.1133
-20.0 0.2918 0.1370 0.1258
-18.0 0.3932 0.1240 0.1370
-16.0 0.4947 0.1109 0.1482
-14.0 0.6004 0.1009 0.1571
-12.0 0.7061 0.0908 0.1660
-10.0 0.7880 0.0836 0.1677
-8.0 0.8700 0.0765 0.1694
-6.0 0.8358 0.0748 -0.1470
-4.0 0.8162 0.0731 -0.1259
-2.0 0.6603 0.0755 -0.0876
0.0 0.5199 0.0780 -0.0506
2.0 0.2636 0.0780 -0.0008
4.0 -0.0906 0.0708 0.0696
6.0 0.1656 0.0748 0.0197
8.0 0.4475 0.0859 -0.0272
10.0 0.7071 0.0999 -0.0671
12.0 0.9540 0.1115 -0.1033
14.0 1.1891 0.1207 -0.1369
16.0 1.4183 0.1368 -0.1687
18.0 1.6392 0.1500 -0.1989
20.0 1.8216 0.1689 -0.2252
22.0 1.9837 0.2066 -0.2509
24.0 2.0985 0.3092 -0.2747
26.0 2.1904 0.4344 -0.2966
28.0 2.2541 0.5512 -0.3171
30.0 2.2731 0.6732 -0.3335
32.0 2.2740 0.7756 -0.3485
```

```
33.0 2.2780 0.8209 -0.3466
34.0 2.2658 0.8551 -0.3476
35.0 2.2408 0.8862 -0.3487
36.0 2.2331 0.9141 -0.3427
37.0 2.2134 0.9390 -0.3366
38.0 2.1820 0.9709 -0.3305
39.0 2.1391 0.9996 -0.3244
40.0 2.0951 1.0254 -0.3183
45.0 1.8370 1.1419 -0.3003
50.0 1.5156 1.1615 -0.2914
55.0 1.2008 1.1657 -0.2824
60.0 0.9660 1.1750 -0.2735
65.0 0.7660 1.1778 -0.2636
70.0 0.6428 1.1979 -0.2549
75.0 0.5000 1.2129 -0.2515
80.0 0.3420 1.2608 -0.2462
85.0 0.1736 1.2901 -0.2490
90.0 0.0000 1.3000 -0.2500
95.0 -0.1736 1.2901 -0.2490
100.0 -0.3420 1.2608 -0.2462
105.0 -0.5000 1.2129 -0.2415
110.0 -0.6428 1.1479 -0.2349
115.0 -0.7660 1.0678 -0.2266
120.0 -0.8660 0.9750 -0.2165
125.0 -0.9397 0.8723 -0.2048
130.0 -0.9848 0.7629 -0.1915
135.0 -1.0000 0.6500 -0.1768
140.0 -0.9848 0.5371 -0.1607
145.0 -0.9397 0.4277 -0.1434
150.0 -0.8660 0.3250 -0.1250
155.0 -0.7660 0.2322 -0.1057
160.0 -0.6428 0.1521 -0.0855
165.0 -0.5000 0.0871 -0.0647
170.0 -0.3420 0.0392 -0.0434
175.0 -0.1736 0.0099 -0.0218
180.0 0.0000 0.0000 0.0000
'Ri/R
```

```
0.2734
'alfa   Cl     Cd   Cm
-180.0 0.0000 0.0000 0.0000
-175.0 0.1736 0.0099 0.0218
-170.0 0.3420 0.0392 0.0434
-165.0 0.5000 0.0871 0.0647
-160.0 0.6428 0.1521 0.0855
-155.0 0.7660 0.2322 0.1057
-150.0 0.8660 0.3250 0.1250
-145.0 0.9397 0.4277 0.1434
-140.0 0.9848 0.5371 0.1607
-135.0 1.0000 0.6500 0.1768
-130.0 0.9848 0.7629 0.1915
-125.0 0.9397 0.8723 0.2048
-120.0 0.8660 0.9750 0.2165
-115.0 0.7660 1.0678 0.2266
-110.0 0.6428 1.1479 0.2349
-105.0 0.5000 1.2129 0.2415
-100.0 0.3420 1.2608 0.2462
-95.0 0.1736 1.2901 0.2490
-90.0 0.0000 1.3000 0.2500
-85.0 -0.1736 1.2901 0.2490
-80.0 -0.3420 1.2608 0.2462
-75.0 -0.5000 1.2129 0.2415
-70.0 -0.6428 1.1479 0.2349
-65.0 -0.7660 1.0678 0.2266
-60.0 -0.8660 0.9750 0.2165
-55.0 -0.9397 0.8723 0.1978
-50.0 -0.9848 0.7629 0.1775
-45.0 -1.0000 0.6500 0.1558
-40.0 -0.9816 0.5352 0.1246
-39.0 -0.9539 0.5136 0.1106
-38.0 -0.9262 0.4851 0.0966
-37.0 -0.8885 0.4565 0.0825
-36.0 -0.8508 0.4279 0.0655
-35.0 -0.8231 0.3924 0.0585
-34.0 -0.7854 0.3638 0.0484
```

```
-33.0 -0.7477 0.3383 0.0384
-32.0 -0.7011 0.3123 0.0305
-30.0 -0.6208 0.2663 0.0200
-28.0 -0.5406 0.2402 0.0094
-26.0 -0.4694 0.2169 -0.0006
-24.0 -0.3881 0.1936 -0.0106
-22.0 -0.3161 0.1732 -0.0197
-20.0 -0.2442 0.1529 -0.0289
-18.0 -0.1641 0.1355 -0.0368
-16.0 -0.0841 0.1180 -0.0448
-14.0 0.0021 0.1035 -0.0510
-12.0 0.0883 0.0890 -0.0572
-10.0 0.1722 0.0773 -0.0604
-8.0 0.2561 0.0656 -0.0636
-6.0 0.3179 0.0563 -0.0605
-4.0 0.3798 0.0470 -0.0574
-2.0 0.3573 0.0405 -0.0351
0.0 0.3348 0.0341 -0.0128
2.0 0.5652 0.0316 -0.0494
4.0 0.8769 0.0343 -0.0894
6.0 1.0425 0.0451 -0.1117
8.0 0.9487 0.0700 -0.1208
10.0 0.9088 0.0886 -0.1376
12.0 0.9761 0.0993 -0.1594
14.0 1.1130 0.1070 -0.1823
16.0 1.3065 0.1163 -0.2066
18.0 1.5414 0.1317 -0.2315
20.0 1.8049 0.1570 -0.2566
22.0 2.0020 0.2757 -0.2806
24.0 2.1216 0.4224 -0.3057
26.0 2.1916 0.5610 -0.3294
28.0 2.2291 0.6861 -0.3520
30.0 2.2322 0.7958 -0.3710
32.0 2.2188 0.8915 -0.3878
33.0 2.2092 0.9229 -0.3845
34.0 2.1927 0.9472 -0.3806
35.0 2.1625 0.9664 -0.3747
```

```
 36.0 2.1313 0.9889 −0.3687
 37.0 2.0878 1.0073 −0.3626
 38.0 2.0435 1.0284 −0.3565
 39.0 1.9984 1.0521 −0.3504
 40.0 1.9418 1.0769 −0.3443
 45.0 1.6775 1.1697 −0.3233
 50.0 1.2856 1.1965 −0.3044
 55.0 1.0308 1.1957 −0.2954
 60.0 0.8660 1.1900 −0.2865
 65.0 0.7660 1.1928 −0.2766
 70.0 0.6428 1.2029 −0.2649
 75.0 0.5000 1.2129 −0.2515
 80.0 0.3420 1.2608 −0.2462
 85.0 0.1736 1.2901 −0.2490
 90.0 0.0000 1.3000 −0.2500
 95.0 −0.1736 1.2901 −0.2490
 100.0 −0.3420 1.2608 −0.2462
 105.0 −0.5000 1.2129 −0.2415
 110.0 −0.6428 1.1479 −0.2349
 115.0 −0.7660 1.0678 −0.2266
 120.0 −0.8660 0.9750 −0.2165
 125.0 −0.9397 0.8723 −0.2048
 130.0 −0.9848 0.7629 −0.1915
 135.0 −1.0000 0.6500 −0.1768
 140.0 −0.9848 0.5371 −0.1607
 145.0 −0.9397 0.4277 −0.1434
 150.0 −0.8660 0.3250 −0.1250
 155.0 −0.7660 0.2322 −0.1057
 160.0 −0.6428 0.1521 −0.0855
 165.0 −0.5000 0.0871 −0.0647
 170.0 −0.3420 0.0392 −0.0434
 175.0 −0.1736 0.0099 −0.0218
 180.0 0.0000 0.0000 0.0000
'Ri/R
 0.3274
 'alfa   Cl    Cd   Cm
 −180.0 0.0000 0.0000 0.0000
```

```
−175.0 0.1736 0.0099 0.0218
−170.0 0.3420 0.0392 0.0434
−165.0 0.5000 0.0871 0.0647
−160.0 0.6428 0.1521 0.0855
−155.0 0.7660 0.2322 0.1057
−150.0 0.8660 0.3250 0.1250
−145.0 0.9397 0.4277 0.1434
−140.0 0.9848 0.5371 0.1607
−135.0 1.0000 0.6500 0.1768
−130.0 0.9848 0.7629 0.1915
−125.0 0.9397 0.8723 0.2048
−120.0 0.8660 0.9750 0.2165
−115.0 0.7660 1.0678 0.2266
−110.0 0.6428 1.1479 0.2349
−105.0 0.5000 1.2129 0.2415
−100.0 0.3420 1.2608 0.2462
−95.0 0.1736 1.2901 0.2490
−90.0 0.0000 1.3000 0.2500
−85.0 −0.1736 1.2901 0.2490
−80.0 −0.3420 1.2608 0.2462
−75.0 −0.5000 1.2129 0.2415
−70.0 −0.6428 1.1479 0.2349
−65.0 −0.7660 1.0678 0.2266
−60.0 −0.8660 0.9750 0.2165
−55.0 −0.9397 0.8723 0.2048
−50.0 −0.9848 0.7629 0.1915
−45.0 −1.0000 0.6500 0.1768
−40.0 −0.9716 0.5352 0.1416
−39.0 −0.9639 0.5136 0.1346
−38.0 −0.9462 0.4851 0.1276
−37.0 −0.9285 0.4635 0.1205
−36.0 −0.9108 0.4349 0.1135
−35.0 −0.8931 0.4064 0.0965
−34.0 −0.8854 0.3778 0.0794
−33.0 −0.8677 0.3523 0.0624
−32.0 −0.8564 0.3315 0.0447
−30.0 −0.8378 0.2777 0.0327
```

```
-28.0 -0.8191 0.2338 0.0208
-26.0 -0.7924 0.2045 0.0102
-24.0 -0.7756 0.1751 -0.0004
-22.0 -0.7441 0.1513 -0.0089
-20.0 -0.7126 0.1274 -0.0174
-18.0 -0.6678 0.1085 -0.0229
-16.0 -0.6231 0.0896 -0.0285
-14.0 -0.5742 0.0748 -0.0300
-12.0 -0.5252 0.0600 -0.0314
-10.0 -0.4827 0.0485 -0.0279
-8.0 -0.4402 0.0370 -0.0244
-6.0 -0.2983 0.0294 -0.0359
-4.0 -0.1564 0.0219 -0.0474
-2.0 0.1744 0.0203 -0.0782
0.0 0.5053 0.0187 -0.1090
2.0 0.8241 0.0188 -0.1329
4.0 1.1209 0.0196 -0.1510
6.0 1.3897 0.0213 -0.1630
8.0 1.6254 0.0240 -0.1691
10.0 1.8109 0.0279 -0.1683
12.0 1.8589 0.0365 -0.1585
14.0 1.8159 0.0760 -0.1558
16.0 1.7786 0.1165 -0.1670
18.0 1.7560 0.1571 -0.1809
20.0 1.7630 0.2063 -0.1960
22.0 1.8002 0.3057 -0.2143
24.0 1.8495 0.4153 -0.2365
26.0 1.8775 0.5163 -0.2588
28.0 1.8828 0.6069 -0.2797
30.0 1.8689 0.6892 -0.2983
32.0 1.8439 0.7625 -0.3147
33.0 1.8349 0.7954 -0.3166
34.0 1.8297 0.8232 -0.3106
35.0 1.8136 0.8446 -0.3047
36.0 1.7854 0.8684 -0.2987
37.0 1.7669 0.8912 -0.2926
38.0 1.7269 0.9066 -0.2865
```

```
39.0 1.6864 0.9255 -0.2844
40.0 1.6458 0.9385 -0.2803
45.0 1.4473 1.0290 -0.2633
50.0 1.1356 1.0715 -0.2544
55.0 0.9808 1.0857 -0.2454
60.0 0.8660 1.1000 -0.2365
65.0 0.7660 1.1278 -0.2366
70.0 0.6428 1.1629 -0.2389
75.0 0.5000 1.2129 -0.2415
80.0 0.3420 1.2608 -0.2462
85.0 0.1736 1.2901 -0.2490
90.0 0.0000 1.3000 -0.2500
95.0 -0.1736 1.2901 -0.2490
100.0 -0.3420 1.2608 -0.2462
105.0 -0.5000 1.2129 -0.2415
110.0 -0.6428 1.1479 -0.2349
115.0 -0.7660 1.0678 -0.2266
120.0 -0.8660 0.9750 -0.2165
125.0 -0.9397 0.8723 -0.2048
130.0 -0.9848 0.7629 -0.1915
135.0 -1.0000 0.6500 -0.1768
140.0 -0.9848 0.5371 -0.1607
145.0 -0.9397 0.4277 -0.1434
150.0 -0.8660 0.3250 -0.1250
155.0 -0.7660 0.2322 -0.1057
160.0 -0.6428 0.1521 -0.0855
165.0 -0.5000 0.0871 -0.0647
170.0 -0.3420 0.0392 -0.0434
175.0 -0.1736 0.0099 -0.0218
180.0 0.0000 0.0000 0.0000
'Ri/R
0.3772
'alfa   Cl    Cd   Cm
-180.0 0.0000 0.0000 0.0000
-175.0 0.1736 0.0099 0.0218
-170.0 0.3420 0.0392 0.0434
-165.0 0.5000 0.0871 0.0647
```

```
-160.0 0.6428 0.1521 0.0855
-155.0 0.7660 0.2322 0.1057
-150.0 0.8660 0.3250 0.1250
-145.0 0.9397 0.4277 0.1434
-140.0 0.9848 0.5371 0.1607
-135.0 1.0000 0.6500 0.1768
-130.0 0.9848 0.7629 0.1915
-125.0 0.9397 0.8723 0.2048
-120.0 0.8660 0.9750 0.2165
-115.0 0.7660 1.0678 0.2266
-110.0 0.6428 1.1479 0.2349
-105.0 0.5000 1.2129 0.2415
-100.0 0.3420 1.2608 0.2462
-95.0 0.1736 1.2901 0.2490
-90.0 0.0000 1.3000 0.2500
-85.0 -0.1736 1.2901 0.2490
-80.0 -0.3420 1.2608 0.2462
-75.0 -0.5000 1.2129 0.2415
-70.0 -0.6428 1.1479 0.2349
-65.0 -0.7660 1.0678 0.2266
-60.0 -0.8660 0.9750 0.2165
-55.0 -0.9397 0.8723 0.2048
-50.0 -0.9848 0.7629 0.1915
-45.0 -1.0000 0.6500 0.1768
-40.0 -1.0216 0.5352 0.1416
-39.0 -1.0239 0.5066 0.1346
-38.0 -1.0162 0.4851 0.1276
-37.0 -1.0185 0.4565 0.1205
-36.0 -1.0108 0.4279 0.1135
-35.0 -1.0031 0.3994 0.0965
-34.0 -0.9954 0.3708 0.0794
-33.0 -0.9877 0.3353 0.0624
-32.0 -0.9835 0.3097 0.0515
-30.0 -0.9703 0.2663 0.0389
-28.0 -0.9672 0.2229 0.0263
-26.0 -0.9441 0.1941 0.0154
-24.0 -0.9310 0.1654 0.0045
```

```
−22.0 −0.9047 0.1417 −0.0039
−20.0 −0.8784 0.1181 −0.0123
−18.0 −0.8459 0.0986 −0.0175
−16.0 −0.8134 0.0792 −0.0227
−14.0 −0.7728 0.0643 −0.0235
−12.0 −0.7322 0.0495 −0.0244
−10.0 −0.6935 0.0381 −0.0227
−8.0 −0.6547 0.0267 −0.0210
−6.0 −0.4507 0.0204 −0.0389
−4.0 −0.2467 0.0140 −0.0569
−2.0 0.0295 0.0129 −0.0717
0.0 0.3056 0.0118 −0.0865
2.0 0.5670 0.0119 −0.0954
4.0 0.8199 0.0125 −0.1024
6.0 1.0614 0.0136 −0.1071
8.0 1.2874 0.0152 −0.1094
10.0 1.4840 0.0180 −0.1080
12.0 1.6388 0.0224 −0.1026
14.0 1.7327 0.0303 −0.0952
16.0 1.7142 0.0539 −0.0910
18.0 1.6828 0.0954 −0.0979
20.0 1.6567 0.1435 −0.1103
22.0 1.6444 0.2280 −0.1300
24.0 1.6329 0.3148 −0.1533
26.0 1.6333 0.3926 −0.1760
28.0 1.6175 0.4623 −0.1966
30.0 1.5975 0.5266 −0.2149
32.0 1.5708 0.5855 −0.2313
33.0 1.5758 0.6215 −0.2366
34.0 1.5571 0.6562 −0.2406
35.0 1.5475 0.6897 −0.2447
36.0 1.5268 0.7148 −0.2487
37.0 1.5259 0.7464 −0.2496
38.0 1.5139 0.7762 −0.2455
39.0 1.4918 0.7982 −0.2444
40.0 1.4596 0.8197 −0.2423
45.0 1.2951 0.9122 −0.2373
```

```
 50.0 1.1256 0.9665 -0.2354
 55.0 0.9808 0.9957 -0.2324
 60.0 0.8660 1.0350 -0.2335
 65.0 0.7660 1.0828 -0.2336
 70.0 0.6428 1.1479 -0.2349
 75.0 0.5000 1.2129 -0.2415
 80.0 0.3420 1.2608 -0.2462
 85.0 0.1736 1.2901 -0.2490
 90.0 0.0000 1.3000 -0.2500
 95.0 -0.1736 1.2901 -0.2490
 100.0 -0.3420 1.2608 -0.2462
 105.0 -0.5000 1.2129 -0.2415
 110.0 -0.6428 1.1479 -0.2349
 115.0 -0.7660 1.0678 -0.2266
 120.0 -0.8660 0.9750 -0.2165
 125.0 -0.9397 0.8723 -0.2048
 130.0 -0.9848 0.7629 -0.1915
 135.0 -1.0000 0.6500 -0.1768
 140.0 -0.9848 0.5371 -0.1607
 145.0 -0.9397 0.4277 -0.1434
 150.0 -0.8660 0.3250 -0.1250
 155.0 -0.7660 0.2322 -0.1057
 160.0 -0.6428 0.1521 -0.0855
 165.0 -0.5000 0.0871 -0.0647
 170.0 -0.3420 0.0392 -0.0434
 175.0 -0.1736 0.0099 -0.0218
 180.0 0.0000 0.0000 0.0000
'Ri/R
 0.4687
 'alfa   Cl    Cd   Cm
 -180.0 0.0000 0.0000 0.0000
 -175.0 0.1736 0.0114 0.0218
 -170.0 0.3420 0.0452 0.0434
 -165.0 0.5000 0.1005 0.0647
 -160.0 0.6428 0.1755 0.0855
 -155.0 0.7660 0.2679 0.1057
 -150.0 0.8660 0.3750 0.1250
```

```
−145.0 0.9397 0.4935 0.1434
−140.0 0.9848 0.6197 0.1607
−135.0 1.0000 0.7500 0.1768
−130.0 0.9848 0.8803 0.1915
−125.0 0.9397 1.0065 0.2048
−120.0 0.8660 1.1250 0.2165
−115.0 0.7660 1.2321 0.2266
−110.0 0.6428 1.3245 0.2349
−105.0 0.5000 1.3995 0.2415
−100.0 0.3420 1.4548 0.2462
−95.0 0.1736 1.4886 0.2490
−90.0 0.0000 1.5000 0.2500
−85.0 −0.1736 1.4886 0.2490
−80.0 −0.3420 1.4548 0.2462
−75.0 −0.5000 1.3995 0.2415
−70.0 −0.6428 1.3245 0.2349
−65.0 −0.7660 1.2321 0.2266
−60.0 −0.8660 1.1250 0.2165
−55.0 −0.9397 1.0065 0.2048
−50.0 −0.9848 0.8803 0.1915
−45.0 −1.0000 0.7500 0.1768
−40.0 −1.0316 0.6095 0.1416
−39.0 −1.0439 0.5845 0.1346
−38.0 −1.0462 0.5516 0.1276
−37.0 −1.0485 0.5267 0.1205
−36.0 −1.0508 0.4937 0.1135
−35.0 −1.0531 0.4608 0.1065
−34.0 −1.0554 0.4279 0.0894
−33.0 −1.0677 0.3869 0.0824
−32.0 −1.0726 0.3347 0.0660
−30.0 −1.0917 0.2862 0.0486
−28.0 −1.1008 0.2277 0.0311
−26.0 −1.1101 0.1750 0.0182
−24.0 −1.1294 0.1423 0.0053
−22.0 −1.1233 0.1183 −0.0029
−20.0 −1.1171 0.0944 −0.0112
−18.0 −1.0870 0.0772 −0.0144
```

```
-16.0 -1.0569 0.0601 -0.0177
-14.0 -1.0238 0.0468 -0.0171
-12.0 -0.9908 0.0335 -0.0166
-10.0 -0.8594 0.0242 -0.0279
-8.0 -0.7279 0.0150 -0.0392
-6.0 -0.4690 0.0126 -0.0530
-4.0 -0.2101 0.0103 -0.0669
-2.0 0.0428 0.0099 -0.0742
0.0 0.2956 0.0096 -0.0816
2.0 0.5435 0.0098 -0.0873
4.0 0.7867 0.0103 -0.0920
6.0 1.0228 0.0112 -0.0956
8.0 1.2474 0.0126 -0.0975
10.0 1.4575 0.0146 -0.0976
12.0 1.6422 0.0175 -0.0949
14.0 1.7824 0.0227 -0.0893
16.0 1.8167 0.0357 -0.0819
18.0 1.7763 0.0649 -0.0793
20.0 1.6608 0.1015 -0.0850
22.0 1.5659 0.1411 -0.0961
24.0 1.4786 0.1809 -0.1075
26.0 1.4098 0.2355 -0.1217
28.0 1.3403 0.2998 -0.1358
30.0 1.2959 0.3640 -0.1519
32.0 1.2412 0.4380 -0.1679
33.0 1.2108 0.4752 -0.1766
34.0 1.1825 0.5083 -0.1806
35.0 1.1640 0.5410 -0.1847
36.0 1.1352 0.5737 -0.1887
37.0 1.1165 0.5980 -0.1926
38.0 1.0977 0.6305 -0.1965
39.0 1.0788 0.6545 -0.2004
40.0 1.0597 0.6785 -0.2043
45.0 1.0043 0.7960 -0.2133
50.0 0.9756 0.8960 -0.2184
55.0 0.9208 1.0104 -0.2214
60.0 0.8660 1.1250 -0.2255
```

```
 65.0 0.7660 1.2321 −0.2306
 70.0 0.6428 1.3245 −0.2349
 75.0 0.5000 1.3995 −0.2415
 80.0 0.3420 1.4548 −0.2462
 85.0 0.1736 1.4886 −0.2490
 90.0 0.0000 1.5000 −0.2500
 95.0 −0.1736 1.4886 −0.2490
 100.0 −0.3420 1.4548 −0.2462
 105.0 −0.5000 1.3995 −0.2415
 110.0 −0.6428 1.3245 −0.2349
 115.0 −0.7660 1.2321 −0.2266
 120.0 −0.8660 1.1250 −0.2165
 125.0 −0.9397 1.0065 −0.2048
 130.0 −0.9848 0.8803 −0.1915
 135.0 −1.0000 0.7500 −0.1768
 140.0 −0.9848 0.6197 −0.1607
 145.0 −0.9397 0.4935 −0.1434
 150.0 −0.8660 0.3750 −0.1250
 155.0 −0.7660 0.2679 −0.1057
 160.0 −0.6428 0.1755 −0.0855
 165.0 −0.5000 0.1005 −0.0647
 170.0 −0.3420 0.0452 −0.0434
 175.0 −0.1736 0.0114 −0.0218
 180.0 0.0000 0.0000 0.0000
'Ri/R
 1.0000
 'Alfa  Cl   Cd  Cm
−180.0 0.0000 0.0000 0.0000
−175.0 0.1736 0.0114 0.0218
−170.0 0.3420 0.0452 0.0434
−165.0 0.5000 0.1005 0.0647
−160.0 0.6428 0.1755 0.0855
−155.0 0.7660 0.2679 0.1057
−150.0 0.8660 0.3750 0.1250
−145.0 0.9397 0.4935 0.1434
−140.0 0.9848 0.6197 0.1607
−135.0 1.0000 0.7500 0.1768
```

```
−130.0 0.9848 0.8803 0.1915
−125.0 0.9397 1.0065 0.2048
−120.0 0.8660 1.1250 0.2165
−115.0 0.7660 1.2321 0.2266
−110.0 0.6428 1.3245 0.2349
−105.0 0.5000 1.3995 0.2415
−100.0 0.3420 1.4548 0.2462
−95.0 0.1736 1.4886 0.2490
−90.0 0.0000 1.5000 0.2500
−85.0 −0.1736 1.4886 0.2490
−80.0 −0.3420 1.4548 0.2462
−75.0 −0.5000 1.3995 0.2415
−70.0 −0.6428 1.3245 0.2349
−65.0 −0.7660 1.2321 0.2266
−60.0 −0.8660 1.1250 0.2165
−55.0 −0.9397 1.0065 0.2048
−50.0 −0.9848 0.8803 0.1915
−45.0 −1.0000 0.7500 0.1768
−40.0 −1.0316 0.6095 0.1416
−39.0 −1.0439 0.5845 0.1346
−38.0 −1.0462 0.5516 0.1276
−37.0 −1.0485 0.5267 0.1205
−36.0 −1.0508 0.4937 0.1135
−35.0 −1.0531 0.4608 0.1065
−34.0 −1.0554 0.4279 0.0894
−33.0 −1.0677 0.3869 0.0824
−32.0 −1.0726 0.3347 0.0660
−30.0 −1.0917 0.2862 0.0486
−28.0 −1.1008 0.2277 0.0311
−26.0 −1.1101 0.1750 0.0182
−24.0 −1.1294 0.1423 0.0053
−22.0 −1.1233 0.1183 −0.0029
−20.0 −1.1171 0.0944 −0.0112
−18.0 −1.0870 0.0772 −0.0144
−16.0 −1.0569 0.0601 −0.0177
−14.0 −1.0238 0.0468 −0.0171
−12.0 −0.9908 0.0335 −0.0166
```

```
−10.0 −0.8594 0.0242 −0.0279
−8.0 −0.7279 0.0150 −0.0392
−6.0 −0.4690 0.0126 −0.0530
−4.0 −0.2101 0.0103 −0.0669
−2.0 0.0428 0.0099 −0.0742
0.0 0.2956 0.0096 −0.0816
2.0 0.5435 0.0098 −0.0873
4.0 0.7867 0.0103 −0.0920
6.0 1.0228 0.0112 −0.0956
8.0 1.2474 0.0126 −0.0975
10.0 1.4575 0.0146 −0.0976
12.0 1.6422 0.0175 −0.0949
14.0 1.7824 0.0227 −0.0893
16.0 1.8167 0.0357 −0.0819
18.0 1.7763 0.0649 −0.0793
20.0 1.6608 0.1015 −0.0850
22.0 1.5659 0.1411 −0.0961
24.0 1.4786 0.1809 −0.1075
26.0 1.4098 0.2355 −0.1217
28.0 1.3403 0.2998 −0.1358
30.0 1.2959 0.3640 −0.1519
32.0 1.2412 0.4380 −0.1679
33.0 1.2108 0.4752 −0.1766
34.0 1.1825 0.5083 −0.1806
35.0 1.1640 0.5410 −0.1847
36.0 1.1352 0.5737 −0.1887
37.0 1.1165 0.5980 −0.1926
38.0 1.0977 0.6305 −0.1965
39.0 1.0788 0.6545 −0.2004
40.0 1.0597 0.6785 −0.2043
45.0 1.0043 0.7960 −0.2133
50.0 0.9756 0.8960 −0.2184
55.0 0.9208 1.0104 −0.2214
60.0 0.8660 1.1250 −0.2255
65.0 0.7660 1.2321 −0.2306
70.0 0.6428 1.3245 −0.2349
75.0 0.5000 1.3995 −0.2415
```

```
80.0 0.3420 1.4548 -0.2462
85.0 0.1736 1.4886 -0.2490
90.0 0.0000 1.5000 -0.2500
95.0 -0.1736 1.4886 -0.2490
100.0 -0.3420 1.4548 -0.2462
105.0 -0.5000 1.3995 -0.2415
110.0 -0.6428 1.3245 -0.2349
115.0 -0.7660 1.2321 -0.2266
120.0 -0.8660 1.1250 -0.2165
125.0 -0.9397 1.0065 -0.2048
130.0 -0.9848 0.8803 -0.1915
135.0 -1.0000 0.7500 -0.1768
140.0 -0.9848 0.6197 -0.1607
145.0 -0.9397 0.4935 -0.1434
150.0 -0.8660 0.3750 -0.1250
155.0 -0.7660 0.2679 -0.1057
160.0 -0.6428 0.1755 -0.0855
165.0 -0.5000 0.1005 -0.0647
170.0 -0.3420 0.0452 -0.0434
175.0 -0.1736 0.0114 -0.0218
180.0 0.0000 0.0000 0.0000
'
 ElmCoeff      100          Wing
'
'                          GroupID    name
 Name       Group          14        YawBearing
 Name       Group          12        DriveTrain
 Name       Group          13        HUB
 Name       Group          11    BLADES
'
'
 GroupDef          14      Mat     8001     !  Yawbearing
'
 GroupDef          12      Mat
                  601     701     602    603     702
                  703     705     706     708
'
```

```
'
'                  PartID    ListType   ElemID .....
 GroupDef            13        Elem
                    501        502        503
'
'                  PartID    ListType   ElemID .....
 GroupDef            11        Elem
                  61004     61005      61006     61007     61008     61009
                  61010     61011      61012     61013     61014     61015
                  61016     61017      61018     61019     61020     61021
                  61022     61023      62004     62005     62006     62007
                  62008     62009      62010     62011     62012     62013
                  62014     62015      62016     62017     62018     62019
                  62020     62021      62022     62023     63004     63005
                  63006     63007      63008     63009     63010     63011
                  63012     63013      63014     63015     63016     63017
                  63018     63019      63020     63021     63022     63023
'
'
#
# ==========================================
#  The model has been processed by TRACO
# ------------------------------------------
#  Date : 2022-02-17 19:39:21
#
#  Control   File: traco.in
#  Original  File: tower_orig.fem
#  Processed File: tower_tran.fem
#
#  Transformation matrix :
#                                  1.000     0.000     0.000
#                                  0.000     1.000     0.000
#                                 -0.000     0.000     1.000
#                                  7.100     0.000     0.000
#
'
' NodeID X Y Z [Boundary  Code]
```

```
#NODE        101      7.1000      0.0000      -5.0000  ! Tower top
 NODE        102      7.1000      0.0000     -20.0000
 NODE        103      7.1000      0.0000     -40.0000
 NODE        104      7.1000      0.0000     -60.0000
 NODE        105      7.1000      0.0000     -80.0000
 NODE        106      7.1000      0.0000    -100.0000
 NODE        107      7.1000      0.0000    -101.0000 ! 1 1 1 1 1 1 ! Fixed
    tower bottom
'
'      ElemID  Nod1  Nod2  Mat  Geo  [LCorr  Ecc1  Ecc2]
 BEAM     101    101   102       101   101
 BEAM     102    102   103       101   102
 BEAM     103    103   104       101   103
 BEAM     104    104   105       101   104
 BEAM     105    105   106       101   105
 BEAM     106    106   107       101   106
'
'      GeoID    Do    Thick   Sy  Sz   D2
 PIPE    101     5.0    0.040   0   0   5.6  ! Conial shape
 PIPE    102     5.6    0.046   0   0   6.2
 PIPE    103     6.2    0.052   0   0   6.8
 PIPE    104     6.8    0.058   0   0   7.4
 PIPE    105     7.4    0.064   0   0   8.0
 PIPE    106     8.0    0.064
'
'        MatID   E-mod    poiss   yield   density  term.exp
 MISOIEP  101  210000e6     0.3    355e6  7850
'
 NODEMASS 101   20E3    ! Turbine model has mass 730 tonnes
'
'
'              PartID      Transp     Red     Green     Blue    Fringe   Smooth
 PartData        101                0     100      100      100        1        1   !
    Tower
'
'                        PartID       name
 Name        Part           101          Tower
```

```
'
 PartElem      101     Mat     101    !  Tower
'
'
 SpriDiag   770100  1e12  1e12   1e12      1e11   1e11   1e12
'
 Sprng2Gr   770100   107  770100

'
'
' ------------------------------------------------------------------------
'
#
# ================================================
#   F i n a l    TRACO     Information :
# ------------------------------------------------
#
#   Number  of  Processed  Nodes     :          7
#   Number  of  Processed  UnitVec  :          0
#   Number  of  Processed  Eccent    :          0
#
#   Successfully  Completed  :)
#
```

B.3 controlB.inp

```
#
 BeginControl_General
#
 Routine ULSALS          !  Use ULSALS    for   5MW fixed  turbine
#
#              no
 Object      1       type   PitchEngine    Element   6010    Blade    1
 Object      2       type   PitchEngine    Element   6020    Blade    2
 Object      3       type   PitchEngine    Element   6030    Blade    3
#
```

```
Object      4      Type   Generator      Element     707
Object      4      Measured    Torque    Element     708   End 2 DOF 4
#
Turbine     NacelNode           500          ! Node no for Acc monitoring
Turbine     TimeLag            0.010         ! Time lag between dem and execut
Turbine     CommInterval       0.010         ! Communication interval to DISCON
#
#
PitchEngine 1     Stiffness          0.0     ! Spring Stiffness (0 = def) [Nm/rad]
PitchEngine 1     dThetadT           0.001   ! Max pitch per step          [rad/stp]
#
PitchEngine 1     MinPitchAng        0.0     ! Min pitch angle             [ deg ]
PitchEngine 1     MaxPitchAng       90.0     ! Max pitch angle             [ deg ]
#
PitchEngine 1     MinPitchRate   -0.018    ! Min pitch rate     Normal: 0.035 Shutdown: 0.087  [rad/s]
PitchEngine 1     MaxPitchRate    0.018    ! Max pitch rate                [rad/s]
#
#               no     Item                Value
Generator    1     Gear                 1.00   ! Gear between gener and shaft
Generator    1     Speed     Min        0.628  ! Minimum Generator speed   [rad/s]
Generator    1     Speed     Rated      1.005  ! Rated    Generator speed   [rad/s]
Generator    1     Speed     Max        1.34   ! Max Generator speed       [rad/s]
#
Generator    1     Torque    Max     15.0e6   ! Max     Rotor torque      [ Nm ]
#
```

```
#
# ——————————————————————————————————————————————————————————————
#
#      UserData is found in DISCON on index 601 ->.
#
#      UserData no 1 is stored on 601
#      UserData no 2 is stored on 602
#      UserData no i is stored on 600 + i etc
#
#
#                          Indx   Value         Description
  Generator 1 UserData    1   1.000E+07   !  Rated power [W]
  Generator 1 UserData    8   2.000E-01   !  Frequency of generator speed
     filter [Hz]
  Generator 1 UserData    9   7.000E-01   !  Damping ratio of speed filter
     [-]
  Generator 1 UserData   10   1.850E+00   !  Frequency of free-free DT
     torsion mode [Hz], if zero no notch filter used
  Generator 1 UserData   11   1.001E+07   !  Optimal Cp tracking K factor [
     kNm/(rad/s)^2]
  Generator 1 UserData   12   6.835E+07   !  Proportional gain of torque
     controller [Nm/(rad/s)]
  Generator 1 UserData   13   1.534E+07   !  Integral gain of torque
     controller [Nm/rad]
  Generator 1 UserData   14   0.000E+00   !  Differential gain of torque
     controller [Nm/(rad/s^2)]
  Generator 1 UserData   15   1           !  Generator control switch [1=
     constant power, 2=constant torque]
  Generator 1 UserData   16   5.245E-01   !  Proportional gain of pitch
     controller [rad/(rad/s)]                              *R2D in
     degree version
  Generator 1 UserData   17   1.412E-01   !  Integral gain of pitch
     controller [rad/rad]                                      *R2D in
     degree version
  Generator 1 UserData   18   0.000E+00   !  Differential gain of pitch
     controller [rad/(rad/s^2)]                            *R2D in
     degree version
```

```
Generator 1 UserData 19 4.000E-09 ! Proportional power error gain [rad/W] *R2D in degree version
Generator 1 UserData 20 4.000E-09 ! Integral power error gain [rad/(Ws)] *R2D in degree version
Generator 1 UserData 21 1.983E+02 ! Coefficient of linear term in aerodynamic gain scheduling, KK1 [deg] *D2R in radian version
Generator 1 UserData 22 6.932E+02 ! Coefficient of quadratic term in aerodynamic gain scheduling, KK2 [deg^2] *D2R**2 in radian version
Generator 1 UserData 23 1.300E+00 ! Relative speed for double nonlinear gain [-]
Generator 1 UserData 33 5.000E-01 ! Lower angle above lowest minimum pitch angle for switch [deg] *D2R in radian version
Generator 1 UserData 34 5.000E-01 ! Upper angle above lowest minimum pitch angle for switch [deg], if equal then hard switch *D2R in radian version
Generator 1 UserData 35 9.500E+01 ! Ratio between filtered speed and reference speed for fully open torque limits [%]
Generator 1 UserData 36 5.000E+00 ! Time constant of 1st order filter on wind speed used for minimum pitch [1/1P]
Generator 1 UserData 37 5.000E+00 ! Time constant of 1st order filter on pitch angle used for gain scheduling [1/1P]
Generator 1 UserData 38 0.000E+00 ! Proportional gain of active DT damper [Nm/(rad/s)]
Generator 1 UserData 44 0.0       ! tau_BP
Generator 1 UserData 45 0.02      ! zeta_BP
Generator 1 UserData 46 0.01      ! zeta1_N Damping ratio 1 notch filter (pitch control)
Generator 1 UserData 47 0.001     ! zeta2_N Damping ratio 2 notch filter (pitch control=
#
Generator 1 UserData 48 0.00      ! XPitch1. Add to pitch bld-1 [deg]
```

```
 Generator 1 UserData 49 0.00        ! XPitch2. Add to pitch bld-2 [
     deg]
 Generator 1 UserData 50 0.00        ! XPitch2. Add to pitch bld-3 [
     deg]
#
#
#                                      - Pitch vs. Wind Speed at Hub
#
#       Key    nUP      WindSpeed      Pitch
 Curve  U_P    6          4.0000      2.8931
                          5.0000      2.1228
                          6.0000      1.0868
                          7.0000      0.0001
                          8.0000      0.0000
                         50.0000      0.0000
#
#
 EndControl_General
#
 BeginULSALS
#
 Scenario    VP_CTR    7      ! Vp Control, no 07
#
#
 PitchAngle  Idling  85  Blade  1 ! Go to 85 deg during shut down,
     Blade 1
 PitchAngle  Idling  85  Blade  2 ! Go to  5 deg during shut down,
     Blade 2
 PitchAngle  Idling  85  Blade  3 ! Go to 85 deg during shut down,
     Blade 3
#
 PitchAngle  Normal   3  Blade  1 ! Use 3 deg for normal operation
     Blade 1
 PitchAngle  Normal   3  Blade  2 ! Use 3 deg for normal operation
     Blade 2
 PitchAngle  Normal   3  Blade  3 ! Use 3 deg for normal operation
     Blade 3
```

```
#
 PitchAngle  StartUp 50  Blade  1 ! Use 50 deg during startup, Blade 1
 PitchAngle  StartUp 50  Blade  2 ! Use 50 deg during startup, Blade 2
 PitchAngle  StartUp 50  Blade  3 ! Use 50 deg during startup, Blade 3
#
 Time     Startup   17              ! Set startup time to 17 seconds
#
#
#
#
 EndULSALS




#
```

Appendix C

MATLAB codes

C.1 SNcurve.m

```
%% SN-curve and damage distribution
clc
clear all
close all

%% Tower bottom characteristics
D = 8000; % Outer diameter [mm]
t = 70; % Thickness [mm]
d = D-t*2; % Inner diameter [mm]
A = pi*((D/2)^2-(d/2)^2);
W = pi*(D^4-d^4)/(32*D); % Section modulus at bottom[mm]

%% Reading data from files
fs = 100;
t = seconds(100:1/fs:700.01-1/fs)';

num = 8; % Number of files

%% From 10m/s simulation
dof = [];
```

```
elem770100_dof5_fasit = readtable('/Users/luciavu/Documents/MasterData/2303/fasit_Time_vs_Element_Force_Elem_770100_End_1_Dof_5.txt');
dof5_fasit = elem770100_dof5_fasit{100.01*fs:end,2}; % Bending moment, fasit [Nm]
dof(:,1) = dof5_fasit;
elem_1006_dof5_5e4 = readtable('/Users/luciavu/Documents/MasterData/dampCoeff/damp5e4_Time_vs_Element_Force_Elem_1006_End_1_Dof_5.txt');
dof5_5e4 = elem_1006_dof5_5e4{100.01*fs:end,2}; % Bending moment, damp = 5e4 [Nm]
dof(:,2) = dof5_5e4;
elem_1006_dof5_1e5 = readtable('/Users/luciavu/Documents/MasterData/dampCoeff/damp1e5_Time_vs_Element_Force_Elem_1006_End_1_Dof_5.txt');
dof5_1e5 = elem_1006_dof5_1e5{100.01*fs:end,2}; % Bending moment, damp = 1e5 [Nm]
dof(:,3) = dof5_1e5;
elem_1006_dof5_3e5 = readtable('/Users/luciavu/Documents/MasterData/dampCoeff/damp3e5_Time_vs_Element_Force_Elem_1006_End_1_Dof_5.txt');
dof5_3e5 = elem_1006_dof5_3e5{100.01*fs:end,2}; % Bending moment, damp = 3e5 [Nm]
dof(:,4) = dof5_3e5;
elem_1006_dof5_5e5 = readtable('/Users/luciavu/Documents/MasterData/dampCoeff/damp5e5_Time_vs_Element_Force_Elem_1006_End_1_Dof_5.txt');
dof5_5e5 = elem_1006_dof5_5e5{100.01*fs:end,2}; % Bending moment, damp = 5e5 [Nm]
dof(:,5) = dof5_5e5;
elem_1006_dof5_7e5 = readtable('/Users/luciavu/Documents/MasterData/dampCoeff/damp7e5_Time_vs_Element_Force_Elem_1006_End_1_Dof_5.txt');
dof5_7e5 = elem_1006_dof5_7e5{100.01*fs:end,2}; % Bending moment, damp = 7e5 [Nm]
dof(:,6) = dof5_7e5;
elem_1006_dof5_1e6 = readtable('/Users/luciavu/Documents/MasterData/dampCoeff/damp1e6_Time_vs_Element_Force_Elem_1006_End_1_Dof_5.txt');
dof5_1e6 = elem_1006_dof5_1e6{100.01*fs:end,2}; % Bending moment, damp = 1e6 [Nm]
dof(:,7) = dof5_1e6;
elem770100_dof5_5e6 = readtable('/Users/luciavu/Documents/MasterData/
```

```
    dampCoeff/damp5e6_Time_vs_Element_Force_Elem_1006_End_1_Dof_5.txt');
dof5_5e6 = elem770100_dof5_5e6{100.01*fs:end,2}; % Bending moment, damp
     = 5e6 [Nm]
dof(:,8) = dof5_5e6;

%% From 12m/s simulation
Xdof = [];

Xelem770100_Mx12 = readtable('/Users/luciavu/Documents/MasterData/
    Mx_var_12/results_0516_Time_vs_Element_Force_Elem_770100_End_1_Dof_5
    .txt');
Xdof5_fasit = Xelem770100_Mx12{100.01*fs:end,2}; % Bending moment,
    fasit [Nm]
Xdof(:,1) = Xdof5_fasit;
Xelem_1006_dof5_5e4 = readtable('/Users/luciavu/Documents/MasterData/
    dampCoeff/damp5e4res_Time_vs_Element_Force_Elem_1006_End_1_Dof_5.txt
    ');
Xdof5_5e4 = Xelem_1006_dof5_5e4{100.01*fs:end,2}; % Bending moment,
    damp = 5e4 [Nm]
Xdof(:,2) = Xdof5_5e4;
Xelem_1006_dof5_1e5 = readtable('/Users/luciavu/Documents/MasterData/
    dampCoeff/damp1e5res_Time_vs_Element_Force_Elem_1006_End_1_Dof_5.txt
    ');
Xdof5_1e5 = Xelem_1006_dof5_1e5{100.01*fs:end,2}; % Bending moment,
    damp = 1e5 [Nm]
Xdof(:,3) = Xdof5_1e5;
Xelem_1006_dof5_3e5 = readtable('/Users/luciavu/Documents/MasterData/
    dampCoeff/damp3e5res_Time_vs_Element_Force_Elem_1006_End_1_Dof_5.txt
    ');
Xdof5_3e5 = Xelem_1006_dof5_3e5{100.01*fs:end,2}; % Bending moment,
    damp = 3e5 [Nm]
Xdof(:,4) = Xdof5_3e5;
Xelem_1006_dof5_5e5 = readtable('/Users/luciavu/Documents/MasterData/
    dampCoeff/damp5e5res_Time_vs_Element_Force_Elem_1006_End_1_Dof_5.txt
    ');
Xdof5_5e5 = Xelem_1006_dof5_5e5{100.01*fs:end,2}; % Bending moment,
    damp = 5e5 [Nm]
```

```
Xdof(:,5) = Xdof5_5e5;
Xelem_1006_dof5_7e5 = readtable('/Users/luciavu/Documents/MasterData/dampCoeff/damp7e5res_Time_vs_Element_Force_Elem_1006_End_1_Dof_5.txt');
Xdof5_7e5 = Xelem_1006_dof5_7e5{100.01*fs:end,2}; % Bending moment, damp = 7e5 [Nm]
Xdof(:,6) = Xdof5_7e5;
Xelem_1006_dof5_1e6 = readtable('/Users/luciavu/Documents/MasterData/dampCoeff/damp1e6res_Time_vs_Element_Force_Elem_1006_End_1_Dof_5.txt');
Xdof5_1e6 = Xelem_1006_dof5_1e6{100.01*fs:end,2}; % Bending moment, damp = 1e6 [Nm]
Xdof(:,7) = Xdof5_1e6;
Xelem_1006_dof5_5e6 = readtable('/Users/luciavu/Documents/MasterData/dampCoeff/damp5e6res_Time_vs_Element_Force_Elem_1006_End_1_Dof_5.txt');
Xdof5_5e6 = Xelem_1006_dof5_5e6{100.01*fs:end,2}; % Bending moment, damp = 5e6 [Nm]
Xdof(:,8) = Xdof5_5e6;

%% From 13m/s simulation
XYdof = [];

XYelem770100_Mx13 = readtable('/Users/luciavu/Documents/MasterData/dampCoeff/1314/results_2505_13_Time_vs_Element_Force_Elem_770100_End_1_Dof_5.txt');
XYdof5_fasit = XYelem770100_Mx13{100.01*fs:end,2}; % Bending moment, fasit [Nm]
XYdof(:,1) = XYdof5_fasit;
XYelem_1006_dof5_5e4 = readtable('/Users/luciavu/Documents/MasterData/dampCoeff/1314/damp5e4_2505_13_Time_vs_Element_Force_Elem_1006_End_1_Dof_5.txt');
XYdof5_5e4 = XYelem_1006_dof5_5e4{100.01*fs:end,2}; % Bending moment, damp = 5e4 [Nm]
XYdof(:,2) = XYdof5_5e4;
XYelem_1006_dof5_1e5 = readtable('/Users/luciavu/Documents/MasterData/dampCoeff/1314/
```

```
damp1e5_2505_13_Time_vs_Element_Force_Elem_1006_End_1_Dof_5.txt');
XYdof5_1e5 = XYelem_1006_dof5_1e5{100.01*fs:end,2}; % Bending moment, damp = 1e5 [Nm]
XYdof(:,3) = XYdof5_1e5;
XYelem_1006_dof5_3e5 = readtable('/Users/luciavu/Documents/MasterData/dampCoeff/1314/damp3e5_2505_13_Time_vs_Element_Force_Elem_1006_End_1_Dof_5.txt');
XYdof5_3e5 = XYelem_1006_dof5_3e5{100.01*fs:end,2}; % Bending moment, damp = 3e5 [Nm]
XYdof(:,4) = XYdof5_3e5;
XYelem_1006_dof5_5e5 = readtable('/Users/luciavu/Documents/MasterData/dampCoeff/1314/damp5e5_2505_13_Time_vs_Element_Force_Elem_1006_End_1_Dof_5.txt');
XYdof5_5e5 = XYelem_1006_dof5_5e5{100.01*fs:end,2}; % Bending moment, damp = 5e5 [Nm]
XYdof(:,5) = XYdof5_5e5;
XYelem_1006_dof5_7e5 = readtable('/Users/luciavu/Documents/MasterData/dampCoeff/1314/damp7e5_2505_13_Time_vs_Element_Force_Elem_1006_End_1_Dof_5.txt');
XYdof5_7e5 = XYelem_1006_dof5_7e5{100.01*fs:end,2}; % Bending moment, damp = 7e5 [Nm]
XYdof(:,6) = XYdof5_7e5;
XYelem_1006_dof5_1e6 = readtable('/Users/luciavu/Documents/MasterData/dampCoeff/1314/damp1e6_2505_13_Time_vs_Element_Force_Elem_1006_End_1_Dof_5.txt');
XYdof5_1e6 = XYelem_1006_dof5_1e6{100.01*fs:end,2}; % Bending moment, damp = 1e6 [Nm]
XYdof(:,7) = XYdof5_1e6;
XYelem_1006_dof5_5e6 = readtable('/Users/luciavu/Documents/MasterData/dampCoeff/1314/damp5e6_2505_13_Time_vs_Element_Force_Elem_1006_End_1_Dof_5.txt');
XYdof5_5e6 = XYelem_1006_dof5_5e6{100.01*fs:end,2}; % Bending moment, damp = 5e6 [Nm]
XYdof(:,8) = XYdof5_5e6;

%% From 14m/s simulation
XYZdof = [];
```

```matlab

XYZelem770100_Mx14 = readtable('/Users/luciavu/Documents/MasterData/dampCoeff/1314/results_2505_14_Time_vs_Element_Force_Elem_770100_End_1_Dof_5.txt');
XYZdof5_fasit = XYZelem770100_Mx14{100.01*fs:end,2}; % Bending moment, fasit [Nm]
XYZdof(:,1) = XYZdof5_fasit;
XYZelem_1006_dof5_5e4 = readtable('/Users/luciavu/Documents/MasterData/dampCoeff/1314/damp5e4_2505_14_Time_vs_Element_Force_Elem_1006_End_1_Dof_5.txt');
XYZdof5_5e4 = XYZelem_1006_dof5_5e4{100.01*fs:end,2}; % Bending moment, damp = 5e4 [Nm]
XYZdof(:,2) = XYZdof5_5e4;
XYZelem_1006_dof5_1e5 = readtable('/Users/luciavu/Documents/MasterData/dampCoeff/1314/damp1e5_2505_14_Time_vs_Element_Force_Elem_1006_End_1_Dof_5.txt');
XYZdof5_1e5 = XYZelem_1006_dof5_1e5{100.01*fs:end,2}; % Bending moment, damp = 1e5 [Nm]
XYZdof(:,3) = XYZdof5_1e5;
XYZelem_1006_dof5_3e5 = readtable('/Users/luciavu/Documents/MasterData/dampCoeff/1314/damp3e5_2505_14_Time_vs_Element_Force_Elem_1006_End_1_Dof_5.txt');
XYZdof5_3e5 = XYZelem_1006_dof5_3e5{100.01*fs:end,2}; % Bending moment, damp = 3e5 [Nm]
XYZdof(:,4) = XYZdof5_3e5;
XYZelem_1006_dof5_5e5 = readtable('/Users/luciavu/Documents/MasterData/dampCoeff/1314/damp5e5_2505_14_Time_vs_Element_Force_Elem_1006_End_1_Dof_5.txt');
XYZdof5_5e5 = XYZelem_1006_dof5_5e5{100.01*fs:end,2}; % Bending moment, damp = 5e5 [Nm]
XYZdof(:,5) = XYZdof5_5e5;
XYZelem_1006_dof5_7e5 = readtable('/Users/luciavu/Documents/MasterData/dampCoeff/1314/damp7e5_2505_14_Time_vs_Element_Force_Elem_1006_End_1_Dof_5.txt');
XYZdof5_7e5 = XYZelem_1006_dof5_7e5{100.01*fs:end,2}; % Bending moment, damp = 7e5 [Nm]
XYZdof(:,6) = XYZdof5_7e5;
```

```
XYZelem_1006_dof5_1e6 = readtable('/Users/luciavu/Documents/MasterData/dampCoeff/1314/damp1e6_2505_14_Time_vs_Element_Force_Elem_1006_End_1_Dof_5.txt');
XYZdof5_1e6 = XYZelem_1006_dof5_1e6{100.01*fs:end,2}; % Bending moment, damp = 1e6 [Nm]
XYZdof(:,7) = XYZdof5_1e6;
XYZelem_1006_dof5_5e6 = readtable('/Users/luciavu/Documents/MasterData/dampCoeff/1314/damp5e6_2505_14_Time_vs_Element_Force_Elem_1006_End_1_Dof_5.txt');
XYZdof5_5e6 = XYZelem_1006_dof5_5e6{100.01*fs:end,2}; % Bending moment, damp = 5e6 [Nm]
XYZdof(:,8) = XYZdof5_5e6;

%% Rainflow counting for 10m/s simulation
stress=[];
cycles=[];
for r = 1 : num
    TT = timetable(t,dof(:,r));
    [c,hist,edges,rmm,idx] = rainflow(TT);
    T = array2table(c,'VariableNames',{'Count','Range','Mean','Start','End'}) ;

    % Bending moment, fasit
    block = 40;
    range = c(:,2); % Bending moment ranges [Nm]
    edgess = linspace(0,max(range)+1,block); % Bending moment ranges, bins edges
    cyclesFasit = zeros(1,length(edgess)); % Number of cycles
    edge_mid = zeros(1,length(edgess)); % Bending moment
    for i = 1:length(range)
        for j = 1:length(edgess)-1
            if range(i) > edgess(j) && range(i) <= edgess(j+1)
                cyclesFasit(j) = cyclesFasit(j) + 1;
            end
            edge_mid(j) = (edgess(j) + edgess(j+1))/2; % Bending moment
        end

```

```
    end
        stress(:,r) = edge_mid*10^3/W; % Stress ranges [N/mm^2]=[MPa]
        cycles(:,r) = cyclesFasit;
end

%% Rainflow counting for 12m/s simulation
Xstress=[];
Xcycles=[];
for r = 1 : num
    XTT = timetable(t,Xdof(:,r));
    [Xc,hist,Xedges,rmm,idx] = rainflow(XTT);
    XT = array2table(Xc,'VariableNames',{'Count','Range','Mean','Start','End'}) ;

    % Bending moment, fasit
    blocks = 40;
    Xrange = Xc(:,2); % Bending moment ranges [Nm]
    Xedgess = linspace(0,max(Xrange)+1,blocks); % Bending moment ranges, bins edges
    XcyclesFasit = zeros(1,length(Xedgess)); % Number of cycles
    Xedge_mid = zeros(1,length(Xedgess)); % Bending moment
    for i = 1:length(Xrange)
        for j = 1:length(Xedgess)-1
            if Xrange(i) > Xedgess(j) && Xrange(i) <= Xedgess(j+1)
                XcyclesFasit(j) = XcyclesFasit(j) + 1;
            end
            Xedge_mid(j) = (Xedgess(j) + Xedgess(j+1))/2; % Bending moment
        end

    end
        Xstress(:,r) = Xedge_mid*10^3/W; % Stress ranges [N/mm^2]=[MPa]
        Xcycles(:,r) = XcyclesFasit;
end

%% Rainflow counting for 13m/s simulation
XYstress=[];
```

```
XYcycles=[];
for r = 1 : num
    XYTT = timetable(t,XYdof(:,r));
    [XYc,hist,XYedges,rmm,idx] = rainflow(XYTT);
    XYT = array2table(XYc,'VariableNames',{'Count','Range','Mean','Start','End'}) ;

    % Bending moment, fasit
    XYblock = 40;
    XYrange = XYc(:,2); % Bending moment ranges [Nm]
    XYedgess = linspace(0,max(XYrange)+1,XYblock); % Bending moment ranges, bins edges
    XYcyclesFasit = zeros(1,length(XYedgess)); % Number of cycles
    XYedge_mid = zeros(1,length(XYedgess)); % Bending moment
    for i = 1:length(XYrange)
        for j = 1:length(XYedgess)-1
            if XYrange(i) > XYedgess(j) && XYrange(i) <= XYedgess(j+1)
                XYcyclesFasit(j) = XYcyclesFasit(j) + 1;
            end
            XYedge_mid(j) = (XYedgess(j) + XYedgess(j+1))/2; % Bending moment
        end

    end
        XYstress(:,r) = XYedge_mid*10^3/W; % Stress ranges [N/mm^2]=[MPa]
        XYcycles(:,r) = XYcyclesFasit;
end

%% Rainflow counting for 14m/s simulation
XYZstress=[];
XYZcycles=[];
for r = 1 : num
    XYZTT = timetable(t,XYZdof(:,r));
    [XYZc,hist,XYZedges,rmm,idx] = rainflow(XYZTT)
    XYZT = array2table(XYZc,'VariableNames',{'Count','Range','Mean','Start','End'}) ;
```

```

    % Bending moment, fasit
    XYZblock = 40;
    XYZrange = XYZc(:,2); % Bending moment ranges [Nm]
    XYZedgess = linspace(0,max(XYZrange)+1,XYZblock); % Bending moment ranges, bins edges
    XYZcyclesFasit = zeros(1,length(XYZedgess)); % Number of cycles
    XYZedge_mid = zeros(1,length(XYZedgess)); % Bending moment
    for i = 1:length(XYZrange)
        for j = 1:length(XYZedgess)-1
            if XYZrange(i) > XYZedgess(j) && XYZrange(i) <= XYZedgess(j+1)
                XYZcyclesFasit(j) = XYZcyclesFasit(j) + 1;
            end
            XYZedge_mid(j) = (XYZedgess(j) + XYZedgess(j+1))/2; % Bending moment
        end

    end
        XYZstress(:,r) = XYZedge_mid*10^3/W; % Stress ranges [N/mm^2]=[MPa]
        XYZcycles(:,r) = XYZcyclesFasit;
end


%% Figures for damping coefficients
figure(1)
for i=2:num
    loglog(cycles(:,i), stress(:,i), 'o', 'MarkerEdgeColor',[0 0.4470 0.7410],'MarkerFaceColor',[10-i 10-i 10-i]*0.1);
    grid on
    hold on
end
loglog(cycles(:,1), stress(:,1), '*','MarkerEdgeColor',[0.9290 0.6940 0.1250],'MarkerSize',11 );
grid on
hold on
```

```
legend({'C = 5e4', 'C = 1e5', 'C = 3e5', 'C = 5e5','C = 7e5','C = 1e6',
    'C = 5e6','Assembled turbine'},'Location','southeast','NumColumns'
    ,2);
set(gca,'Fontsize',16)
title('Analysed stress distribution, U_{mean} = 10 m/s')
xlabel('Number of cycles, N')
ylabel('Stress range, \Delta \sigma [MPa]')


figure(2)
for i=2:num
    loglog(Xcycles(:,i), Xstress(:,i), 'o', 'MarkerEdgeColor',[0 0.4470
        0.7410],'MarkerFaceColor',[10-i 10-i 10-i]*0.1);
    grid on
    hold on
end
loglog(Xcycles(:,1), Xstress(:,1), '*','MarkerEdgeColor',[0.9290 0.6940
    0.1250], 'MarkerSize',11);
grid on
hold on
legend({'C = 5e4', 'C = 1e5', 'C = 3e5', 'C = 5e5','C = 7e5','C = 1e6',
    'C = 5e6','Assembled turbine'},'Location','southeast','NumColumns'
    ,2);
set(gca,'Fontsize',16)
title('Analysed stress distribution, U_{mean} = 12 m/s')
xlabel('Number of cycles, N')
ylabel('Stress range, \Delta \sigma [MPa]')

figure(3)
for i=2:num
    loglog(XYcycles(:,i), XYstress(:,i), 'o', 'MarkerEdgeColor',[0
        0.4470 0.7410],'MarkerFaceColor',[10-i 10-i 10-i]*0.1);
    grid on
    hold on
end
loglog(XYcycles(:,1), XYstress(:,1), '*','MarkerEdgeColor',[0.9290
    0.6940 0.1250], 'MarkerSize',11);
```

```
grid on
hold on
legend({'C = 5e4', 'C = 1e5', 'C = 3e5', 'C = 5e5','C = 7e5','C = 1e6',
    'C = 5e6','Assembled turbine'},'Location','southeast','NumColumns'
    ,2);
set(gca,'Fontsize',16)
title('Analysed stress distribution, U_{mean} = 13 m/s')
xlabel('Number of cycles, N')
ylabel('Stress range, \Delta \sigma [MPa]')

figure(4)
for i=2:num
    loglog(XYZcycles(:,i), XYZstress(:,i), 'o', 'MarkerEdgeColor',[0
        0.4470 0.7410],'MarkerFaceColor',[10-i 10-i 10-i]*0.1);
    grid on
    hold on
end
loglog(XYZcycles(:,1), XYZstress(:,1), '*','MarkerEdgeColor',[0.9290
    0.6940 0.1250], 'MarkerSize',11);
grid on
hold on
legend({'C = 5e4', 'C = 1e5', 'C = 3e5', 'C = 5e5','C = 7e5','C = 1e6',
    'C = 5e6','Assembled turbine'},'Location','southeast','NumColumns'
    ,2);
set(gca,'Fontsize',16)
title('Analysed stress distribution, U_{mean} = 14 m/s')
xlabel('Number of cycles, N')
ylabel('Stress range, \Delta \sigma [MPa]')
%% Fatigue damage accumulation 10 m/s

% N > e6
loga2Bar = 15.606;
m2 = 5;
n = cycles / 600 * 31556926 * 20; % Number of cycles within 20
    operating years

DD_bin = [];
```

```
DD_temp = zeros(1,num);
for l = 1 : num
    for p = 1 : block % Looping through p number of stress blocks

        DD_temp(l) = DD_temp(l) + n(p,l)*stress(p,l)^m2;

        if l == 1 % Assembled
            DD_bin(1,p) = n(p,l)*stress(p,l)^m2;
        elseif l == 3 % 1e5
            DD_bin(2,p) = n(p,l)*stress(p,l)^m2;
        elseif l == 4 % 3e5
            DD_bin(3,p) = n(p,l)*stress(p,l)^m2;
        elseif l == 5 % 5e5
            DD_bin(4,p) = n(p,l)*stress(p,l)^m2;
        else
            cc = 1;
        end

    end
end

DD = 1/10^loga2Bar * DD_temp;
DD_bins = 1/10^loga2Bar * DD_bin;
%% Fatigue damage accumulation 12 m/s

Xn = Xcycles / 600 * 31556926 * 20;% Number of cycles within 20
    operating years

XDD_bin = [];
XDD_temp = zeros(1,num);
for l = 1 : num
    for p = 1 : blocks % Looping through p number of stress blocks

        XDD_temp(l) = XDD_temp(l) + Xn(p,l)*Xstress(p,l)^m2;

        if l == 1 % Assembled
            XDD_bin(1,p) = Xn(p,l)*Xstress(p,l)^m2;
```

```
            elseif l == 3 % 1e5
                XDD_bin(2,p) = Xn(p,l)*Xstress(p,l)^m2;
            elseif  l == 4 % 3e5
                XDD_bin(3,p) = Xn(p,l)*Xstress(p,l)^m2;
            elseif l == 5 % 5e5
                XDD_bin(4,p) = Xn(p,l)*Xstress(p,l)^m2;
            else
                cc = 1;
            end

        end
end

XDD = 1/10^loga2Bar * XDD_temp;
XDD_bins = 1/10^loga2Bar * XDD_bin;

%% Fatigue damage accumulation 13 m/s

XYn = XYcycles / 600 * 31556926 * 20;% Number of cycles within 20
    operating years

XYDD_bin = [];
XYDD_temp = zeros(1,num);
for l = 1 : num
    for p = 1 : XYblock % Looping through p number of stress blocks

        XYDD_temp(l) = XYDD_temp(l) + XYn(p,l)*XYstress(p,l)^m2;

            if l == 1 % Assembled
                XYDD_bin(1,p) = XYn(p,l)*XYstress(p,l)^m2;
            elseif l == 3 % 1e5
                XYDD_bin(2,p) = XYn(p,l)*XYstress(p,l)^m2;
            elseif  l == 4 % 3e5
                XYDD_bin(3,p) = XYn(p,l)*XYstress(p,l)^m2;
            elseif l == 5 % 5e5
                XYDD_bin(4,p) = XYn(p,l)*XYstress(p,l)^m2;
            else
```

```
                cc = 1;
            end

        end
end

XYDD = 1/10^loga2Bar * XYDD_temp;
XYDD_bins = 1/10^loga2Bar * XYDD_bin;

%% Fatigue damage accumulation 14 m/s

XYZn = XYZcycles / 600 * 31556926 * 20;% Number of cycles within 20
    operating years

XYZDD_bin = [];
XYZDD_temp = zeros(1,num);
for l = 1 : num
    for p = 1 : XYZblock % Looping through p number of stress blocks

        XYZDD_temp(l) = XYZDD_temp(l) + XYZn(p,l)*XYZstress(p,l)^m2;

        if l == 1 % Assembled
            XYZDD_bin(1,p) = XYZn(p,l)*XYZstress(p,l)^m2;
        elseif l == 3 % 1e5
            XYZDD_bin(2,p) = XYZn(p,l)*XYZstress(p,l)^m2;
        elseif  l == 4 % 3e5
            XYZDD_bin(3,p) = XYZn(p,l)*XYZstress(p,l)^m2;
        elseif l == 5 % 5e5
            XYZDD_bin(4,p) = XYZn(p,l)*XYZstress(p,l)^m2;
        else
            cc = 1;
        end

    end
end

XYZDD = 1/10^loga2Bar * XYZDD_temp;
```

```
XYZDD_bins = 1/10^loga2Bar * XYZDD_bin;

%% Plot Damage contribution 10 m/s
edgess_stress = edgess*10^3/W;
figure(5)
b = bar(edgess_stress,DD_bins);
legend('Assembled turbine', 'EqDamp, C = 1e5', 'EqDamp, C = 3e5', '
    EqDamp, C = 5e5');
set(gca,'Fontsize',16)
title('Damage contribution, U_{mean} = 10 m/s')
xlim([5 22.5])
ylim([0 0.024])
xlabel('Stress range, \Delta \sigma [MPa]')
ylabel('Damage, D [-]')

%% Plot Damage contribution 12 m/s
Xedgess_stress = Xedgess*10^3/W;
figure(6)
Xb = bar(Xedgess_stress,XDD_bins);
legend('Assembled turbine', 'EqDamp, C = 1e5', 'EqDamp, C = 3e5', '
    EqDamp, C = 5e5');
set(gca,'Fontsize',16)
title('Damage contribution, U_{mean} = 12 m/s')
xlim([5 28])
xlabel('Stress range, \Delta \sigma [MPa]')
ylabel('Damage, D [-] ')

%% Plot Damage contribution 13 m/s
XYedgess_stress = XYedgess*10^3/W;
figure(7)
XYb = bar(XYedgess_stress,XYDD_bins);
legend('Assembled turbine', 'EqDamp, C = 1e5', 'EqDamp, C = 3e5', '
    EqDamp, C = 5e5');
set(gca,'Fontsize',16)
title('Damage contribution, U_{mean} = 13 m/s')
xlim([5 29])
xlabel('Stress range, \Delta \sigma [MPa]')
```

```
ylabel('Damage, D [-] ')

%% Plot Damage contribution 14 m/s
XYZedgess_stress = XYZedgess*10^3/W;
figure(8)
XYZb = bar(XYZedgess_stress,XYZDD_bins);
legend('Assembled turbine', 'EqDamp, C = 1e5', 'EqDamp, C = 3e5', '
    EqDamp, C = 5e5');
set(gca,'Fontsize',16)
title('Damage contribution, U_{mean} = 14 m/s')
xlim([5 23.7])
ylim([0 0.02])
xlabel('Stress range, \Delta \sigma [MPa]')
ylabel('Damage, D [-] ')
```

Lucia Hanh Tran Vu

NTNU
Norwegian University of
Science and Technology